POLITECNICO DI MILANO

School of Civil, Environmental and Land Management Engineering

Master of Science in Civil Engineering for Risk Mitigation

Master of Science Thesis

Structural Response of Heavily-Reinforced Concrete Columns Subjected to Fire

Supervisor: Prof. Patrick BAMONTE

Candidate: Batuhan DER

Abstract

Heavily-reinforced concrete columns can be used in high-rise buildings due to the several advantages. The cost-effectiveness of using high-strength concrete is a major reason why construction companies should make use of them in demanding structures. With the increasing height of buildings, vertical supporting elements, as columns and walls, are subjected to successive load increments due to the construction of the overlying floors, showing significant axial shortenings. These elastic deformations increase in time due to creep and shrinkage of concrete. Large amounts of steel, such as in heavily reinforced members, reduces the impact of long-term phenomena. Naturally, their performance in fire is an important topic, yet not completely investigated and not even to the same extent as normal reinforced concrete members. The focus of this thesis is on the fire response of heavily-reinforced high strength concrete columns subjected to fire.

In this thesis, twenty heavily-reinforced columns tested in laboratory were used to compare experimental results with numerical simulations obtained by using finite element code. The numerical simulation of heavily reinforced concrete columns was conducted with the traditional approach adopted for reinforced concrete columns and a comparison was made between test data and numerical simulation results, including comparisons between explicit and implicit models for the load-induced thermal strain. The agreement between test results and numerical simulations for temperature, axial deformation and failure time was found to be good, with no major difference between explicit and implicit transient creep models. The role of concrete in heavily-reinforced concrete columns was also investigated. The mechanical analysis of the columns was performed by using the three strength classes currently provided by EC2 for high strength concretes, as well as the provisions devised in the same standard for ordinary siliceous

concrete. Results indicated that normal siliceous concrete strength can be used for Class 1 and Class 2, with no major loss of accuracy, whereas more significant differences were observed when using normal siliceous concrete strength decay instead Class 3.

Acknowledgments

Foremost, I would like to express my sincere gratitude to my advisor Prof. Patrick Bamonte for the continuous support of my master study, for his patience, motivation, and immense knowledge.

Table of Contents

Acknowledgments iv

List of Figures ix

List of Tables xvii

Chapter 1 Introduction 1

1 Introduction 1

1.1 General 1

1.2 Composite Structures 2

1.3 Advantages of Steel-Concrete Composite Structures 3

1.4 Structural Performance of Composite Columns Exposed to Fire 3

1.5 Objective 3

1.6 Thesis Layout 5

Chapter 2 Literature Review 6

2 Literature Review 6

2.1 Fire Scenario 6

2.1.1 ISO 834 Fire Curve 6

2.1.2 ASTM E119 Fire Curve 7

2.1.3 Hydrocarbon Fire 7

2.1.4 External Fire 8

2.2 Thermal Properties of Materials at Elevated Temperatures 9

2.2.1 Concrete 9

2.2.1.1 Thermal Conductivity 9

2.2.1.2 Specific Heat 11

2.2.1.3 Density 12

2.2.2 Steel 13

2.2.2.1 Thermal Conductivity 13

2.2.2.2 Specific Heat 14
2.2.2.3 Density 15
2.3 Mechanical Properties of Materials at Elevated Temperature 15
2.3.1 Concrete 15
2.3.1.1 Compressive Strength 15
2.3.1.2 Poisson's Ratio 17
2.3.1.3 Tensile Strength 17
2.3.1.4 Modulus of Elasticity 18
2.3.1.5 Stress-Strain Response 20
2.3.2 Steel 22
2.3.2.1 Stress-Strain Response 23
2.3.2.2 Yield Strength 24
2.3.2.3 Elastic Modulus 25
2.4 Deformation Properties of Materials at Elevated Temperature 26
2.4.1 Concrete 26
2.4.1.1 Thermal Strain 26
2.4.1.2 Creep Strain 27
2.4.1.3 Transient Strain 29
2.4.1.3.1 Implicit and Explicit Models 31
2.4.2 Steel 32
2.4.2.1 Thermal Strain 32
2.4.2.2 Creep Strain 33
2.4.2.3 Stress-Related Strain 34
2.5 High Strength Concrete 34
2.6 Spalling of Concrete Due to Fire 36
2.7 Previous Studies on Fire Resistance of RC Column 37

2.7.1 Analytical Study by Lie and Irwin (1990) 37
2.7.2 Experimental and Analytical Study by Zhu and Lie (1993) 37
2.7.3 Experimental and Analytical Study by Kodur and Raut (2011) 38
Chapter 3 Thermal Behavior Modelling 39
3 THERMAL BEHAVIOR MODELLING 39
3.1 Introduction 39
3.2 Software Description 39
3.3 Experimental Studies 41
3.3.1 Test Conditions 42
3.3.2 Test Specimens 42
3.4 Numerical Studies 48
3.4.1 Cross Section Discretization 48
3.4.2 Boundary Conditions 49
3.4.3 Thermal Properties of Materials 49
3.4.3.1 Thermal Conductivity 49
3.4.3.2 Specific Heat 50
3.4.3.3 Density 51
3.5 Results and Discussions 51
Chapter 4 Structural Behavior Modelling 53
4 Structural Behavior Modelling 53
4.1 Introduction 53
4.2 Software Description 53
4.3 Experimental Studies 54
4.3.1 Test Conditions 54
4.3.2 Test Specimens 55
4.4 Numerical Studies 55

4.4.1 Mechanical Properties of Materials 56
4.4.2 Boundary Conditions 56
4.5 Results and Discussions 56
Chapter 5 Concluding Remarks 62
5 Concluding Remarks 62
5.1 Genaral 62
5.2 Conclusions 62
References 65
Appendices 69
Appendix A 69

List of Figures

Figure 1. 1 Physicochemical processes in Portland cement concrete during heating, Khoury (2000) 2

Figure 2. 1 ISO 834 standard fire curve 6

Figure 2. 2 ASTM E119 standard fire curve 7

Figure 2. 3 Hydrocarbon fire curve 8

Figure 2. 4 External Fire Curve 9

Figure 2. 5 Thermal conductivity of concrete proposed by a) Eurocode and b) ASCE 11

Figure 2. 6 Thermal conductivity of high strength concrete for different type of aggregate 11

Figure 2. 7 Specific heat of concrete proposed by a) Eurocode and b) ASCE 12

Figure 2. 8 Density of concrete proposed by Eurocode 13

Figure 2. 9 Thermal conductivity of steel 14

Figure 2. 10 Specific heat of steel 14

Figure 2. 11 Compressive strength of normal strength concrete at elevated temperature 16

Figure 2. 12 Compressive strength of high strength concrete at high temperature 17

Figure 2. 13 Normalized tensile strength of concrete 18

Figure 2. 14 Reduction of elastic modulus of concrete at high temperature (Adopted from ASCE, according to experimental results of Bazant and Kaplan (1996)) 19

Figure 2. 15 Normalized elastic modulus of concrete at high temperatures (proposed by EN 1992-1-2 and ASCE) 20

Figure 2. 16 Model for stress-strain relationship for concrete under compression at elevated temperatures according to EC2. 21

Figure 2. 17 Stress-strain curves for concrete with a cylinder strength of 35 MPa at various temperatures 22

Figure 2. 18 Mathematical model of the stress-strain relationship for reinforcing steel at elevated temperatures according to EC2 23

Figure 2. 19 The reduction factor of yield strength by proposed by ASCE and EN1992-1-2 for hot rolled and cold worked reinforcing steel at elevated temperatures 25

Figure 2. 20 The reduction factor of elastic modulus by proposed by ASCE and EN1992-1-2 for hot rolled and cold worked reinforcing steel at elevated temperatures 25

Figure 2. 21 Thermal strain for concrete proposed by Eurocode and ASCE 27

Figure 2. 22 Variation of creep strain of concrete for several temperatures under a) 22.5% b) 45% stress levels 29

Figure 2. 23 Thermal strain of steel proposed by Eurocode and ASCE 33

Figure 2. 24 Typical creep curve for steel from ASCE model 34

Figure 3. 1 Flow chart of thermal analysis used in SAFIR 41

Figure 3. 2 Reinforced concrete column sections considered: a) PC1, b) PC3 45

Figure 3. 3 Reinforced concrete column sections considered: a) PC2, b) PC4 45

Figure 3. 4 Reinforced concrete column sections considered: a) PC5, b) PC6 45

Figure 3. 5 Reinforced concrete column sections considered: a) PC7, b) PC8 46

Figure 3. 6 Reinforced concrete column sections considered: a) PC9, b) PC10 46

Figure 3. 7 Reinforced concrete column sections considered: a) PC11, b) PC12 46

Figure 3. 8 Reinforced concrete column sections considered: PC14 47

Figure 3. 9 Reinforced concrete column sections considered: a) PC16, b) PC17 47

Figure 3. 10 Reinforced concrete column sections considered: a) PC18, b) PC19 47

Figure 3. 11 Reinforced concrete column sections considered: a) PC20, b) PC21 48

Figure 3. 12 Reinforced concrete column sections considered: PC22 48

Figure 3. 13 Meshes of modelled RC columns cross sections 49

Figure 3. 14 Thermal conductivity of concrete 50

Figure 3. 15 Specific heat of the modelled concrete 51

Figure 4. 1 Comparison of failure times from test data and numerical results 57

Figure 4. 2 Comparison of axial deformations from test data and numerical results 58

Figure 4. 3 Deformation shapes of tested columns namely PC 1 to 8 from left to right 59

Figure 4. 4 Deformation shapes of tested columns namely PC 9 to 16 from left to right 59

Figure 4. 5 Deformation shapes of tested columns namely PC 17 to 22 from left to right 60

Figure 4. 6 Deformation shape of column from numerical analysis 60

Figure B. 1 Temperature map for PC1 at a) 45 min b) 90 min and c) failure time 69

Figure B. 2 The calculated and measured temperature in thermocouples 70

Figure B. 3 Comparison of calculated axial deformations with measured axial deformations for PC1 70

Figure B. 4 Axial deformations for different concrete compressive strengths 71

Figure B. 5 Temperature map for PC2 at a) 100 min b) 160 min and c) failure time 71

Figure B. 6 The calculated and measured temperature in thermocouples 72

Figure B. 7 The calculated and measured temperature in thermocouples 72

Figure B. 8 Comparison of calculated axial deformations with measured axial deformations for PC2..... 73

Figure B. 9 Axial deformations for different concrete compressive strengths 73

Figure B. 10 Temperature map for PC3 at a) 60 min b) 120 min and c) failure time 74

Figure B. 11 The calculated and measured temperature in thermocouples 75

Figure B. 12 Comparison of calculated axial deformations with measured axial deformations for PC3..... 75

Figure B. 13 Axial deformations for different concrete compressive strengths 76

Figure B. 14 Temperature map for PC4 at a) 50 min b) 100 min and c) failure time 76

Figure B. 15 The calculated and measured temperature in thermocouple..... 77

Figure B. 16 The calculated and measured temperature in thermocouples 77

Figure B. 17 Comparison of calculated axial deformations with measured axial deformations for PC4..... 78

Figure B. 18 Axial deformations for different concrete compressive strengths 78

Figure B. 19 Temperature map for PC5 at a) 30 min b) 60 min and c) failure time 79

Figure B. 20 The calculated and measured temperature in thermocouples 80

Figure B. 21 Comparison of calculated axial deformations with measured axial deformations for PC5..... 80

Figure B. 22 Axial deformations for different concrete compressive strengths 81

Figure B. 23 Temperature map for PC6 at a) 42 min b) 84 min and c) failure time 82

Figure B. 24 The calculated and measured temperature in thermocouples 83

Figure B. 25 Comparison of calculated axial deformations with measured axial deformations for PC6..... 83

Figure B. 26 Axial deformations for different concrete compressive strengths 84

Figure B. 27 Temperature map for PC7 at a) 50 min b) 100 min and c) failure time 84

Figure B. 28 The calculated and measured temperature in thermocouples 85

Figure B. 29 Comparison of calculated axial deformations with measured axial deformations for PC7..... 85

Figure B. 30 Axial deformations for different concrete compressive strengths 86

Figure B. 31 Temperature map for PC8 at a) 42 min b) 84 min and c) failure time 87

Figure B. 32 The calculated and measured temperature in thermocouples 88

Figure B. 33 Comparison of calculated axial deformations with measured axial deformations for PC8..... 88

Figure B. 34 Axial deformations for different concrete compressive strengths 89

Figure B. 35 Temperature map for PC9 at a) 60 min b) 120 min and c) failure time 90

Figure B. 36 The calculated and measured temperature in thermocouples 90

Figure B. 37 The calculated and measured temperature in thermocouples 91

Figure B. 38 Comparison of calculated axial deformations with measured axial deformations for PC9..... 91

Figure B. 39 Axial deformations for different concrete compressive strengths 92

Figure B. 40 Temperature map for PC10 at a) 67 min b) 134 min and c) failure time 92

Figure B. 41 The calculated and measured temperature in thermocouples 93

Figure B. 42 The calculated and measured temperature in thermocouples 93

Figure B. 43 Comparison of calculated axial deformations with measured axial deformations for PC10..... 94

Figure B. 44 Axial deformations for different concrete compressive strengths 94

Figure B. 45 Temperature map for PC11 at a) 50 min b) 100 min and c) failure time 95

Figure B. 46 The calculated and measured temperature in thermocouple..... 96

Figure B. 47 Comparison of calculated axial deformations with measured axial deformations for PC11..... 96

Figure B. 48 Axial deformations for different concrete compressive strengths 97

Figure B. 49 Temperature map for PC12 at a) 34 min b) 87 min and c) failure time 97

Figure B. 50 The calculated and measured temperature in thermocouples 98

Figure B. 51 The calculated and measured temperature in thermocouples 98

Figure B. 52 Comparison of calculated axial deformations with measured axial deformations for PC12..... 99

Figure B. 53 Axial deformations for different concrete compressive strengths 99

Figure B. 54 Temperature map for PC14 at a) 60 min b) 120 min and c) failure time 100

Figure B. 55 The calculated and measured temperature in thermocouple..... 100

Figure B. 56 The calculated and measured temperature in thermocouples 101

Figure B. 57 Comparison of calculated axial deformations with measured axial deformations for PC14..... 101

Figure B. 58 Axial deformations for different concrete compressive strengths 102

Figure B. 59 Temperature map for PC16 at a) 50 min b) 100 min and c) failure time 103

Figure B. 60 The calculated and measured temperature in thermocouples 104

Figure B. 61 Comparison of calculated axial deformations with measured axial deformations for PC16..... 104

Figure B. 62 Axial deformations for different concrete compressive strengths 105

Figure B. 63 Temperature map for PC17 at a) 50 min b) 100 min and c) failure time 105

Figure B. 64 The calculated and measured temperature in thermocouple..... 106

Figure B. 65 The calculated and measured temperature in thermocouple..... 106

Figure B. 66 The calculated and measured temperature in thermocouple..... 107

Figure B. 67 Comparison of calculated axial deformations with measured axial deformations for PC17..... 107

Figure B. 68 Axial deformations for different concrete compressive strengths 108

Figure B. 69 Temperature map for PC18 at a) 60 min b) 120 min and c) failure time 108

Figure B. 70 The calculated and measured temperature in thermocouple..... 109

Figure B. 71 The calculated and measured temperature in thermocouple..... 109

Figure B. 72 Comparison of calculated axial deformations with measured axial deformations for PC18..... 110

Figure B. 73 Axial deformations for different concrete compressive strengths 110

Figure B. 74 Temperature map for PC19 at a) 60 min b) 120 min and c) failure time 111

Figure B. 75 The calculated and measured temperature in thermocouple..... 112

Figure B. 76 The calculated and measured temperature in thermocouple..... 112

Figure B. 77 The calculated and measured temperature in thermocouple..... 113

Figure B. 78 Comparison of calculated axial deformations with measured axial deformations for PC19 113

Figure B. 79 Axial deformations for different concrete compressive strengths 114

Figure B. 80 Temperature map for PC20 at a) 60 min b) 120 min and c) failure time 115

Figure B. 81 The calculated and measured temperature in thermocouple 116

Figure B. 82 Comparison of calculated axial deformations with measured axial deformations for PC20 116

Figure B. 83 Axial deformations for different concrete compressive strengths 117

Figure B. 84 Temperature map for PC21 at a) 25 min b) 50 min and c) failure time 117

Figure B. 85 The calculated and measured temperature in thermocouple 118

Figure B. 86 The calculated and measured temperature in thermocouple 118

Figure B. 87 Comparison of calculated axial deformations with measured axial deformations for PC21 119

Figure B. 88 Axial deformations for different concrete compressive strengths 119

Figure B. 89 Temperature map for PC22 at a) 50 min b) 100 min and c) failure time 120

Figure B. 90 The calculated and measured temperature in thermocouple 121

Figure B. 91 Comparison of calculated axial deformations with measured axial deformations for PC22 121

Figure B. 92 Axial deformations for different concrete compressive strengths 122

List of Tables

Table 3. 1 Density and moisture content of columns at test date 43

Table 3. 2 Characteristics of the test columns with internal hole 43

Table 3. 3 Characteristics of the square test columns 43

Table 3. 4 Characteristics of the oval test columns 44

Table 3. 5 Characteristics of the round test columns 44

Table 3. 6 Characteristics of the rectangular test columns 44

Table 4. 1 Summary of test parameters for columns 55

Table 4. 2 The calculated and tested values of fire resistance 61

Chapter 1
Introduction

1 Introduction

1.1 General

Fire is considered one of the most serious potential risks for concrete structures although concrete is well known for its good fire resistance and the best possible response in case of fire among the different building materials. The use of concrete can strongly decrease many problems due to fire risk. As a construction material it does not burn and does not contribute to the fire load. Moreover, its insulating power brings in low increasing rate of temperature across a cross section. There is a significant difference between temperature of internal zone and surface exposed to the elevated temperature owing to concrete low thermal conductivity. Another essential feature related to human health is that concrete does not produce toxic gases and smokes when heated. Concrete can be considered as an effective fire barrier and therefore fire spreading can not take place. Chemical and physical changes can take place while concrete is heated to elevated temperature during fire. Many experimental results indicate that the mechanical properties of non protected concrete reduce drastically above 300°C.

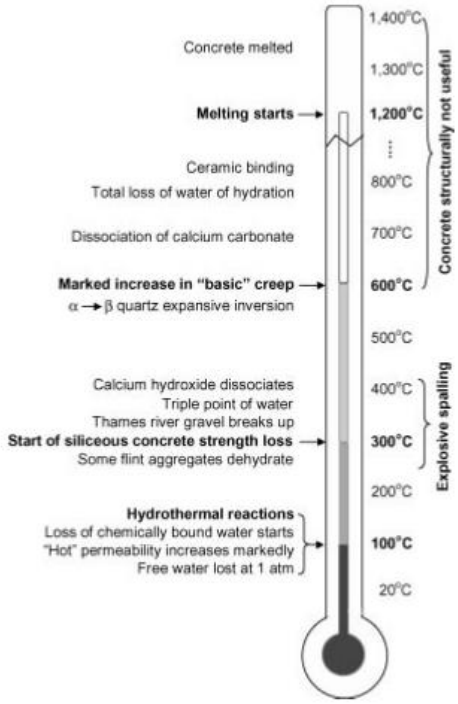

Figure 1. 1 Physicochemical processes in Portland cement concrete during heating, Khoury (2000)

1.2 The Steel-Concrete Composite Structures

Composite structures are made up of two or more different materials. The steel-concrete composite is the most common form of composite in construction. The heavily-reinforced high strength concrete is also consider as a steel-concrete composite structure.

Steel columns have a less fire resistance than steel-concrete composite columns due to the thermal mass of concrete. The composite columns were developed to improve the fire resistance of steel columns. Fully encased steel sections, partially encased steel sections and concrete filled tabular sections are the most common composite columns. In addition to them, by means of using high reinforcement ratio, reinforced concrete columns can behave like composite columns. In composite structures, concrete is used to protect steel from fire as insulator material.

In concrete-steel composite structures, the major problem of concrete section is spalling and expansion of steel reinforcement. Steel expands and contracts more on variations in temperature as compared to composites.

1.3 Advantages of Steel-Concrete Composite Structures

As a material, concrete works well in compression and steel is very strong in tension even when used in relatively small amounts. Compressive strength of concrete alongside steel's resistance to tension are used in steel-concrete composite members and provide the most effective utilization of the two materials. This combination results in cost effective, faster and very stable construction. Additionally, the concrete cover protects steel from buckling, corrosion and fire. Composite construction takes the advantages of the speed of construction, light weight and strength of steel, and the higher mass, stiffness, damping, ductility of reinforced concrete. High ductility of steel leads to better seismic resistance of the composite section. Area occupied by the composite column is less than the area occupied by an RC column. Therefore, there are more free places for people to use in buildings. RC construction has more cost of formwork than composite construction.

1.4 Structural Performance of Composite Columns Exposed to Fire

The performance of a building structure in a fire event depends greatly on the behavior of the columns.

The fire safety of any building can be provided by increasing its fire resistance which depends on the combustibility and the properties of the main structural elements in structure. The response of a composite structure subjected to fire is affected by the properties of its constituent materials, concrete and steel, at elevated temperature.

The behaviour of the columns influences the response of the structure in case of fire. The column subjected to fire can have a deficient behaviour and it can lead to the partial (or even global) failure of the building. The fire rating of a reinforced concrete column is influenced primarily by the column size and the aggregate type. The heated column tends to elongate while restrained in its elongation when the rest of structure remains at lower temperature. The behavior of steel-concrete composite columns subjected to fire is predicted by carrying out thermal stress analysis. This could be made by two different methods: fully coupled thermal stress analysis and sequentially coupled thermal stress analysis.

The traditional approach of evaluating the fire resistance of reinforced concrete column is through full-scale fire standard tests, finite element software, numerical and analytical methods. Furnaces are used to perform the full-scale fire standard tests by heating the column. One of the standard fire curves such as ISO 834 or ASTM E119 can be used to define the ambient temperature surrounding the column. Fire resistance tests are generally more expensive and time consuming than calculation methods.

A concrete column, compared to other structural members, has most often to deal with vertical forces and bending moments from slabs and beams. Furthermore, second-order effects play an important role for columns subjected to axial loads and bending moments. The material and geometric non-linearities due to the non-linear behavior of concrete should be considered when designing reinforced concrete columns. The reasons of the non-linear behavior of reinforced concrete are concrete cracking and yielding of the reinforcement. Bending moments in the initial undeformed configuration of the column axis are called first order moments. The additional moments caused by deformations are called second order moments. If the case is that second order effects cannot be ignored, a nonlinear analysis must be made, taking into account the role played by displacements and rotations on the equilibrium equations (geometric non linearity).

1.5 Objective

The main goal of this thesis is to compare the test results on reinforced concrete columns characterized by high reinforcement ratio exposed to fire with numerical simulations of the 2D structural response with the non-linear software SAFIR developed at the University of Liege (Franssen, 2005) and (Gernay and Franssen, 2017). The temperature measured in thermocouples, the axial deformations and the failure times of the columns are used to compare the test data with the numerical results. Based on the thermal response validation, a different thermal conductivity derived from thermal conductivity of concrete proposed by Eurocode is used instead of using the two limit curves from Eurocode. In mechanical analysis, the axial deformations and the failure times are measured by using different concrete models including the transient creep strain implicitly and explicitly. Then, the influence of reduction factors of concrete compressive strength for different types of concrete strength are investigated to understand the possibility of using the reduction factor of normal concrete strength for high strength concretes.

1.6 Thesis Layout

The thesis is divided into 5 main chapters.

In Chapter 2, a comprehensive literature review is given and the focus of the chapter are the thermal and mechanical properties and deformation properties that influence the behavior at elevated temperature of the materials used in reinforced concrete columns, as well as previous studies about the fire resistance of reinforced concrete columns subjected to fire. There are also informations about high strength concrete and concrete spalling due to fire. Additionally, some previous experimental and numerical studies are introduced.

In the beginning, Chapter 3 briefly describes the main features of thermal analysis and the computer code (SAFIR) used to perform the thermal analysis briefly. Twenty previous studied RC columns were modelled in SAFIR and the numerical results compared with the experiment results. Finally, numerical results were discussed.

Chapter 4 contains the structural response of reinforced concrete columns exposed to fire. Numerical analysis is performed by using SAFIR for twenty tested reinforced concrete columns. The axial deformations and the failure times are calculated for each of column based on Eurocode implicit transient creep model and explicit transient creep model. The influence of reduction factor of concrete compressive strength at elevated temperatures is investigated by using four different reduction factors: normal strength concrete and high strength concrete classified into Class 1, Class 2 and Class 3.

In Chapter 5, conclusions drawn from the whole thesis and recommendations for future work were provided.

Chapter 2
Literature Review

2 Literature Review

2.1 Fire Scenario

The impact of fires on structures is simulated using time-temperature curves. In the following, the most common temperature-time curves used in fire tests are briefly introduced and discussed.

2.1.1 ISO 834 Fire Curve

This fire curve is one of the most popular fire curves for predicting the fire resistance of structural members and products. The temperature-time relationship is defined in equation below and shown in Figure 2.1.

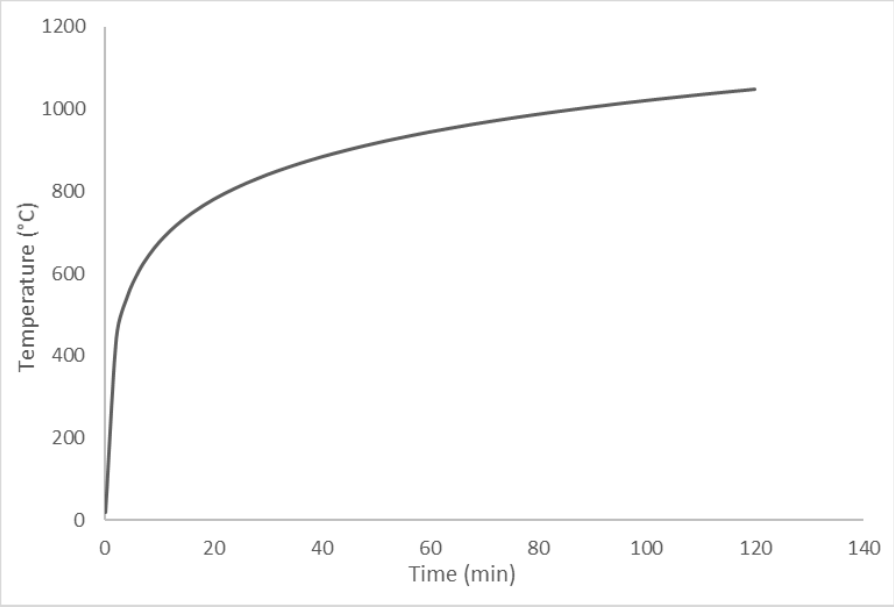

Figure 2. 1 ISO 834 standard fire curve

$$T = 345 \times log_{10}(8t + 1) + T_0$$

where T is the temperature of the environment [°C],

T_0 is the ambient temperature [°C] and

t is the time [min]

2.1.2 ASTM E119 Fire Curve

ASTM E 119 standard temperature-time curve is shown in figure by using the following equation.

$$T = 750\left(1 - e^{-3.79553\sqrt{t_h}}\right) + 170.41\sqrt{t_h} + T_0$$

T is the temperature of boundary [°C]

T_0 is the ambient temperature

t is the time [hour]

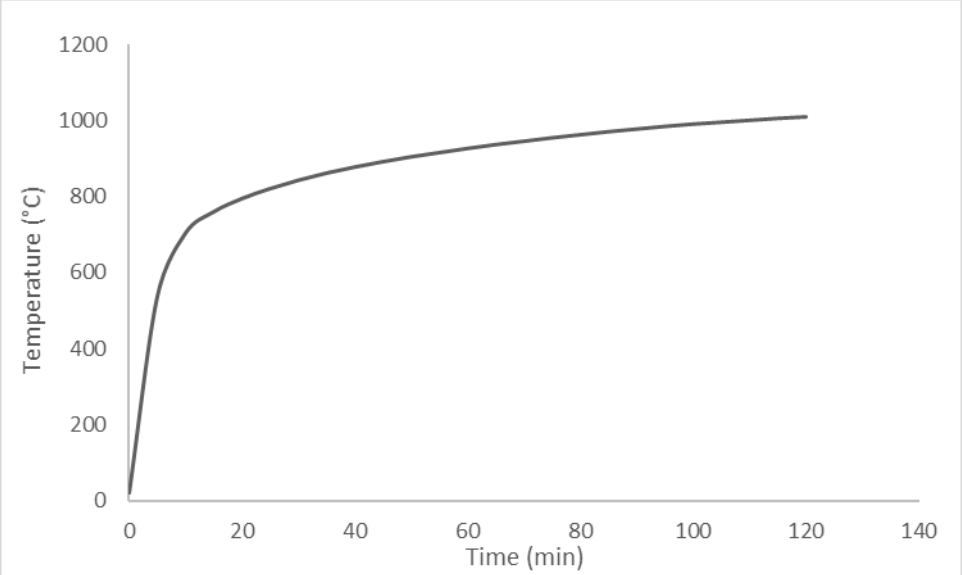

Figure 2. 2 ASTM E119 standard fire curve

2.1.3 Hydrocarbon Fire

The hydrocarbon fire curve can be applied for possible petroleum. This type of fire is defined as follows:

$$T = T_0 + 1080(1 - 0.325e^{-0.167t} - 0.675e^{-2.5t})$$

T is the temperature of boundary [°C]

T_0 is the ambient temperature

t is the time [min]

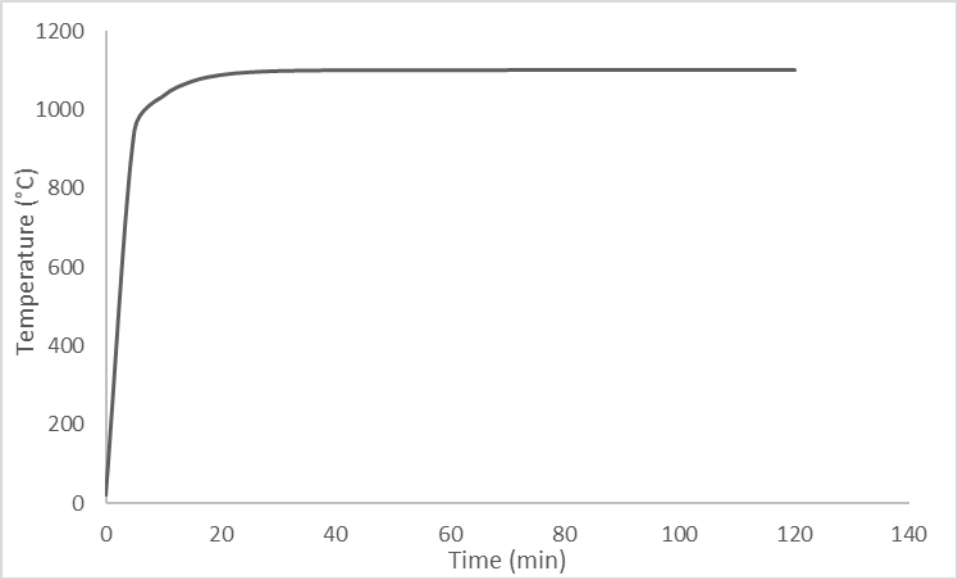

Figure 2. 3 Hydrocarbon fire curve

2.1.4 External Fire

The external fire curve, which is defined via the following equation, presents the time-temperature relationship for members outside the fire compartment.

$$T = 20 + 660(1 - 0.686e^{-0.32t} - 0.313e^{-3.8t})$$

T is the temperature of boundary [°C]

T_0 is the ambient temperature

t is the time [min]

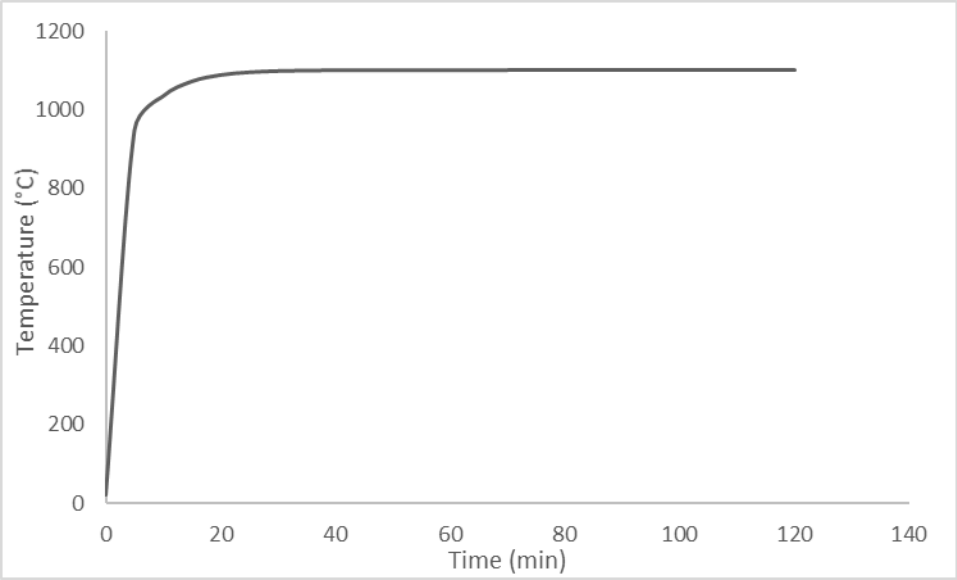

Figure 2. 4 External Fire Curve

2.2 Thermal Properties of Materials at Elevated Temperatures

2.2.1 Concrete

Concrete is considered an isotropic material in temperature calculations. Thermal conductivity, specific heat, mass loss and thermal diffusivity are mainly affected by the moisture content, the aggregate type and constituents of concrete mix (Kodur, 2014). Thermal properties affect the temperature increase and distribution in concrete members. The strength class (normal and high) and weight class (normal and light) of concrete also affect the thermal response.

The most common used thermal properties of concrete are those proposed by Eurocode (2004) and ASCE (1992).

2.2.1.1 Thermal Conductivity

Thermal conductitiy is one of the main feature to affect the change in temperature of concrete. It is the ability of material to conduct heat. Heat flux is calculated by Fourier's law and its unit is joules per second per square meter in the case of °C.

$$q = -\lambda \frac{dT}{dx}$$

where λ is thermal conductivity (W/m K), q is heat flux (W/m²), x is thickness or length in meter and temperature difference K or °C.

Thermal conductivity of concrete is dependent on conductivity of its constituents. There are many factors affect thermal conductivity. These are the type of aggregate (siliceous and calcareous), the moisture content of concrete, test conditions, the temperature of concrete, mix proportion and density of concrete. (Schneider, 1988)

Concrete has higher thermal conductivity resulting from heavier aggregates. The moisture content has an important effect on thermal conductivity because in comparision with air, water has higher conductivity. As a result of the dehydration of cement paste and the loss of pore water, the increasing in temperature causes reducing in thermal conductivity.

Steady state or transient test methods help us to measure the thermal conductivity and transient test is more favorite method than steady state test in case of moist concrete.

The thermal conductivity of concrete is determined between lower and upper limit values in Eurocode models. The proposal does not depend on type of aggregate or strength class of concrete. In concrete structures the lower limit is better than upper limit to obtain closer result to real temperatures. In ASCE model, there are different expressions for different types of aggregate which is main component of concrete whereas this consideration is not taken into account in Eurocode. Due to physico-chemical processes, proposals of ASCE may describe behaviour of concrete in better way. Thermal conductivity proposed by both models is plotted as a function of temperature (Figure 2.5)

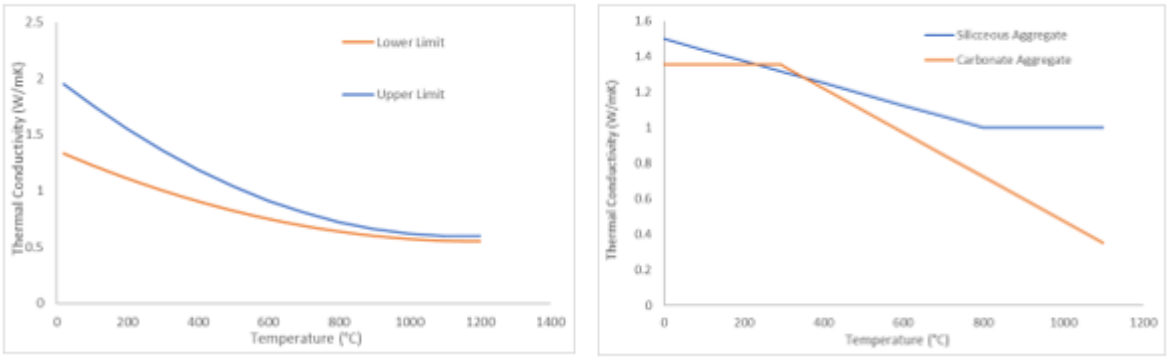

Figure 2. 5 Thermal conductivity of concrete proposed by a) Eurocode and b) ASCE

For high strength concrete there is no agreement about the values of thermal conductivity throughout fire. In research of Kodur and Sultan (1998), the thermal conductivity of high strength concrete is plotted in Figure 2.6. It can be seen that the effect of type of aggretae for both high strength and normal strength concrete is similar.

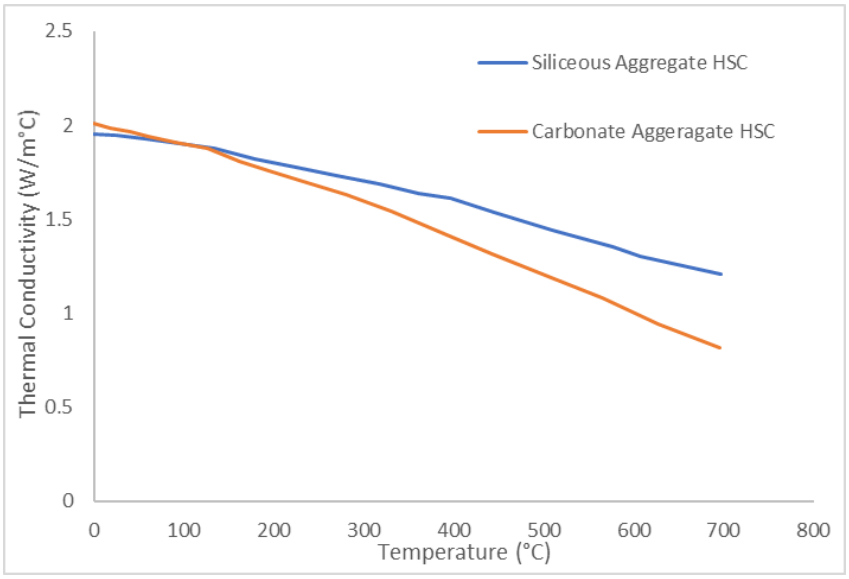

Figure 2. 6 Thermal conductivity of high strength concrete for different type of aggregate

2.2.1.2 Specific Heat

Specific heat measures the quantity of heat per unit mass to raise to temperature by 1°C. Specific heat is also determined by in regard to thermal capacity that is product of density and specific heat of concrete. It increases with a reducing in the density of concrete and with an increasing in temperature.

Moisture content, density and aggregate type of concrete have an essential effect on the specific heat. The higher water to cement ratio concrete has, the more value of specific heat increases. The specific heat is also related to the chemical and physical transformations happen in concrete at high temperatures. For examples, the vaporization of free water, the dissociation of calcium hydroxide about 400°C and quartz expansive inversion above 600°C.

In Eurocode model, specific heat can be affected by several factors especially the moisture content. It increases with the moisture of content. In Eurocode model, there is a peak between 100°C and 200°C because of necessary energy to evaporate water. In ASCE model different representations are found for different types of aggregate. ASCE considers specific heat and density together. In figure 1. 3 the specific heat of concrete is plotted according to ASCE and Eurocode model.

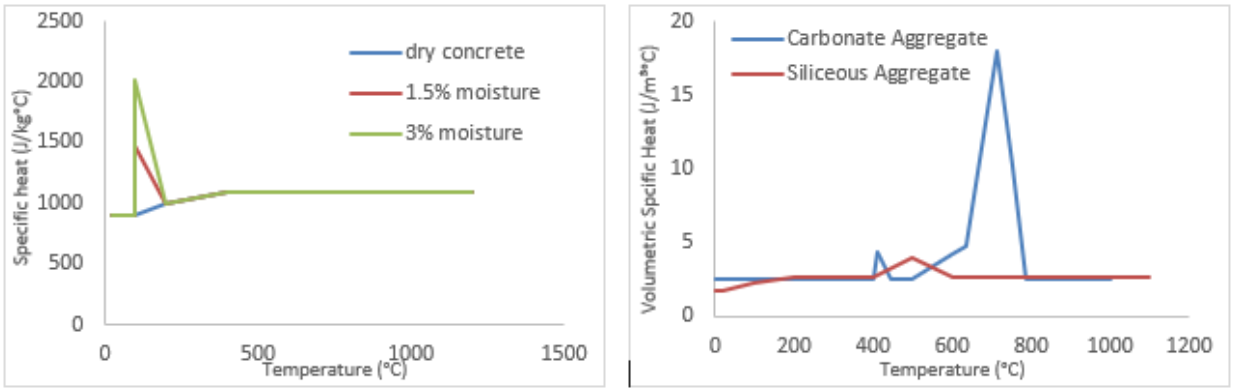

Figure 2. 7 Specific heat of concrete proposed by a) Eurocode and b) ASCE

2.2.1.3 Density

Density of concrete depends on the mix design of concrete and type of aggregate. Concerete can be grouped by density as normal weight (between 2150-2450 kg/m³) and lightweight (between 1350-1850 kg/m³) concrete. Density is mainly influenced by water loss that occurs at 100°C where free water evaporates and decreases with increasing temperature due to the water loss. Thermal response is not significantly affected by the evaporation of free water. The density of limestone aggregate stone changes much at elevated temperature due to decomposition above 800°C. For ASCE, density consists in heat capacity which is product of density and specific heat.

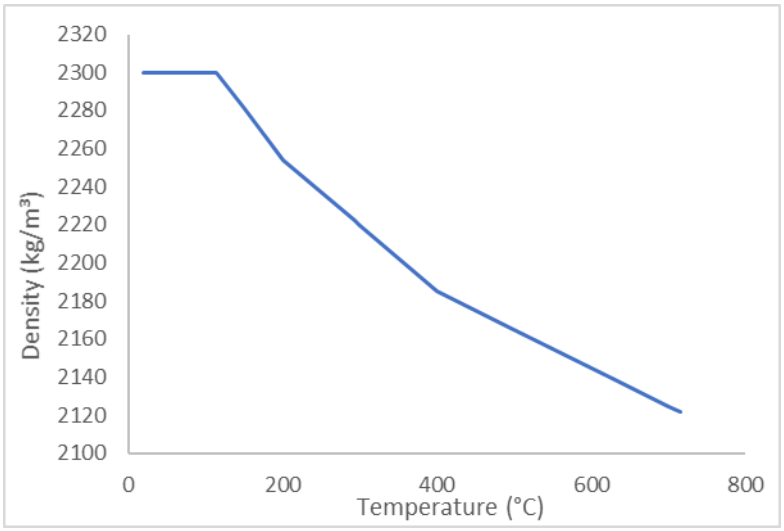

Figure 2. 8 Density of concrete proposed by Eurocode

2.2.2 Steel

Steel is an isotropic material in thermal analysis as well as concrete. Specific heat and thermal conductivity are the material thermal properties that have influence on increasing in temperature and heat distribution. The reinforcing steel does not have a significant effect on thermal analysis because of small amount of area.

2.2.2.1 Thermal Conductivity

Heat transfer analysis which is a function of thermal conductivity is used to evaluate temperature history. Steel becomes an excellent conductor on account of relatively high thermal conductivity. Therefore, when thermal analysis of reinforced concrete is conducted there is an ssumption that temperature of steel equals to temperature in surrounding concrete.

The thermal conductivity of steel varies according to temperature.In EN 1992-1-2 it is decreasing linearly from 54 W/mK at 0°C to 27.3 W/mK at 800°C. ASCE (1992) also demonstrates the same tendency like Eurocode.

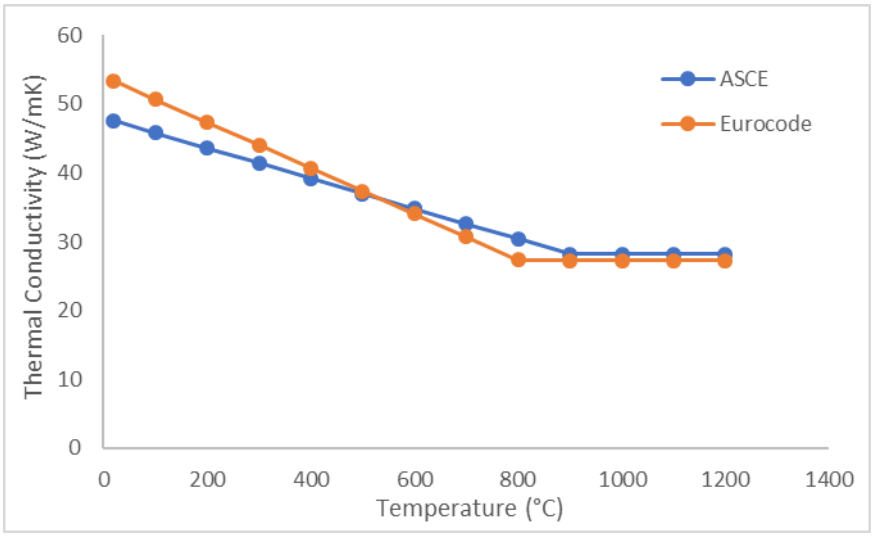

Figure 2. 9 Thermal conductivity of steel

2.2.2.2 Specific Heat

The specific heat is the amount of heat per unit mass required to increase the temperature by one degree Celsius. ASCE and Eurocode propose emprical formulation for specific heat as a function of temperature. There is a spike around 750°C for Eurocode as consequences of metallurgical change whereas ASCE has a relatively lower peak point.

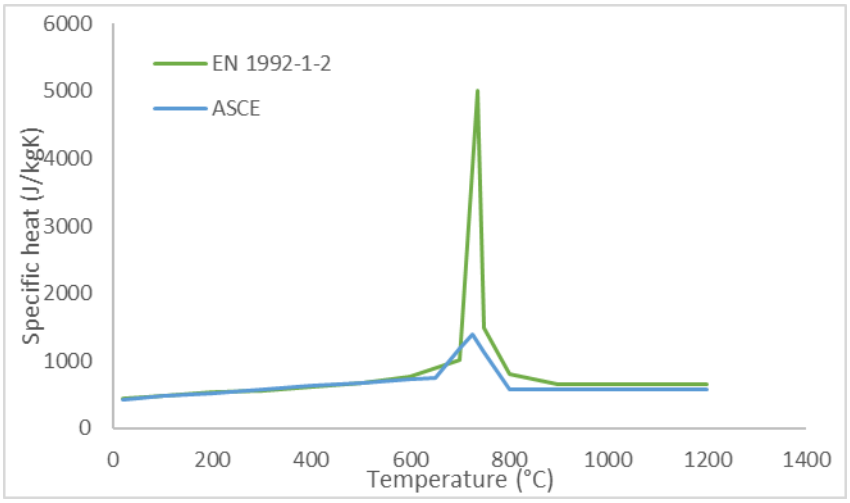

Figure 2. 10 Specific heat of steel

2.2.2.3 Density

Density of steel does not vary according to temperature and the standard value for the density of structural steel offered by EN 1992-1-2 is 7850 kg/m^3.

2.3 Mechanical Properties of Materials at Elevated Temperature

As a structural component is subjected to fire, time dependent high temperature gradients and stress gradients occur. The mechanical properties such as modulus of elasticity, tensile and yield strength reduce under fire load. Furthermore, fire temperatures induce new strains, thermal and transient creep (Youssef and Moftah, 2007). They might also result in explosive spalling of concrete surface (Khoury, 2000).

2.3.1 Concrete

Compressive strength, tensile strength, modulus of elasticity and stress-strain response of constituent materials are parameters that influence the fire performance of RC elements. These are nonlinear functions of temperature. The values of mechanical properties are based on steady and transient states tests. In the steady state test, the concrete specimen is heated to a desired temperature and then loaded under constant elevated temperature. In the transient test, firstly the concrete specimen is loaded upto a given constant load and then heated under the constant load.

2.3.1.1 Compressive Strength

The fundamental property of fire resistance design is the compressive strength of concrete at elevated temperature.

Schneider(1988) indicates that the concrete strength in compression at elevated temperature is dependent mainly on aggregate-cement ratio , type and maximum size of aggregate and level of applied stress during heating. On the other hand, original strength, water-cement ratio, cement type and heating rate are factors that have little influence on concrete strength in compressive.

Mehta and Monteiro’s (2006) study emphasizes that compressive strength of concrete is also affected by type of admixture curing conditions and aggregate-paste interface.

As Naus (2005) has noted, “the reasons of decreasing in compressive strength during heating are aggregate damage due to physical and chemical changes,development of crackings and weakening of the cement-aggregate bond and cement paste.

Reduction factors for compressive strength are offered by EN 1992-1-2 according to type of aggregate. The rate of decreasing in compressive strength is more noticeable for siliceous aggregate than for carbonate aggregate. Up to 400°C decreasing in compressive strength is not hazardous because as summarized (Naus,2005) large number of aggregate indicates the thermally stable behaviour up to 350°C. When the temperature reached above 400°C, compressive strength had severe decline. It can be seen that decay of compressive strength is more detrimental. Meanwhile, the ambient temperature exceeds 800°C and then concrete does not have compressive strength at 1200°C.

Unlike Eurocode, ASCE suggests the same reduction factor for all the aggregate types. Compressive strength remained stable up to 450°C. From 450°C to 875°C reduction factor drops dramatically to 0.

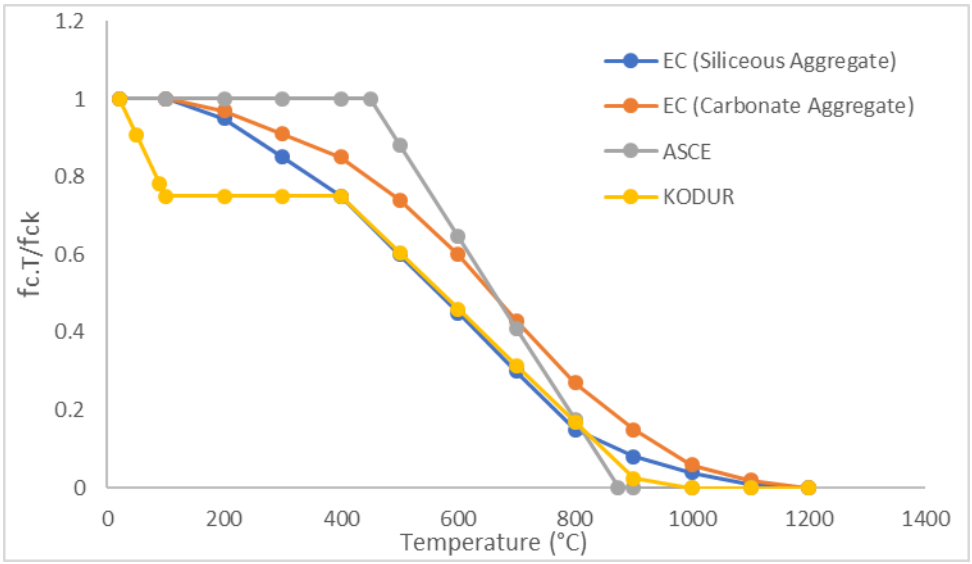

Figure 2. 11 Compressive strength of normal strength concrete at elevated temperature

In addition EC2 provides the values of relative compressive strength for three classes of high strength concrete. The recommended class for concrete C 55/67 and C 60/75 is Class 1, for concrete C 70/85 and C80/95 is Class 2 and for concrete C90/105 is Class 3.

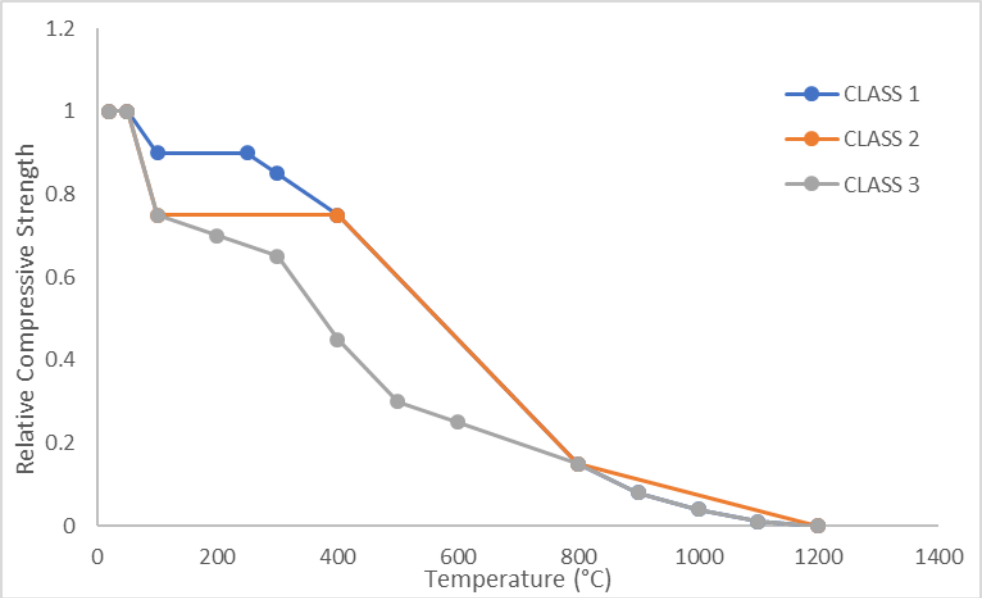

Figure 2. 12 Compressive strength of high strength concrete at high temperature

2.3.1.2 Poisson's Ratio

Concrete specimen under a uniaxial load produces a longitudinal strain in the same direction with the applied load, meanwhile, lateral strain occurs with opposite sign.

At normal ambient conditions, Poisson's ratio for concrete can vary from 0.11 to 0.32. Poisson's ratio of concrete decreases with increasing temperature because of loss of evaporable water in the mixture. When the concrete reaches to 300°C, the amaount of poisson's ratio falls by half from the range of 0.22-0.3 to the range of 0.13-0.19. (Kassir, 1996)

2.3.1.3 Tensile Strength

As Kodur (2014) notes that concrete has relatively high compressive strength but considerably lower tensile strength, and hence tensile strength of concrete is ignorable for strength calculation at ambient temperatures. Due to this reason, ASCE does not propose reduction factor for tensile strength at ambient temperature. However, from perspective of fire resistance, it is a crucial mechanical property because cracking generally occurs because of tensile strength in concrete.

In proposal of EN1992-1-2, tensile strength is retained for the temperatures up to 100°C, followed by linear decay up to 600°. Felicetti and Gambrova (1999) conducted an experiment to

evaluate the response of concrete tensile strength of high strength concrete at elevated temperature. It can be seen from the figure 1.9 that the trend of loss of tensile strength for both concrete is similar but the rate of decay of tensile strength for high strength concrete is slightly higher than for normal strentgh concrete.

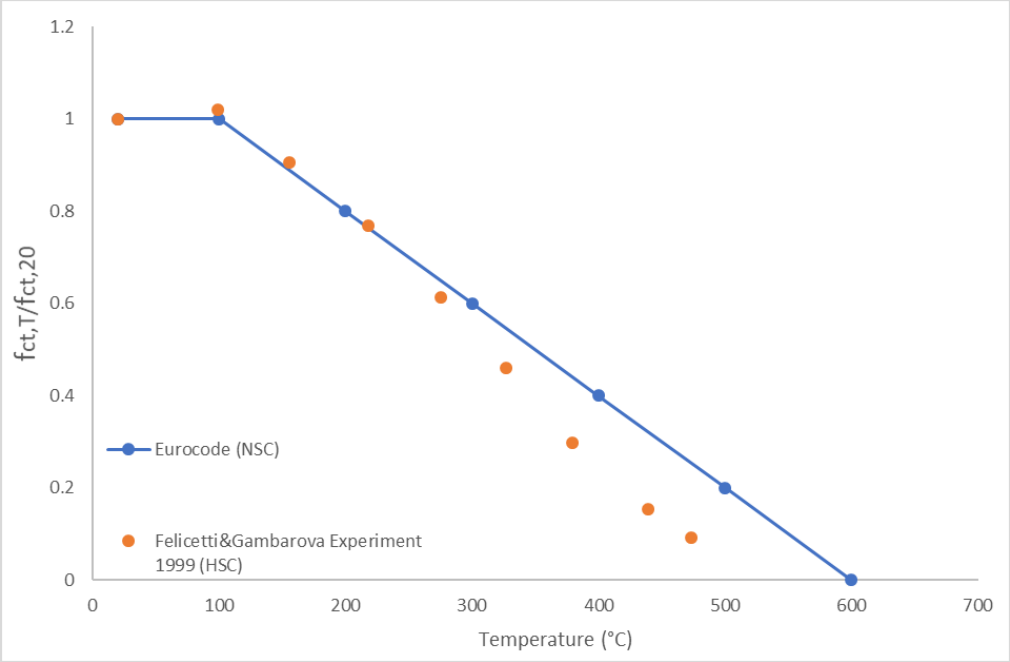

Figure 2. 13 Normalized tensile strength of concrete

2.3.1.4 Modulus of Elasticity

The modulus of elasticity reduces quickly with increasing temperature. The reason of the decreasing is breakage of bonds of cement paste at high temperature. (Linus, 2004)

As defined in (Naus, 2005), elastic modulus of concrete is the ability of material to resist deformation. Therefore increasing temperature is an unfavorable situation for mechanical response of structure under fire. Stress-strain curve of conrete is nonlinear and therefore modulus of elasticity is determined by using some methods such as tangent modulus, secant modulus or initial tangent modulus.

Main factors influencing the modulus of elasticity are (Kodur, 2014) the water/cement ratio (low ratio raises modulus), the age of concrete, the method of conditioning and nature and amount of aggregates. In addition, Schneider (1988) reports that stress conditions has important influence on elasticity-temperature behaviour.

Modulus of elasticity decays at elevated temperatures, aggregate type and load level (Schneider, 1988) are mostly controlling the trend.

The reduction factor for elastic modulus of concrete with siliceous, carbonate aggregate as well as lightweight concrete are plotted in (ASCE, 1992). There is no significant difference between all the three concretes.

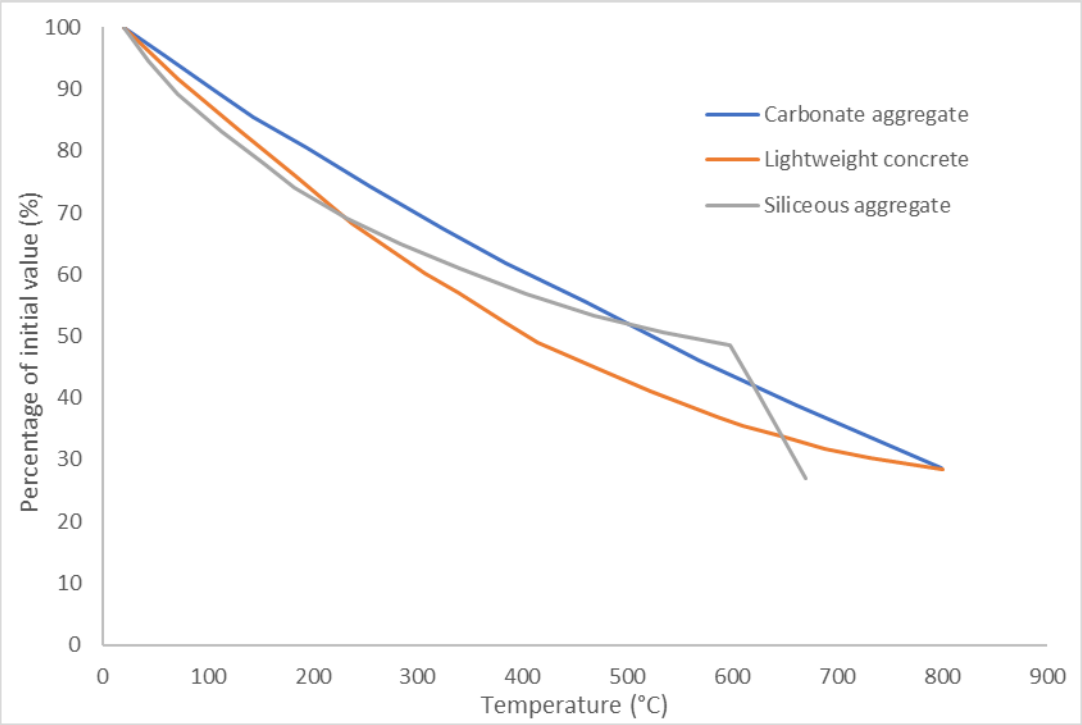

Figure 2. 14 Reduction of elastic modulus of concrete at high temperature (Adopted from ASCE, according to experimental results of Bazant and Kaplan (1996))

It can be seen from figure 1. 11 that there is a decline in the reduction factors of elastic modulus with increasing temperatures for both Eurocode and ASCE model. ASCE proposes the unique reduction factor for all type of aggregates.In Eurocode, different types of aggregate are considered to measure the reduction factor for the modulus of elasticity. Carbonate is somewhat more durable than siliceous. The decay rate in Eurocode model little bit higher than in ASCE model.

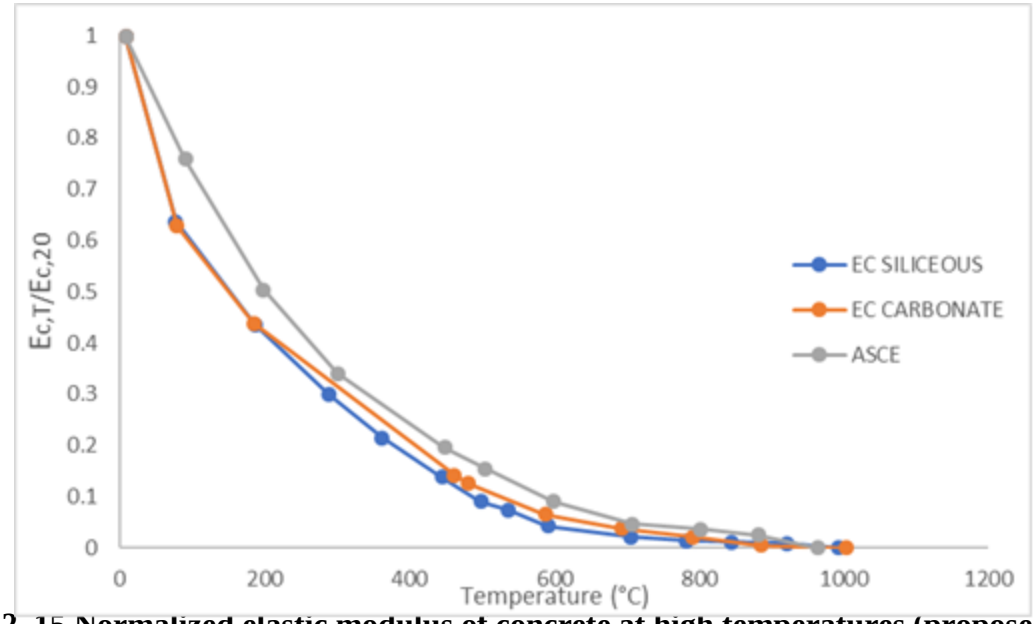

Figure 2. 15 Normalized elastic modulus of concrete at high temperatures (proposed by EN 1992-1-2 and ASCE)

2.3.1.5 Stress-Strain Response

The stress-strain relations are usually used to define the mechanical response of concrete for evaluating the fire resistance of concrete structure members. There are several researches offered different stress-strain models. In concrete, high temperature induces a particular phenomenon: the transient creep strain. Transient creep strain is considered in two different ways; explicitly and implicitly.

The stress-strain curves can be analysed by using three variables; peak strain $\varepsilon_{c1,\theta}$, ultimate strain $\varepsilon_{cu1,\theta}$ and peak compressive strength $f_{c,\theta}$. A unique curve can be plotted for each temperature due to the time temperature dependent parameters.

Reduction of compressive strength and rise in ductility of concrete induce the reduction in the slope stress-strain curve with increasing time. Main factor that has influence on stress-strain relation at both ambient and elevated temperature is the concrete strength.

The compressive strength and the strain corresponding to the peak stress are used to define the stress-strain for defined temperature in Eurocode model. It can be seen that Eurocode model

proposes a nonlinear ascending branch and linear or nonlinear descending branch. Following expression is provided for the ascending part of curve.

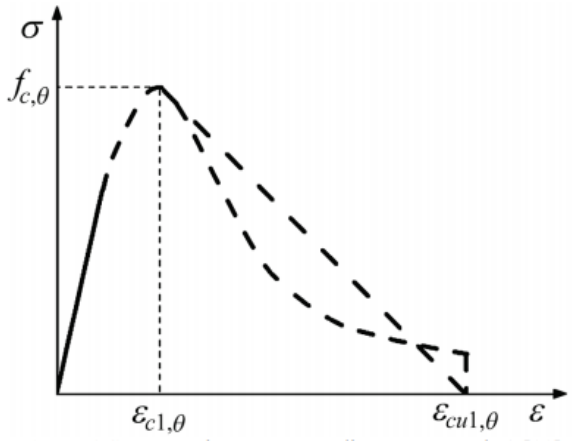

Figure 2. 16 Model for stress-strain relationship for concrete under compression at elevated temperatures according to EC2.

$$\sigma(\theta) = 3\frac{\varepsilon_{c,\theta}}{\varepsilon_{c1,\theta}}\frac{f_{c,\theta}}{2 + (\frac{\varepsilon_{c,\theta}}{\varepsilon_{c1,\theta}})^3}$$

In Figure 2.17, it can be seen that there are stress-strain curves for concrete with a cylinder strength of 35 MPa at various temperatures by proposed ASCE model. These curves are defined by means of following equations;

$$\varepsilon_c \leq \varepsilon_{max}$$

$$f_c = f_c^{'}[1 - \left(\frac{\varepsilon_{max} - \varepsilon_c}{\varepsilon_{max}}\right)^2]$$

$$\varepsilon_c > \varepsilon_{max}$$

$$f_c = f_c^{'}[1 - \left(\frac{\varepsilon_c - \varepsilon_{max}}{3\varepsilon_{max}}\right)^2]$$

where

$$f_c^{'} = f_{co}^{'}[2.011 - 2.353\frac{T-20}{100}] \text{ if } T \geq 450°C$$

$$\varepsilon_{max} = 0.0025 + (6T + 0.04T^2) \times 10^{-6}$$

f_c is compressive strength of concrete at temperature T, f_c' is cylinder strength of concrete at temperature T, f_{co}' is cylinder strength of concrete at 20°C, ε_c is strain of the concrete and ε_{max} is strain corresponding to maximum stress.

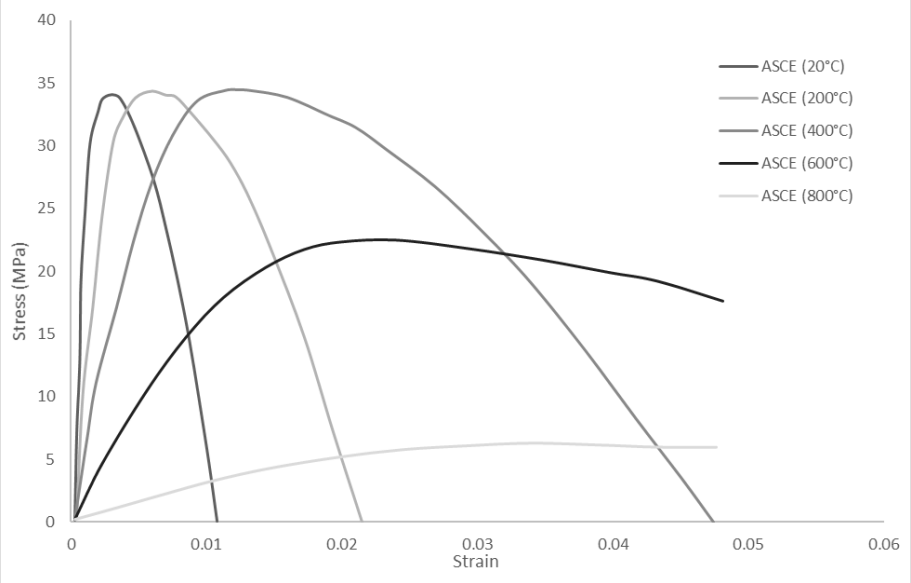

Figure 2. 17 Stress-strain curves for concrete with a cylinder strength of 35 MPa at various temperatures

2.3.2 Steel

As the steel member is heated, the mechanical properties such as modulus of elasticity, yield strength and stress-strain response. .

In Eurocode model, $\varepsilon_{sy,\theta}$, $\varepsilon_{st,\theta}$ and $\varepsilon_{su,\theta}$ are not temperature dependent parameters and these are assigned as 0.02, 0.15 and 0.2 respectively (for Class B and C reinfircement) and 0.02, 0.05 and 0.1 respectively (for Class A reinforcement). Therefore, change in temperature does not have an influence on the ductility of reinforcement. (Elghazouli et al., 2009)

The material models indicated in EN 1993 1.2 are valid only for heating rates between 2 and 50 K/min.

2.3.2.1 Stress-Strain Response

Stress-strain curve is used to describe the mechanical behaviour of materials under different loading. It is unique for each material and for each temperature and is plotted by storing deformation's amount at noticeable intervals of compressive and tensile loading. 3 important parameters such as modulus of elasticity, ultimate and effective yield strength are derived from the stress-strain curves.

The stress-strain behaviour of carbon steel at elevated temperature is significantly different from that at ambient temperature and there is not distinctly visible yield plateu.

The definitions of effective yield strength ($f_{y,\theta}$), proportional limit ($f_{p,\theta}$) and slope of linear elastic range ($E_{a,\theta}$) are built up on the fundamental characteristic of the stress-strain model for steel at elevated temperatures presented by EN1993-1.2. The Eurocode model of stress-strain relationship as a result of tensioning the reinforcing steel at elevated temperatures is based on Anderberg's model ()

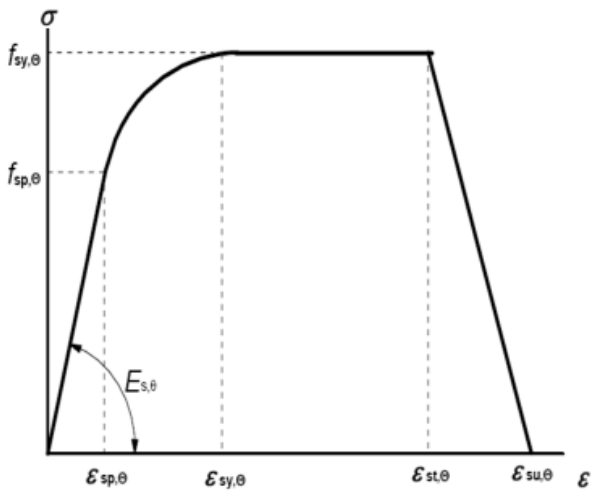

Figure 2. 18 Mathematical model of the stress-strain relationship for reinforcing steel at elevated temperatures according to EC2

Figure 2.13 indicates that in the first part of curve, there is a linear line until proportional limit is reached and elastic modulus is equal to the slope of this linear line. Then material demonstrates

plastic behaviour that is referred to parabolic branch. Strength remains steady by modelling elastic-perfectly plastic behaviour when the strains exceed yield limit strain. Apparently it can be seen from the stress-strain curve that stiffness and strength of steel are decreasing at elevated temperatures.

There are two test methods to obtain stress-strain relationship at high temperatures; steady state and transient tests.

2.3.2.2 Yield Strength

Yield strength represents the maximum stress that can be applied in the steel without plastic deformation. If the stress exceeds the yield strength, it will pass from elastic range to plastic range and will cause irreversible deformations.

The reduction factor for strength and stiffness of steel reinforcement with increasing temperature is dependent on the manufacturing process of the reinforcing bars. (Elghazouli et al., 2009)

Hot rolled steel which shows clearly yield plateau is usally used for standard reinforcing bars at room temperature. This situation makes the yield strength easier to determine at room temperature and changes at elevated temperature because high temperature induces the stress-strain curves to become more rounded. Cold worked steel, typically used in prestressed steel bars, does not indicate yield plateau at any temperature.

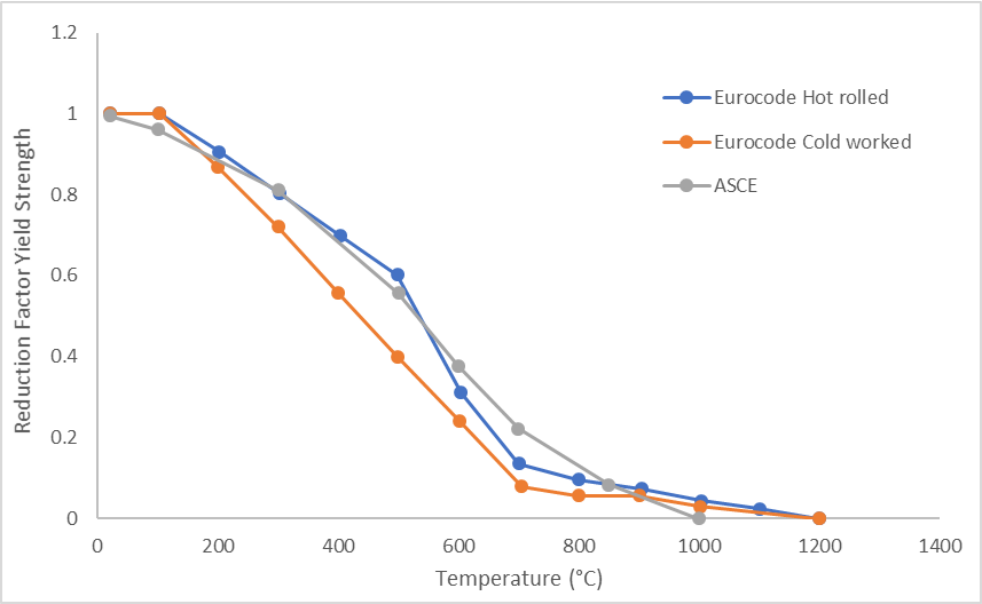

Figure 2. 19 The reduction factor of yield strength by proposed by ASCE and EN1992-1-2 for hot rolled and cold worked reinforcing steel at elevated temperatures

2.3.2.3 Elastic Modulus

The modulus of elasticity of a material is a measure of its stiffness. Elastic modulus of steel defines the relationship between applied stress and elastic strain. Initial stiffness for each type of steel decreases with increasing temperature. The modulus of elasticity is used to calculate buckling. The elastic modulus is also needed for elastic deformation calculation but it is not often attempted because plastic deformation occurs quickly at elevated temperature. The decay rate of elasic modulus exhibits the same behaviour as reduction in yield strength.

In Figure 2.20, normalized elastic modulus of reinforcing steel with reduction factors offered by ASCE and Eurocode has been indicated. The decay of modulus of elasticty indicates the same trend as the reduction in yield strength for both models.

In Eurocode model, the reduction factor for stiffness of bot hot rolled and cold worked steel has a similar trend but cold worked steel suffers more pronounced decay.

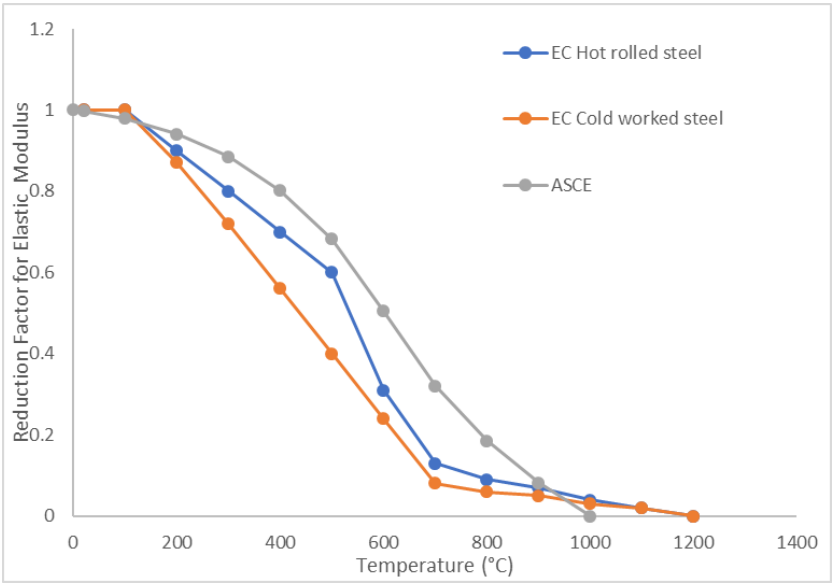

Figure 2. 20 The reduction factor of elastic modulus by proposed by ASCE and EN1992-1-2 for hot rolled and cold worked reinforcing steel at elevated temperatures

2.4 Deformation Properties of Materials at Elevated Temperature

2.4.1 Concrete

There are four components of the total strain to describe the deformation of concrete at elevated temperature.

$$\varepsilon = \varepsilon_{th}(T) + \varepsilon_{\sigma}(\sigma, T) + \varepsilon_{cr}(\sigma, T, t) + \varepsilon_{tr}(\sigma, T)$$

$\varepsilon_{th}(T)$ is thermal strain being a function only of temperature, $\varepsilon_{\sigma}(\sigma, T)$ is the stress related strain, being a function of both the applied stress σ and the temperature, $\varepsilon_{cr}(\sigma, T, t)$ is the creep strain, $\varepsilon_{tr}(\sigma, T)$ is the transient strain (Buchanan, 2001).

As suggested in (Anderberg and Thelandersson, 1973) deformation properties of concrete that contain thermal, mechanical, creep nd transient strain are remarkably dependent on concrete mix proportions and physical nature of its constituents, age and curing conditions of concrete prior to heating and loading, loss of moisture from the specimen during the test, heating procedure (level and history of temperature, heating rate and duration, presence of temperature gradients) and external loading (magnitude and duration of loading, stress history in relation to temperature history).

2.4.1.1 Thermal Strain

Kodur (2014) describes thermal strain as the expansion (or shrinkage) of unit length of a material when the temperature of concrete is increased by one degree. When material shrinks, thermal strain is assumed to be negative otherwise positive. Thermal expansion of concrete is defined by the coefficient of thermal expansion that refers to change in length per unit temperature change.

As summarized in (Anderberg and Thelandersson, 1973) type of aggregate and cement paste have significant impact on the thermal strain of concrete. Furthermore, thermal expansion of concrete is affected by the aggregate rather than cement paste because the fundamental

constituent of concrete is aggregate. When the temperature of concrete is increased, the cement paste tends to shrink above about 150°C while aggregates expand.

EN 1992-1-2 offers set of equations to evaluate thermal elongation of different types of aggregate such as siliceous and calcerous aggregate. As can be seen from the figure that concrete made with calcerous aggregate has a lower thermal expansion that that of siliceous aggregate concrete. However, ASCE model provides an unique variation which increasing monotonically for both siliceous and carbonate aggregate concrete.

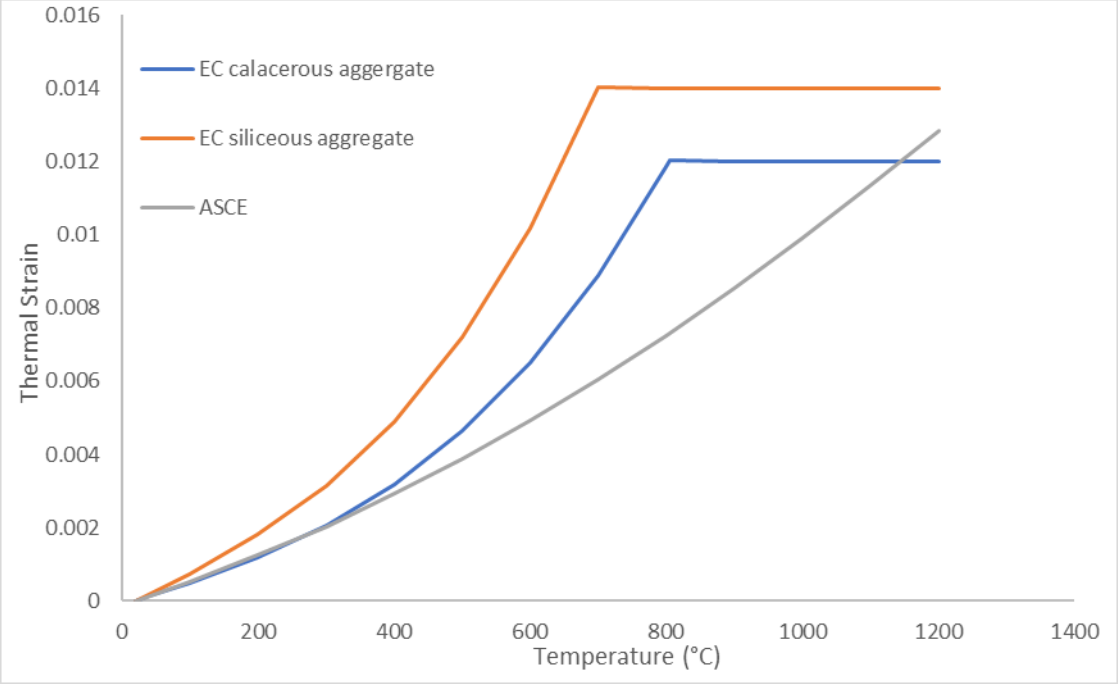

Figure 2. 21 Thermal strain for concrete proposed by Eurocode and ASCE

The decay of thermal expansion rate for high strength concrete is observed between 600-800°C due to the loss of chemically bound water in hydrates. Nonetheless, softening of concrete and excessive micro and macrocrack development make the rate of thermal expansion increased again. (Kodur, 2014)

2.4.1.2 Creep Strain

In overview of Kodur (2014), creep strain is expressed as time dependent inelastic deformation of a material and is an insignificant property at ambient temperatures and normal stress. However, creep can be detrimental at higher temperatures and higher stress levels.

The temperature dependent stress-strain relations for concrete proposed by ASCE and EN 1992-1-2 include creep effects implicitly. Nonetheless, it is recommended to consider the creep effect explicitly to carry out better fire resistance analysis.

As stated in Kodur (2014) there are two fundamental mechanisms that expedites the process of creep: (1) motion of moisture and dehydration of concrete as a result of high temperature and (2) acceleration in the process of bond breakage in cement gel (C-S-H).

Test methods play a critical role in measuring the creep in concrete at high temperatures. These are steady-state and transient-state method. In the steady-state test method, the temperature of concrete is uniformly increased to a targeted temperature and then the specified load level is imposed on concrete at constant elevated temperature. This method is little relevant to real fire stiuation. Therefore, it is obvious that the steady-state tests do not provide reliable results.

Bazant (2001) states that creep strain has a linear relationship with stress level in case of absences of crack at service stress in structure element.

ASCE (1992) explains the main factors affect the creep strain at elevated temperature based on 5 hour test for carbonate aggregate concrete under 45% of room temperature strength performed by Cruz (1968). These factors are age, moisture conditions, type and strength of concrete and stress-strength ratio.

ASCE (1992) also mentions that 3 hour creep strain test under different stress levels i.e 22.5% and 45% of concrete strength for several temperatures. This experience presents that creep strain becomes essential for the response of concrete above 400°C.

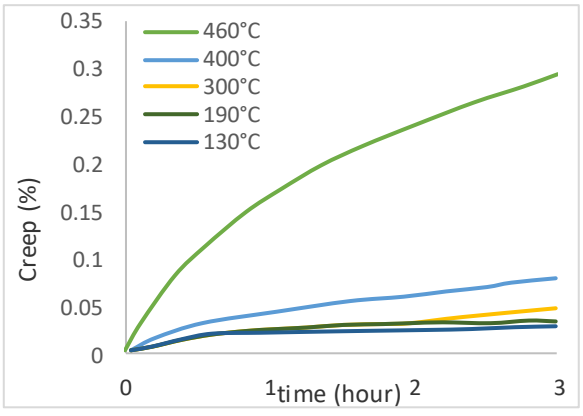

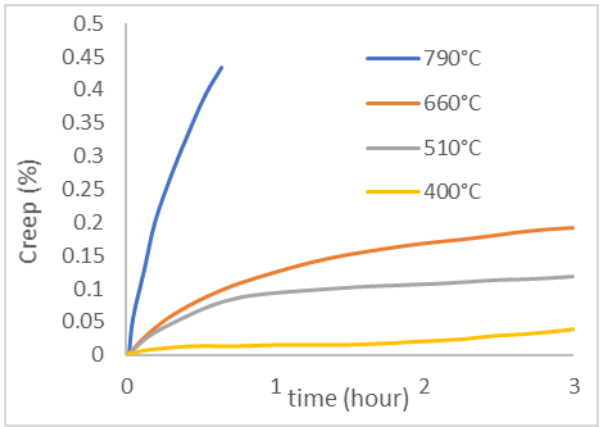

Figure 2. 22 Variation of creep strain of concrete for several temperatures under a) 22.5% b) 45% stress levels

2.4.1.3 Transient Strain

Transient strain is the additional irrecovarable strain which occurs during first time heating of loaded concrete and is dependent on the stress applied during heating and the temperature. Transient creep strain is expressed by means of the comparison of two tests. The difference in strain between results from steady-state and transient tests is called as transient strain.(Gernay and Franssen, 2011).

High temperature entails changes in moisture content and chemical substances of cement paste. Furthermore, the thermal incompatibility occurs between cement paste and aggregates due to the opposite thermal responses. Hence, these factors cause thermal strain with appearing of microcracks and developing of internal stresses (Schneider 1988).

As summarized in Kodur (2014), main factors that affect transient strain are temperature, strength, moisture content, loading and mix proportions.

Load Induced Thermal Strain is defined as the difference between the deformation of loaded and non-loaded concrete. Type of aggregate is not the main factor which influence load induced thermal strain. Despite the internal creep of concrete's constituent, non-loaded concrete expands through heating. On the other hand loaded concrete yields to the load and conctracts as a consequence of transient creep (Kowalski, 2010).

Sadaoui and Khennane (2009) analyzed that the influence of transient creep strain on the fire resistance of reinforced concrete columns by using two different approaches based on the way of measuring of transient creep strain. For both explicit and implict approach, the transient creep strain causes additional contributions to bending which can lead to the failure of structure.

It is the fact that transient strain plays a significant role to understand the behavior of concrete structure under fire load. EN 1992-1-2 proposes uniaxial concrete material model that contains transient strain impicitly. The characteristics of transient strain implictly have not been dealt with

in depth. On the contrary, there are several models that are able to predict transient creep strain explicitly in the literature.

Anderberg (1976) states that the transient creep strain was assumed to be proportional to the applied stress and to free thermal strain and can be found by the following equation;

$$\varepsilon_{tr}(\sigma, T) = -2.35 \times \frac{\sigma}{f_{c,20}} \times \varepsilon_{th}$$

where ε_{tr} is the transient srain, $\frac{\sigma}{f_{c,20}}$ is the ratio between the compressive stress and the compressive strength of concrete at room temperature and ε_{th} is the thermal expansion. All parameters are unitless.

The transient creep strain is dependent on the type of aggregate but afterwards Khoury (1985) indicated that the transient creep strain is not physically related to free thermal strain. Terro (1998) affirms that the transient creep strain has nonlinear proportion to the temperature by means of experimental results by Khoury and volume fraction of aggregates has a contribution to transient strain

$$\varepsilon_{tr} = \varepsilon_{0.3} \times (0.032 + 3.226\frac{f_c}{f_c'})\frac{V_a}{0.65}$$

where V_a is the volume fraction of aggregates, $\varepsilon_{0.3}$ is the transient creep strain for initial axial stress of $0.3f_c'$ which is the compressive strength of concrete at room temperature

In Schneider's model, it is revealed that the transient creep strain depends on the initial stress before heating together with the applied stress, the temperature, modulus of elasticity and strength

Gernay and Franssen (2012) proposed a generic transient model based on the generic constitiutive model for concrete at elevated temperatures taken from EN 1992-1-2 and experimental stress-strain relationships. The main importance of this model is calculating the transient strain explicitly.

2.4.1.3.1 Implicit and Explicit Models

EN 1992-1-2 proposes the most widely used implicit stress-strain model. In the implicit models, the total strain ε_{tot} can be represented as sum of two (or possibly three) components; free thermal strain ε_{th}, mechanical strain ε_m and possibly basic creep strain ε_{cr}.

$$\varepsilon_{tot} = \varepsilon_{th} + \varepsilon_m \ (+\varepsilon_{cr})$$

The stress is directly relevant to mechanical strain, without calculation of transient creep strain. In implicit methods, there are two major limitations. For example, there is no difference between loading at elevated temperature and heating under stress. Furthermore, unlike physical nature, transient creep strain demonstrates reversible behaviour during unloading, because the initial tangent of the constitutive curve in terms of ($\varepsilon_m; \sigma$) is used for the elastic modulus at a given temperature. (Gernay and Franssen, 2010)

In the explicit models, the total strain ε_{tot} is seperated to three (or possibly four) components; free thermal strain ε_{th}, instantaneous stress-related strain ε_σ is a sum of elastic and plastic contribution, transient creep strain ε_{tr} and possibly basic creep strain ε_{cr}.

$$\varepsilon_{tot} = \varepsilon_{th} + \varepsilon_\sigma + \varepsilon_{tr} \ (+\varepsilon_{cr})$$

In explicit models, the stress is directly related to the instantaneous stress-related strain. Experimental results give the relationship from steady-state test at any temperature, by subtracting the free thermal strain to the total strain. Transeint creep strain is not treated as reversible during unloading and cooling. This is because, the initial tangent of instantaneous stress-strain curve is used for the elastic modulus. (Gernay and Franssen, 2011)

As indicated in models proposed by several authors (Anderberg (1976), Schneider (1985) and Terro (1998)). ETC also formulate transient creep strain by adopting previous researches.

$$\varepsilon_{tr} = \Phi(T)\frac{\sigma}{f_{ck}}$$

where $\Phi(T)$ is a nonlinear function of temperature and f_{ck} is the compressive strength at 20°C.

When stress is constant and temperature increases, the correct behaviour of concrete can only be indicated by implicit models. This is a particular situation which is not very common.

2.4.2 Steel

Thermal, mechanical and creep strain are the deformation properties to express the response of steel at elevated temperature.

$$\Delta\varepsilon = \varepsilon - \varepsilon_i = \varepsilon_{th}(T) + \varepsilon_{\sigma}(\sigma, T) + \varepsilon_{cr}(\sigma, T, t)$$

where ε is the total strain at time t, ε_i is the initial strain at time t=0, $\varepsilon_{th}(T)$ is the thermal strain, $\varepsilon_{\sigma}(\sigma, T)$ isthe stress related strain and $\varepsilon_{cr}(\sigma, T, t)$ is the creep strain.

2.4.2.1 Thermal Strain

The thermal strain is the well known thermal expansion which defines the change in unit length of steel when the temperature is increased by one degree. The thermal expansion of steel can be related to its temperature by a thermal expansion coefficient. At room temperature, the coefficient of thermal expansion is assumed as $11.7\times 10^{-6}/°C$ but at higher temperature the coefficient increases.

ASCE proposes nonlinear function of temperatures for thermal strain; main difference with respect to EN 1992-1-2 is that there is not any plateau with constant value of thermal strain in the narrow temperature range from 750°C to 860°C. In ASCE model, thermal expansion increases monotonically with temperature and is higher than in Eurocode model.

EN 1993-1-2 proposes a linear coefficient of $14 \times 10^{-6}\ /°C$ and linear function of thermal elongation for steel.

$$\Delta L/_{L} = 14 \times 10^{-6}\,(T - 20)$$

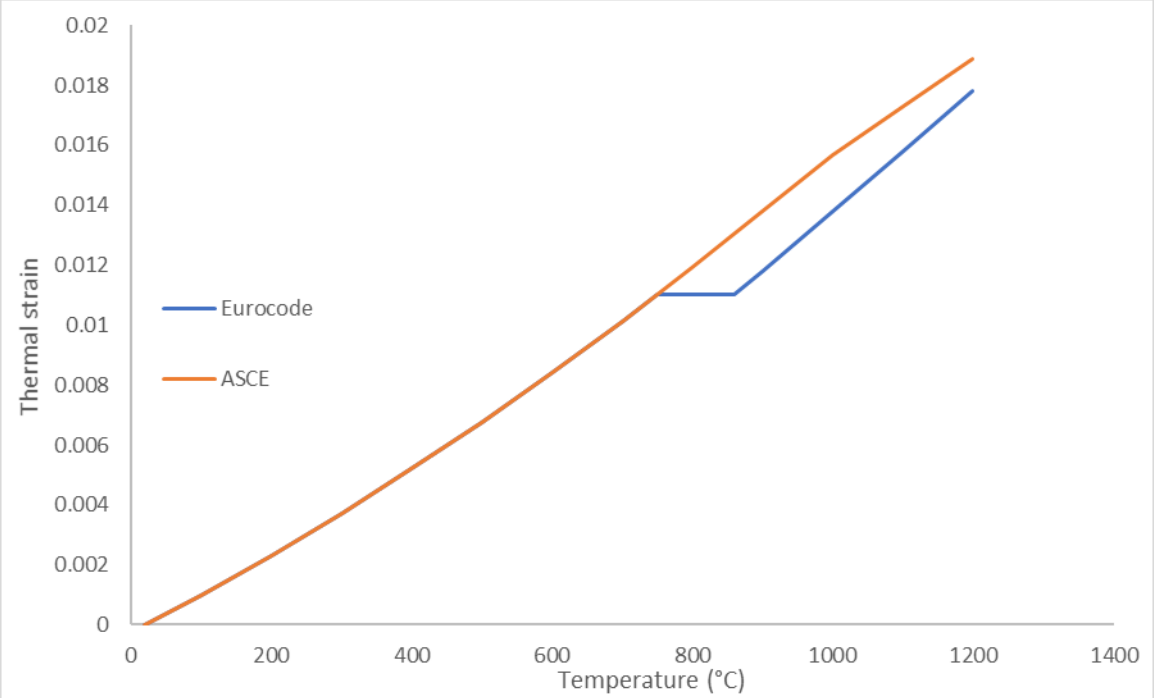

Figure 2. 23 Thermal strain of steel proposed by Eurocode and ASCE

2.4.2.2 Creep Strain

Creep is the time dependent deformation of a material that is simultaneously subjected to high temperature and high stress over time.

In ASCE, creep is specified by three periods such as the primary, secondary and tertiary. Primary phase, which is described by parabola, provides decrease creep rate. In the secondary phase, there is nearly linear increasing. Tertiary indicates a rapid increase in the creep rate because of reduction in cross section area of material. Inasmuch as fire is generally lasting a short time, only primary and secondary creep strains can be considered (Wang and Yong 2002).

At normal temperature creep is relatively unimportant for structural steel whereas it has a significant effect above 400°C for reinforcing steel. (Buchanan 2001)

On the other hand, notwithstanding being significant, the influence of creep strain is implicitly introduced in the stress-strain models of steel like Eurocodes. Kirby and Preston (1988) states that the creep strain significantly depends on stress level and temperature by conducting a series of transient creep tests.

Kirby and Preston (1988) where it can be seen that the creep is highly dependent on temperature and stress level from 25 to 350 MPa. The creep deformations accelerate rapidly where the creep strain curve becomes nearly vertical.

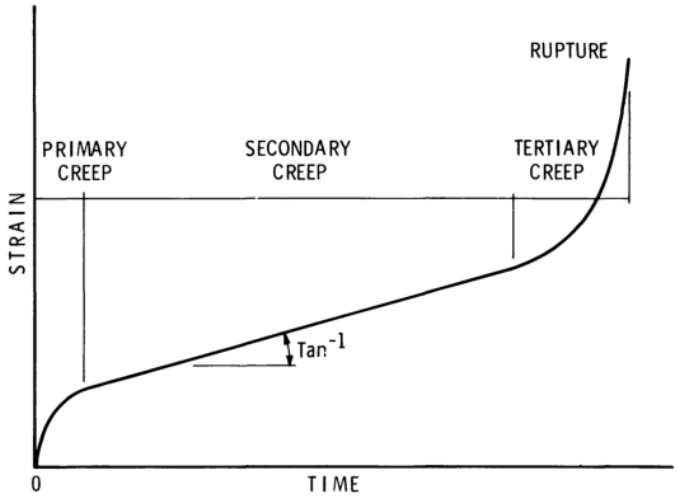

Figure 2. 24 Typical creep curve for steel from ASCE model

2.4.2.3 Stress-Related Strain

This type of strain is developed from stress in case of fire situations or under normal conditions. Stress strain relations can be obtained directly from the steady state tests or derived from the transient tests at elevated temperatures (Buchanan, 2002).

2.5 High Strength Concrete

In the beginning of 1980s, concretes with increasing compressive strengths started to become commercially available and primarily utilized in the construction of high-rise buildings. High-performance concrete (HPC) exceeds the properties and constructability of normal concrete.

High-performance concrete has been primarily used in tunnels, bridges, and tall buildings for its strength, durability, and high modulus of elasticity. High strength concretes are prepared with carefully special high-quality ingredients and optimized mixture designs; these are batched, mixed, placed, compacted and cured to highest standards. Generally, such concretes have a low water-cement ratio varies from 0.2 to 0.45. HSC considered in Eurocode has a design strength of at least 55 MPa. Size and shape of aggregates, surface textures, mineralogy, and cleaness affect the high strength concretes. The bond or adhesion between the paste and aggregate are also significant factors for the high strength concretes.

There are three different classes of high strength concrete proposed by Eurocode. Class 1 is recommended for concrete C55/67 and C60/75, Class 2 is recommended for concrete C70/85 and C80/95 and Class 3 is recommended for concrete C90/105. During exposure to high temperatures such as during fire event, the mechanical properties of both high strength and normal strength concrete (strength, elastic modulus and volumetric stability) are significantly reduced.

In this case of fire, when high strength concrete is exposed to rapid heating explosive spalling occurs in high strength concrete. The investigation of Phan and Carino (2000) states that high strength concrete has a higher strength loss than normal concrete strength from 25°C to 400°C and above 300°C the possibility of occurrence spalling is high for high strength concrete. Kodur (2003) explains the main factors that affect the fire performance of high strength concretes are concrete strength, moisture content of concrete, concrete density, intensity of load and fire, reinforcements, specimen dimension, concrete cover and type of aggregate. In research of Kodur, Cheng and Wang (2003), it is seen that the usage of addition of steel and polypropylene fibers improve the fire resistane and ductility of high strength concrete columns whereas it decreases the possibility of spalling. The study of Ali (2001) stressed that the higher tensile strength of HSC can compensate the influence of low permeability

Advantage of high strength concrete use is reduction of columns size, thus there are lighter structures with more usable space. The thermal properties given for normal strength concrete may be used for high strength concrete. High strength concrete has one or more of the following properties: low shrinkage, low permeability, a high modulus of elasticity, or high strength.

2.6 Spalling of Concrete Due to Fire

Spalling is a physical process of the breakdown of surafce layers of concrete which crumble into small pieces under high temperatures and/or mechanical pressure. Concrete thermal instability is observed when a concrete structure is totally, or partially, exposed to an accidental fire. It is generally accepted that spalling takes place when water vapour is expelled from the cement paste during heating because pore water pressures exceed the the tensile strength of the concrete.

Concrete spalling has an influence on the fire resistance of reinforced concrete structures, because of a loss of resistant cross-section and a loss of thermal protection of the reinforcing steel bars. Concrete cover which protects reinforcement will be removed due to explosive spalling and thus steel bars will be subjected to fire. This weakens reinforcement bars and led to decrease ultimate load carrying capacity of the reinforced concrete element.

The main factors affecting the explosive spalling of concrete structural elements exposed to fire are heating rate, shape and size of the reinforced concrete element section, age, permeability and moisture content of reinforced concrete, type of aggregate, type of concrete strength, concrete cover distance to reinforcement, applied compressive stress and restrains. The permeability affects the spalling behavior. That is why the tendency of high strength concrete (HSC), which possess low permeability to explosive spalling is higher than the tendency of normal strength concrete.

There is great possibility of explosive spalling occurrence in high strength concrete. The experimental results from Aldea (1997) indicated that early spalling occurs at the corners in high strength concrete with compressive strength of 90 Mpa. The circular cross section shape does not prevent the occurence of spalling (Franssen and Dotreppe, 2003). Ali (2007) states that increasing in load level does not increase the possibility of explosive spalling and under high heating rate high strength conrete with compressive strengh grater than 90 Mpa does not have a good response to fire.

2.7 Previous Studies on Fire Resistance of RC Column

2.7.1 Analytical Study by Lie and Irwin (1990)

Lie and Irwin (1990) proposed a mathematical model to calculate the fire resistance of reinforced concrete columns with rectangular cross section examined by Lie and Woolerton (1988). The aim of study in 1988 was understanding the influence of cross section shape, reinforcement, cover thickess, load, aggregate type and load eccentricity on the fire resistance of reinforced concrete columns. It was shown that carbonate aggregate and heavy reinorcement have a positive contribution to fire resistance of reinforced concrete.

The columns were tested under concentric load until failure time and were exposed to ASTM E119 standard fire. There are two steps: calculation of temperature in column and its strength and deformationss during fire exposure. The temperatures in columns were calculated by finite element method. Traingular elements were used to mesh surface whereas for column square elements were used. Based on the results of study, fire resistance of reinfırced concrete columns could be affected by significant parameters such as load, column section size, column length, concrete strength and and reinforcement ratio and under comensurate loads rectangular columns had higher fire resistance than square columns.

2.7.2 Experimental and Analytical Study by Zhu and Lie (1993)

Fire response of seven reinforced concrete columns exposed to ISO 834 standard fire were performed by Zhu and Lie (1993). Thermal properties of siliceous and carbonate aggregaete concretes were determined to carry out the numerical studies for columns. The study indicated the comparison between experimental and numerical results for rectangular RC columns that made of materials commonly used in China under concentric and eccentric load. The temperatures at several distances along the centerline of a column and the axial deformation of columns, obtained from experiment and numerical calculations, were shown as a function of time in this study. The temperatures in columns were calculated by finite element method and load deflection analysis was used to calculate the strength of colum. There was a dramatic increasing in temperature at the centres of the columns during experiment and it was not

predicted by calculation methods. The measured and calculated axial deformation of the columns during fire exposure were presented graphically.

2.7.3 Experimental and Analytical Study by Kodur and Raut (2011)

Experimental studies and numerical model were done to evaluate the fire resistance of different types of concrete under design fire exposure by Kodur and Raut (2011) at MSU. Columns were made of three batches of concrete such as normal strength, high strength and high strength with polypropylene. The columns were of 3.35 m high, with the middle 1.7 m of the column height exposed to fire due to the dimension of furnace. The only concentric axial loads were applied on columns. For numerical procedure, time dependent moment-curvature relationships were used to determine the response of RC structural members loaded up to failure under fire load. The comparative performance of NSC, HSC, HSCP columns under different conditions is evaluated by studying the thermal response, structural response and spalling progression. Based on experiemental and numerical studies presented, it was seen that concrete permeability and load level have significant effect on spalling and fire resistance of high strength columns.

Chapter 3
Thermal Behavior Modelling

3 THERMAL BEHAVIOR MODELLING

3.1 Introduction

The thermal analysis is usually performed while the structure is exposed to fire. From this analysis, the temperature across the cross section are obtained and are stored for subsequent structural analysis.

The fire resistance of a reinforced concrete column can be numarically evaluated by modelling its mechanical response under fire condition and the mechanical properties of reinforcing steel and concrete depends on change in temperature, hence the temperature distiribution for different moments should be calculated in the cross section of the reinforced concrete column. This can be numerically predicted and it is called as thermal behavior modelling.

Inasmuch as the temperature field through the cross section is not affected by stress or strain state, the heat transfer problem is uncoupled from the mechanical problem. On the contrary the stress strain field is significantly dependent on the temperature field. In brief, the thermal analysis and the mechanical analysis are performed seperately and subsequently.

The thermal response model depends on the evaluation of heat transfer through the reinforced concrete columns considering the temperature-dependent thermal properties of its constituents.

3.2 Software Description

The thermal analyses were performed by means of SAFIR software. SAFIR is a nonlinear finite element based computer program that can analyse the structure at ambient and elevated temperature. SAFIR can perform uncoupled heat transfer and sequentially coupled thermo-mechanical analysis. 2D thermal calculation can be conducted on the cross section of a beam-column finite element. The geometry of the cross-section at study is discretized into a number of triangular or quadrilateral finite elements.

The purpose of SAFIR in thermal analysis is evaluating of temperature field that develops in a structure subjected to fire. Isothermal surfaces,each of which connects all points of the field having the same temperature, are used to represent graphically a temperature field.

Theoretical basis of the phenomena and physical laws on which SAFIR is based;

Heat transfer happens in the three different mechanisms: conduction, convection and radiation.

SAFIR premises heat exchange on Fourirer equation for conduction in solids, assuming the following main hypotheses; the materials are isotropic that means values of a property are identical in all directions, not compressible and have no mechanical dissipation, not compressible and there is no contact thermal resistane exist at the interface between adjacent materials (Franssen 2005). It is described by equation in Cartesian system of coordinates.

$$\frac{\partial}{\partial \mathrm{x}}\left(k\frac{\partial \mathrm{T}}{\partial \mathrm{x}}\right)+\frac{\partial}{\partial \mathrm{y}}\left(k\frac{\partial \mathrm{T}}{\partial \mathrm{y}}\right)+\frac{\partial}{\partial \mathrm{z}}\left(k\frac{\partial \mathrm{T}}{\partial \mathrm{z}}\right)+Q=c\rho\frac{\partial \mathrm{T}}{\partial \mathrm{t}}$$

where {x,y,z} is the vector of Cartesian coordinates [m], k is the thermal conductivity [W/Mk], T is the temperature [K], ρ is the specific mass [kg/m^3], Q is a term that accounts for internal generation of heat [W/m^3], c is the specific heat [J/kg/K], t is time [t].
Linear convection is the mechanism of heat transfer at the surface and in internal cavities.

$$\ddot{h}_c = h(T_g - T_s)$$

where $\ddot{h}_c$ is the convective heat flux between a gas and a solid [W/m^2], h is convection coefficient [W/m^{2}K], T_g is the gas temperature [K] and T_s is the temperature at the surface of the solid. The value of convection coefficient is taken as 25 W/m^{2}K and 9 W/m^{2}K for hot or cold environment, respectively.

In fire situations, radiation is extremely significant because it is the fundamental mechanism for heat transfer from hot flames to fuel surfaces, from hot smoke to building objects and from a burning building to an adjacent building. (Buchanan, 2001)

$$\ddot{h}_r = \sigma\,\varepsilon\,T_s^4$$

where $\ddot{h}_r$ is the radiative heat flux emitted by a solid [W/m²], σ is the Stefan-Boltzmann constant [5.67×10^{-8} W/mK^4], ε is the emissivity of solid [no unit] and T_s is the temperature at the surface of solid [K].

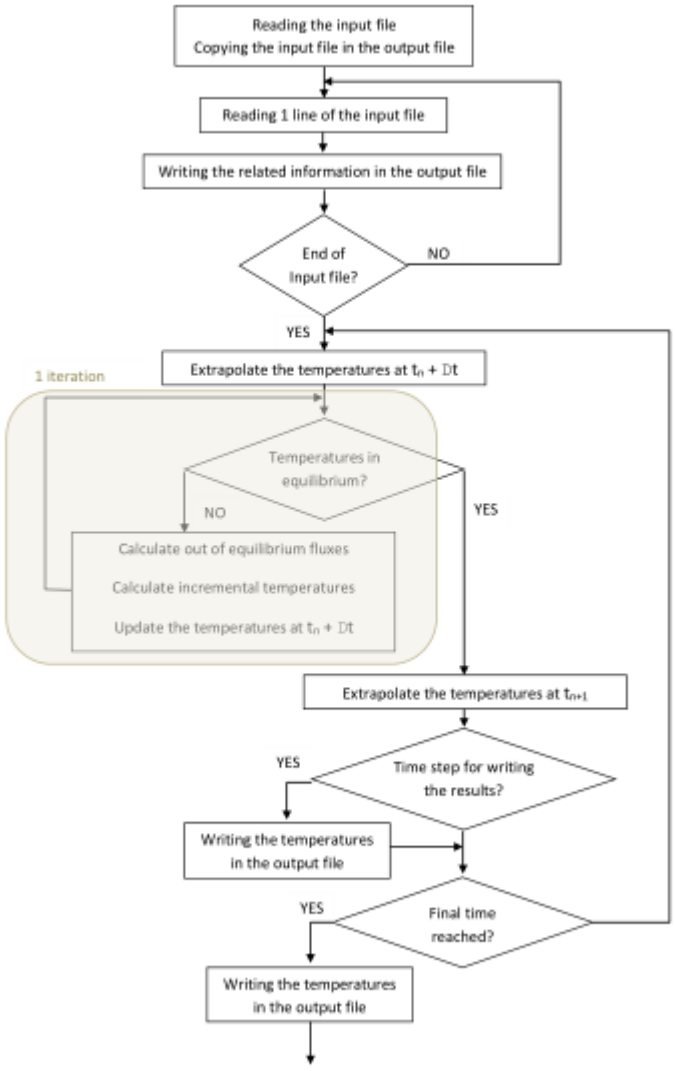

Figure 3. 1 Flow chart of thermal analysis used in SAFIR

3.3 Experimental Studies

The experimental research carried out had the main objective of studying the behavior of concrete columns with high reinforcement steel ratio subjected to fire.

3.3.1 Test Conditions

The tested columns were designed as per Eurocode specifications. For each column, there were reference cubes to specify the thermal and mechanical properties of column at the test day. The fire resistance tests were carried out with the column test furnace according to Eurocode specifications. There were six type K Chromel-alumel thermocouples as per ISO 834 distributed throughout the test chamber to monitor the furnace temperature during a fire test. The test furnace was designed to produce the conditions to which a member might be exposed during a fire, i.e. temperatures, structural loads and heat transfer.

The temperatures in the test specimens were measured by type K thermocouples, 0.5 mm, located in different sections in the vertical direction of the test columns but the results measured by thermocouples installed at mid-height in the columns were used to compare with calculated temperatures in SAFIR.

3.3.2 Test Specimens

The test specimens were picked from experiments conducted in MFPA Leipzig GmbH and TU Braunschweig. The experimental study consisted of conducting fire resistance tests on twenty reinforced concrete columns, namely PC from 1 to 22 (excluding 13 and 15). Each of the columns had different height and four different types of cross sections (square, rectangular, oval and round). Some of test specimens had an internal hole inside the cross section.

Table 3. 1 indicates the values for density and moisture content of columns that measured at the test date. The moisture content of tested concrete ranges from 2.84 to 3.91. For density of columns, there is a smal interval between 2340 kg/m³ and 2440 kg/m³.

Columns	Moisture Content (%)	Density (kg/m³)	Columns	Moisture Content (%)	Density (kg/m³)
PC1	3	2340	PC11	3	2410
PC2	3	2450	PC12	3.05	2340
PC3	3	2400	PC14	3.47	2370
PC4	3	2400	PC16	2.85	2360
PC5	3	2400	PC17	3.44	2420
PC6	3	2400	PC18	3.37	2440
PC7	3	2400	PC19	3.49	2420
PC8	2.84	2410	PC20	3.16	2390
PC9	3.91	2370	PC21	3.37	2400
PC10	3.47	2350	PC22	3.23	2400

Table 3. 1 Density and moisture content of columns at test date

The following tables indicated characteristics of the test columns are separated according to the type of cross sections. The characteristics that shown in tables are dimensions of cross sections, diameter of hole (if any), cover distance between the surface of lateral reinforcement to the outer surface column and, number and dimension of longitudinal and lateral reinforcements.

Columns	Dimensions (mm)	Hole Diameter (mm)	Cover Distance (mm)	Longitudinal Reinforcement (mm)	Stirrups (mm)
PC4	500×300	140	30	8Φ30	Φ8
PC6	300×300	120	30	8Φ34	Φ8
PC8	Φ300	100	30	8Φ34	Φ7

Table 3. 2 Characteristics of the test columns with internal hole

Columns	Dimensions (mm)	Cover Distance (mm)	Longitudinal Reinforcement (mm)	Stirrups (mm)
PC5	150×150	20	8Φ16	Φ8
PC9	250×250	30	8Φ30	Φ8
PC12	250×250	30	8Φ30	Φ8
PC16	250×250	30	8Φ30	Φ10
PC17	250×250	30	12Φ34	Φ6
PC20	250×250	30	8Φ20	Φ6

Table 3. 3 Characteristics of the square test columns

Columns	Dimensions (mm)	Cover Distance (mm)	Longitudinal Reinforcement (mm)	Stirrups (mm)
PC2	500×250	30	14Φ40	Φ8
PC10	500×245	30	8Φ40	Φ10
PC18	450×250	30	18Φ40	Φ6

Table 3. 4 Characteristics of the oval test columns

Columns	Dimensions (mm)	Cover Distance (mm)	Longitudinal Reinforcement (mm)	Stirrups (mm)
PC1	Φ246	30	14Φ40	Φ7
PC11	Φ300	20	15Φ40	Φ8
PC21	Φ150	20	18Φ14	Φ6
PC22	Φ250	40	5Φ40	Φ6

Table 3. 5 Characteristics of the round test columns

Columns	Dimensions (mm)	Cover Distance (mm)	Longitudinal Reinforcement (mm)	Stirrups (mm)
PC3	300×250	20	10Φ40	Φ8
PC7	300×200	30	10Φ30	Φ8
PC13	300×250	20	10Φ40	Φ8
PC14	450×140	25	12Φ26	Φ10
PC19	450×250	30	18Φ40	Φ6

Table 3. 6 Characteristics of the rectangular test columns

From figure 3. 2 to figure 3. 13, the shape of cross sections and the location of thermal couples are demonstrated. The thermal couples are located on the surface of reinforcements. In the captions, “a” represents cross section on the left side whereas “b” represents cross section on the right side.

Figure 3. 2 Reinforced concrete column sections considered: a) PC1, b) PC3

Figure 3. 3 Reinforced concrete column sections considered: a) PC2, b) PC4

Figure 3. 4 Reinforced concrete column sections considered: a) PC5, b) PC6

Figure 3. 5 Reinforced concrete column sections considered: a) PC7, b) PC8

Figure 3. 6 Reinforced concrete column sections considered: a) PC9, b) PC10

Figure 3. 7 Reinforced concrete column sections considered: a) PC11, b) PC12

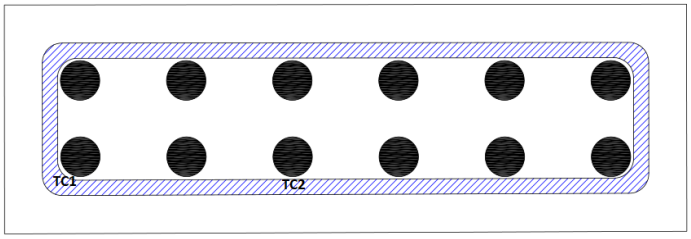

Figure 3. 8 Reinforced concrete column sections considered: PC14

Figure 3. 9 Reinforced concrete column sections considered: a) PC16, b) PC17

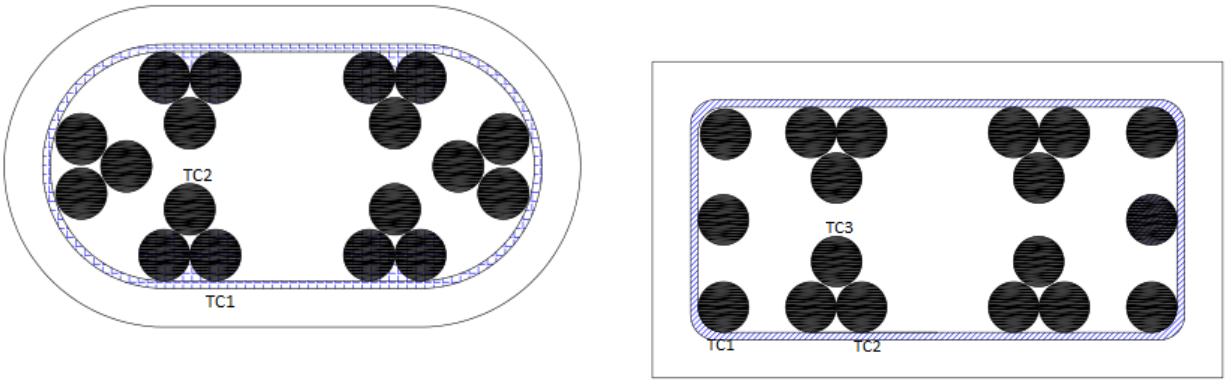

Figure 3. 10 Reinforced concrete column sections considered: a) PC18, b) PC19

Figure 3. 11 Reinforced concrete column sections considered: a) PC20, b) PC21

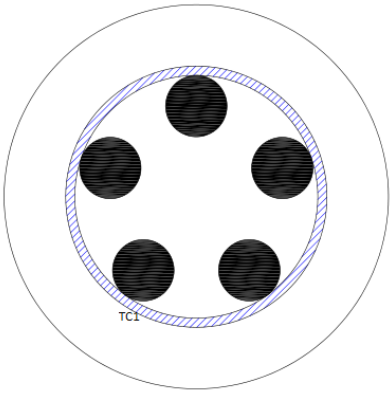

Figure 3. 12 Reinforced concrete column sections considered: PC22

3.4 Numerical Studies

The numerical simulations were conducted by means of SAFIR which is based on a nonlinear finite element method. The thermal analysis was made by using 2D numerical models and was performed for the cross section of each tested column. The effect of concrete spalling cannot be modelled in the analysis, nor can shear behavior. Therefore, the lateral reinforcements in columns were not modelled to calculate the temperature distribution.

3.4.1 Cross Section Discretization

As the software SAFIR is a software based on finite element method, therefore, the modelled cross sections were discretized into finite elements. The triangle elements were used to discretize the cross sections. In figure 3. 13 there is an example to exhibit the discretization of different types of cross sections. The accuracy of the analysis can be affected by number of nodes and the

size of elements. Due to the different shapes of cross sections, there was not a certain number of number of nodes but approximately nine hundred nodes were used for meshes.

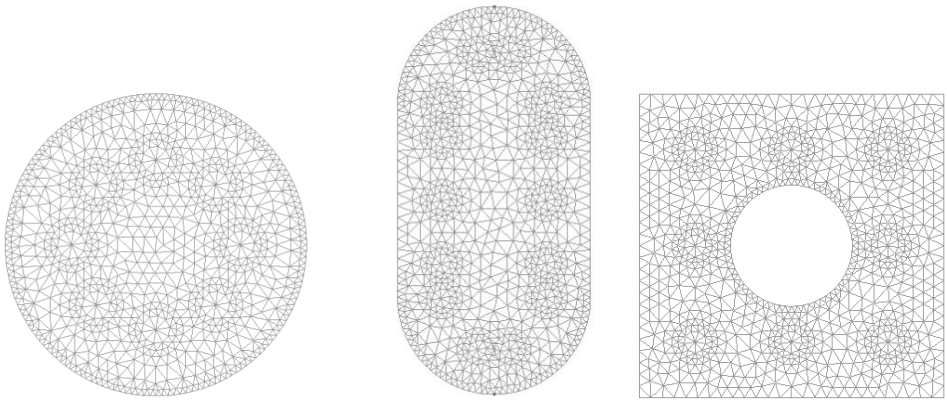

Figure 3. 13 Meshes of modelled RC columns cross sections

3.4.2 Boundary Conditions

Heat transfer includes three main processes: conduction, convection and radiation. There are three parameters needed to calculate the heat transfer in SAFIR. These are the emissivity factor and the convection coefficient for heated and unheated surfaces.

According to Eurocode models for both concrete and reinforcing steel, the emissivity factor and the convection coefficient of hot and cold environment were taken as 25 W/m²K, 9 W/m²K and 0.7, respectively.

3.4.3 Thermal Properties of Materials

All the thermal properties used in this analysis follow the recommendations of the EN 1992 and EN 1993 except from thermal conductivity of concrete.

3.4.3.1 Thermal Conductivity

The graph of thermal conductivity-temperature for concrete that used in thermal analysis is shown in figure 3. 14. The thermal conductivity of concrete follows the same trend with upper limit in Eurocode model till 115°C and then it follows the lower limit and is taken from National Anneces of France.

For reinforcing steel, the values of thermal conductivity were obtained directly from EN 1992-1-2.

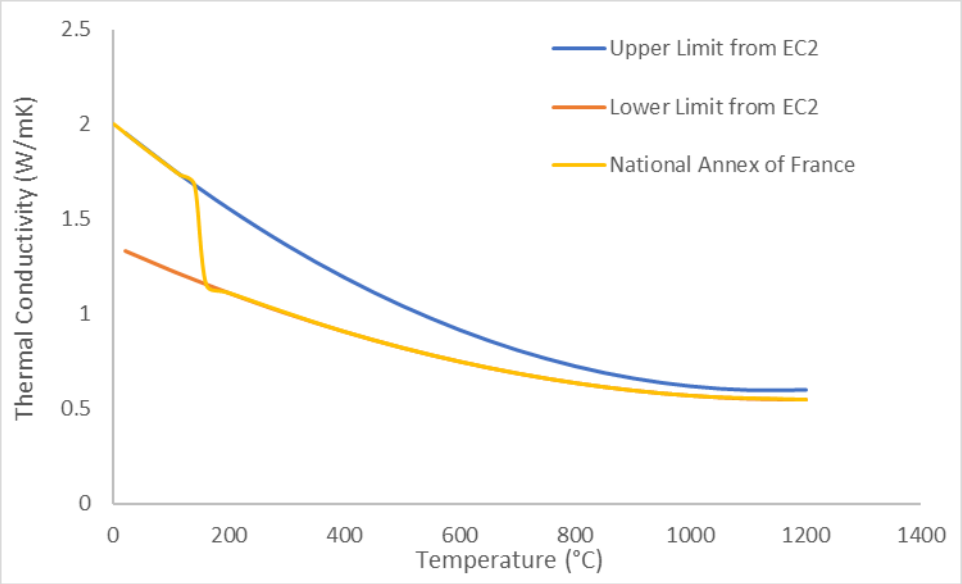

Figure 3. 14 Thermal conductivity of concrete

3.4.3.2 Specific Heat

Due to the moisture content of the tested column in experiments, the peak value of specific heat for moisture content 3% of concrete weight was used in thermal analysis.

For the reinforcing steel, the specific heat is based on EN 1992-1-2.

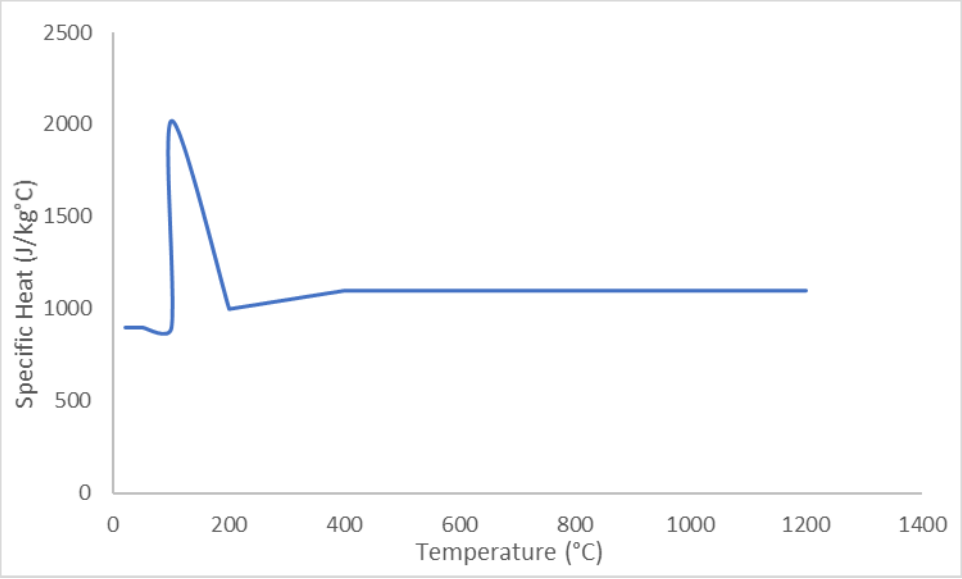

Figure 3. 15 Specific heat of the modelled concrete

3.4.3.3 Density

The density of concrete has different value for each column. The rate of decrease of density for concrete is taken from Eurocode model and steel has a constant density over temperature.

3.5 Results and Discussions

The crosssectional area of the column is subdivided into a number of elements, arranged in a triangular network. The evoluation of temperature on the surface of thermocouples for each cross section of column obtained in the experiment and numerical simulation will be shown in Appendix B. Thermocouples used in experiment for columns were approximately located on the surface of the longitudinal reinforcements. The positions of thermocuples were shown before. There are differences between experiment and numerical simulation due to the spalling phenomenon in the thermal analysis because the concrete cracking and spalling can not be considered in SAFIR. The evoluation of temperature in the cross sections could be affected by size and shape of sections, cover distance to rebars, density and moisture content of concrete and fire duration.

For some columns, there are differences between calculated and measured temperatures on the thermocouples. The measured temperatures are higher than the calculated temperatures especially for columns PC4, PC9, PC14, PC16, PC18, PC21 and PC22. On the other hand, there is an opposite situation for columns PC1, PC2, PC10 and PC20. The reason of differences between test data and numerical results can be the breaking of concrete cover due to spalling because SAFIR does not account for fire induced spalling. The largest amount of difference between measured and calculated temperatures is approximately 50°C when the maximum calculated temperature is around 600°C during the failure time, thus this is a pretty admissible result to validate the tested data.

It is observed that all time-temperature curves generally have similar trend of increase. It can be seen that there is good agreement between calculated and measured temperatures. This indicates that the material model during the thermal analysis performs well. Therefore, it can be said that the thermal properties of normal strength concrete proposed by Eurocode are also proper to

evaluate the temperature of high strength concretes. Then, the used thermal conductivity curve for concrete has a positive effect on evaluating the temperature.

Chapter 4
Structural Behavior Modelling

4 Structural Behavior Modelling

4.1 Introduction

The structural analysis of the reinforced concrete column is conducted based on the thermal analysis results of the heated columns, incorporating the applied loads on the structure. The structural analysis calculates the mechanical response, including the thermal strains, deflections and forces of the structural elements based on the outputs of the thermal analyses. As a result of the elevated temperatures, the reduction of strength and elastic modulus, and thermal expansion are considered.

A column is a structural element, which primarily carries axial loads. If loaded column has a horizontal deflection, it can cause an extra bending moment. This is also called as second order effects and increases under fire load. Internal forces and moments related to fire on columns are usually varied during a fire scenario.

SAFIR software was used to implement the thermo-mechanical analysis for the reinforced concrete columns exposed to fire.

4.2 Software Description

As stated in SAFIR (2016), the mechanical behavior of concrete and reinforcing steel at elevated temperatures can be represented by using the predefined uniaxial material models embedded in the code. For both steel and concrete materials, the models are based on Eurocode model. According to user preference transient strain can be considered implicitly and explicitly. Transient creep is included implicitly in the Eurocode 2 uniaxial concrete material model.

The temperature history of the structure evaluated in thermal analysis was used for the determination of mechanical behavior of structures exposed to fire. The temperature increase induces the loss of strength and stiffness, and thermal elongation in materials which affect the structural behavior.

The methodology of SAFIR for the mechanical analysis is based on a step by step procedure. The mechanical analysis of structures suffered from large displacements is based on the incremental form of principal of virtual work. SAFIR gives the displacement at each node of structure, internal forces and bending moment at integration points in each finite element and strains, stresses and tangent modulus in each mesh at integration points of each finite element as output until structure fails. The structure can be discretized by four different elements; truss, beam, shell and solid elements.

The beam finite element uses a constant section along the longitudinal axis that is a straight line extending between two end nodes. In this element, only longitudinal reinforcement can be modelled because the stress can only be longitudinal along beam or column axis. The derivation of the strains is based on Bernoulli hypothesis, therefore in bending plane sections remain plane. The fiber model is used to integrate the longitudinal stresses and stiffness on the cross section. In this model, the discretization in thermal analysis is used the same. The integrations along the longitudinal axis are performed by a numerical integration of Gauss. (Franssen, 2003)

4.3 Experimental Studies

The experimental tests program of realistic fire exposure tests on twenty reinforced concrete columns, made of high strength concrete. The tested columns had the different geometry, reinforcement ratio and concrete strength. The tests were carried out by exposing the columns to heat in a furnace specially built for testing loaded columns. The columns, with fixed ends, were installed in the furnace by bolting their end plates to the loading head at the top.

4.3.1 Test Conditions

The test specimens were longitudinally loaded with an eccentricity of 7 mm at the top of the columns. In order to apply an eccentric load, each column had brackets at the ends, consisting of a horizontal steel plates overhang with 40x600x600 mm and 30x600x600 mm. The test furnace was designed to produce the conditions to which a member might be exposed during a fire, i.e. temperatures, structural loads and heat transfer. The load was maintained constant throughout the fire test duration. The axial deformation of the test specimen is determined by measuring the displacement of the jack that support columns.

4.3.2 Test Specimens

The average compressive cylinder strength of the concrete measured on the day of testing with concrete classes and applied loads are given in Table 4.1. The test day compressive cylinder strength varies from 64 MPa to 95 MPa. The steel of main longitudinal reinforcement and stirrups had a specified yield strength of 500 MPa.

COLUMNS	Length (mm)	Concrete Strength (Mpa)	Concrete Class	Applied Load (kN)
PC1	3740	75	2	1548
PC2	3740	86	2	3000
PC3	3740	85	2	2500
PC4	3740	88	2	3000
PC5	3740	68	1	225
PC6	3740	88	2	3000
PC7	3740	58	1	1140
PC8	3620	95	3	2230
PC9	3620	88.5	2	1230
PC10	3620	81	2	2955
PC11	3740	86	2	3000
PC12	3620	82.2	2	1810
PC14	3600	65	1	600
PC16	3600	64	1	1500
PC17	3620	96	3	2870
PC18	3620	95	3	4675
PC19	3620	93	2	5555
PC20	3620	89	2	1190
PC21	3620	92	3	230
PC22	3620	89	2	1520

Table 4. 1 Summary of test parameters for columns

4.4 Numerical Studies

Structural analyses are conducted for the heated columns. Three-noded, two-dimensional beam finite elements are used. The time-temperature evolution in the sections is taken from the thermal analyses previously conducted. It also accounts for thermal expansion. The simulations are run up to experimental failure times of ISO fire exposure, and the time to failure of numerical

simulation is recorded as a function of the axial deformations. Axial deformations and failure times of the columns were recorded at one-minute intervals.

4.4.1 Mechanical Properties of Materials

The concrete models are defined according to EN 1992-1-2. For concrete material, parameters to be introduced are type of aggregate (siliceous or calcareous) and concrete strength (normal and high), formulation of transient creep (implicit or explicit), the Poisson's ratio, the compressive strength and the tensile strength.

The reinforcing steel models are based on EN 1992-1-2 as well. Parameters to be introduced are the modulus of elasticity, the Poisson's ratio, the yield strength, the maximum temperature beyond which irreversible behavior occurs during cooling, the decay rate of the residual yield strength if maximum temperature exceeds the threshold, ductility class (A, B and C) and fabrication process (hotrolled or cold worked).

The stress-strain relationships in the load bearing materials are non-linear and are temperature dependent.

4.4.2 Boundary Conditions

In numerical analysis, it is assumed that bottom of colums is fixed and top of columns is restrained in horizontal movement.

4.5 Results and Discussions

All columns have been simulated using SAFIR program. The calculated and tested values of the fire resistance based on the failure time and the maximum axial deformation are compared in Table 2. The comparison of axial deformations and failure times are shown graphically to see the difference between measured results and test data in Figure 4.1 and 4.2.

In numerical analysis, transient creep strain was considered implicitly and explicitly. Explicit transient creep model proposed by Franssen and Gernay and Eurocode model were used to conduct the mechanical analysis. In Table 2, it can also be seen that the comparisons of axial deformations and failure times are indicated.

A steel-concrete composite column is a compression member. To investigate the effect of reduction factors of compressive strength for different type of concrete strength on the measuring axial deformation. Firstly, compressive load capacity of columns was calculated by using the formula ($0.85f_{cd}A_c + A_s f_{yd}$) to understand the concrete contribution to the total load capacity.

The ratio varies from 40% to 80% except from PC11 because PC11 has a 30% concrete contribution which is relatively smaller than others. In Appendix B, the axial deformations of columns were calculated by four different reduction factors of concrete compressive strength: high strength concrete in three classes and normal strength concrete. The results showed that reduction factor curves for normal concrete strength can be used for high strength concrete of Class 1 and Class 2. There is no need to define different curves for Class 1 and Class 2. In case of using reduction factor curve of Class 3, the failure time and the axial deformations were lower than results from other curves.

For PC11, it is enough to use the reduction curve of normal concrete strength due to low contribution of concrete to column load capacity.

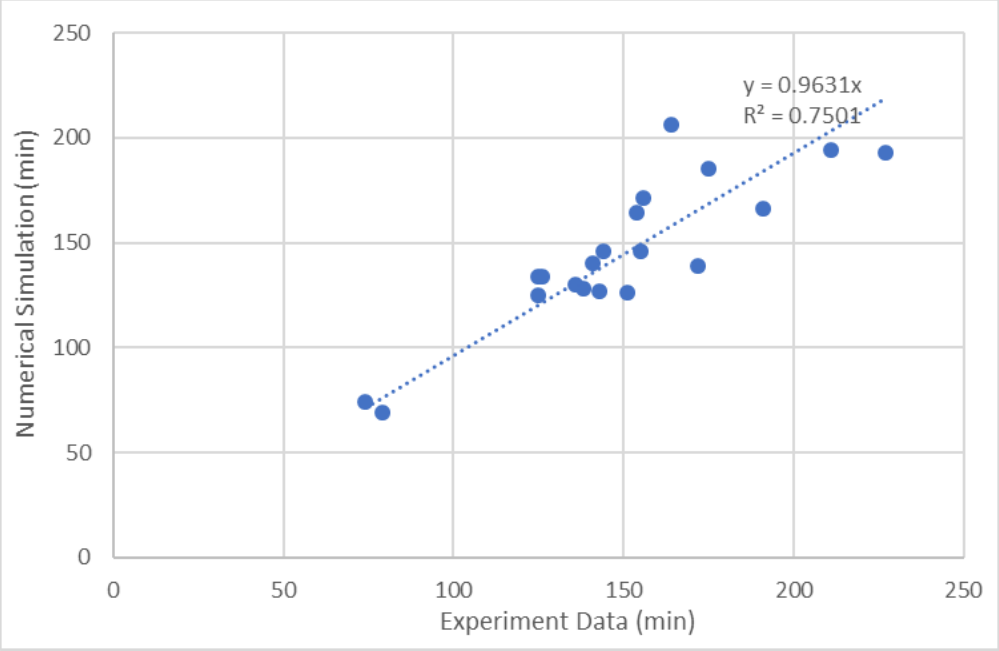

Figure 4. 1 Comparison of failure times from test data and numerical results

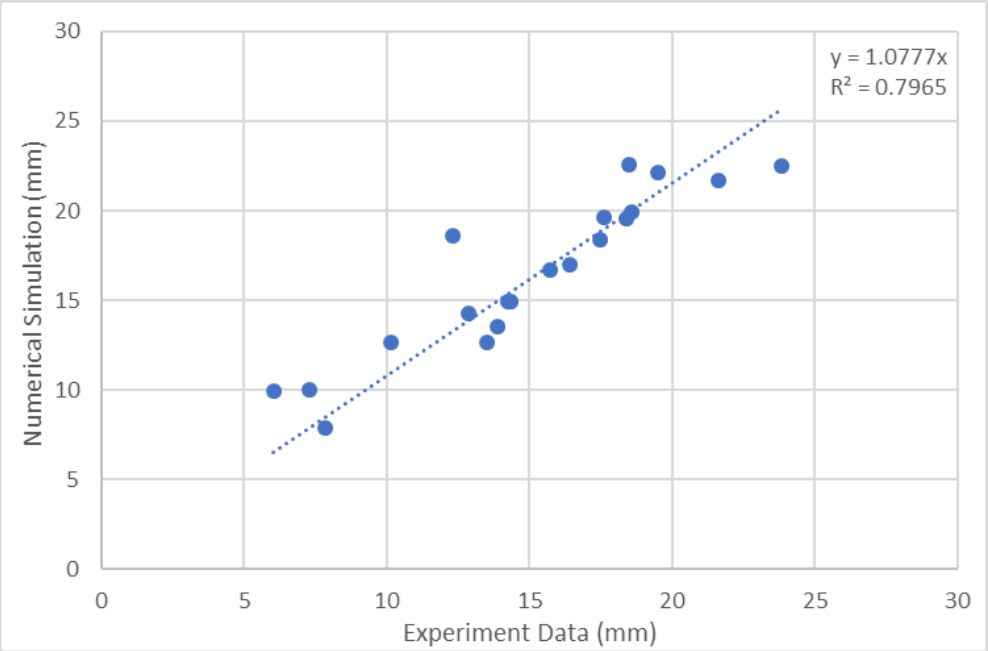

Figure 4. 2 Comparison of axial deformations from test data and numerical results

Figure 4.3, 4.4 and 4.5 shows a representative view of the columns following the fire tests. All the tested specimens were observed to fail by buckling. Explosive spalling on the column surface was observed in any of the specimens. Damage was observed to be concentrated around the little bit upper part of the midpoint of each column, and several distinct longitudinal surface cracks were observed. In numerical simulation, columns had a similar deformed shape as shown in Figure 4.6.

Figure 4. 3 Deformation shapes of tested columns namely PC 1 to 8 from left to right

Figure 4. 4 Deformation shapes of tested columns namely PC 9 to 16 from left to right

Figure 4. 5 Deformation shapes of tested columns namely PC 17 to 22 from left to right

.

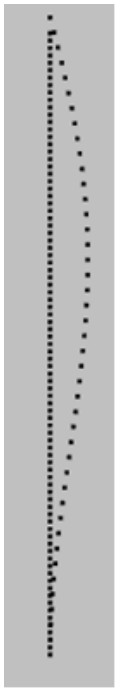

Figure 4. 6 Deformation shape of column from numerical analysis

Columns	Failure Time (min)			Maximum Axial Displacement (mm)		
	Experimental	Numerical		Experimental	Numerical	
		EC	ETC		EC	ETC
PC1	136	127	130	18.4	20.63	19.53
PC2	227	183	193	18.6	20.3	19.9
PC3	144	138	146	17.62	20.3	19.6
PC4	164	194	206	6.03	10.97	9.95
PC5	74	72	74	19.5	22.85	22.15
PC6	125	121	125	7.82	9.06	7.86
PC7	138	128	128	17.5	19.35	18.35
PC8	125	130	134	13.9	14.67	13.56
PC9	156	164	171	12.3	19.9	18.6
PC10	211	184	194	12.86	15.5	14.3
PC11	154	161	164	18.5	23.41	22.55
PC12	126	127	134	10.13	13.98	12.67
PC14	151	124	126	23.85	22.92	22.521
PC16	155	139	146	14.26	16.05	14.95
PC17	143	124	127	14.32	15.84	14.95
PC18	175	181	185	16.4	17.442	17
PC19	191	162	166	13.52	13.42	12.66
PC20	172	126	139	7.3	11.58	10
PC21	79	67	69	21.65	21.8	21.7
PC22	141	138	140	15.72	18.12	16.67

Table 4. 2 The calculated and tested values of fire resistance

In Table 4.2, there are the axial deformations and failure times measured and calculated by explicit and implicit transient creep models. Generally, the maximum axial deformations obtained by explicit model is lower than results from implicit models.

Chapter 5
Concluding Remarks

5 Concluding Remarks

5.1 Genaral

The main goal of this thesis was to predict the behavior of heavily-reinforced high strength concrete columns exposed to fire in terms of temperature, failure time and axial deformation, by performing numerical analysis with the nonlinear software SAFIR developed at the University of Liege. To this end, the experimental results of twenty different columns were used to compare results with numerical simulation. The numerical simulations were performed by using two different transient creep strain models (explicit and implicit) to make comparisons.

Another focus of thesis was to understand the role played by concrete in these columns. The reduction factor for concrete compressive strength during fire is the most important property to calculate the axial deformation and failure time. The possibility of using the normal siliceous concrete strength instead of the three different classes of high strength concretes (as devised in EN 1992-1-2) was also investigated.

5.2 Conclusions

Based on the fire tests and numerical studies presented in this thesis, the following conclusions can be drawn on the behavior of heavily-reinforced high strength concrete columns under ISO 834 standard fire.

The thermal part is well predicted, while the evolution of temperature is significant for the mechanical part. Therefore, the defined thermal conductivity curve and the thermal properties of normal strength concrete can be used to evaluate the temperature distribution in high strength concretes.

In this thesis, the traditional approach adopted for reinforced concrete columns was used to predict the fire response of heavily-reinforced concrete columns and there was a good agreement between test data and numerical results.

The comparison of concrete models that include transient creep strain explicitly and implicitly demonstrates that Eurocode model which considers implicit transient strain gives the lower failure time for tested columns than the explicit transient creep model proposed by Gernay and Franssen (2010) implemented in SAFIR. The maximum axial deformation till failure time measured by Eurocode model is slightly larger than measured by explicit transient creep model. On the whole, however, there is no major difference between explicit and implicit transient creep strain for the investigated columns, as should be expected, since the cooling phase was absent.

The numerical results from the mechanical analysis state that the only one curve, reduction factor of normal–strength siliceous concrete, can be used for high strength concrete of Class 1 and Class 2. When high strength concrete of Class 3 is used, there is a small difference between results obtained from class 3 and normal siliceous concrete. Summing up, the normal siliceous concrete decay can be used instead of the decay classes of high strength concrete, with minor loss of accuracy in two out of three classes.

References

1. **Aldea, C.M., Franssen, J.M. and Dotrppe, J.C. (1997),** "Fire test on normal and high strength reinforced concrete columns", National Institute of Science and Technology – Special Publication, No. 919, Gaithersburg, Maryland, USA

2. **Ali, F.A., O'Connor, D. and Abu-Tair, A (2001)**., "Explosive spalling of high strength concrete columns in fire", Magazine of Concrete Research, V. 53, No. 3, pp. 197-204.

3. **Anderberg Y, Thelandersson S., (1976),** "Stress and deformation characteristics of concrete at high temperatures: 2 experimental investigation and material behaviour model". Bulletin 54. Lund Institute of Technology, Sweden

4. **Anderberg, Y. (1988);** Modelling Steel Behaviour. Fire Safety Journal, 13; p.17-26

5. **ASCE Manual of Practice No. 78 (1992),** Structural Fire Protection, ASCE Committee on Fire Protection, Structural Division, American Society of Civil Engineers, NY, USA

6. **Bazant, Z.P., (2001).** "Creep of Concrete." Complete version of an article whose slightly abbreviated version was printed in Encyclopedia of Materials: Science and Technology, K.H.J. Buschow et al., eds. Elsevier, Amsterdam, Vol. 2C, 1797– 1800

7. **Buchanan A.H., (2001),** Structural design for fire safety, John Wiley and Sons, Chichester, West Sussex (England)

8. **Cruz, C.R. (1968).** "Apparatus for measuring creep of concrete at high temperatures.", PCA Research Department Bulletin 225, Skokie, IL.

9. **Elghazouli A.Y., Cashell K.A. and Izzuddin B.A., (2009),** "Experimental Evaluation of the Mechanical Properties of Steel Reinforcement at Elevated Temperature", Fire Safety Journal, 44, pp.909-919

10. **Eurocode 2 (2004),** EN 1992-1-2: Design of Structures. Part 1-2: General Rules-Structural Fire Design, European Committee for Standardization, Brussels, Belgium

11. **Eurocode 4 (2005),** EN 1994-1-2: Design of Composite Steel and Concrete Structures. Part 1-2: General Rules-Structural Fire Design, European Committee for Standardization, Brussels, Belgium

12. **Franssen, J.M. and Dotreppe, J.C. (2003)**, "Fire tests and calculation methods for circular concrete columns", Fire Technology, V. 39, pp. 89–97.

13. **Franssen, J.M. (2005),** "SAFIR: A thermal-structural program for modelling structures under fire", Engineering Journal, 143–158.

14. **Gernay T. and Franssen J.M (2010),"** Consideration of Transient Creep in the Eurocode Constitutive Model for Concrete in the Fire situation"

15. **Gernay T. and Franssen J.M. (2011),** "A Comparison Between Explicit and Implicit Modelling of Transient Creep Strain in Concrete Uniaxial Constitutive Relationship"

16. **Gernay T. And Franssen J.M (2012),** "A formulation of the Eurocode 2 concrete model at elevated temperature that includes an explicit term for transient creep"

17. **Franssen, J.M., Gernay, T. (2017),** "Modeling structures in fire with SAFIR: Theoretical background and capabilities", Journal of Structural Fire Engineering, 8(3).

18. **John A. Purkiss, (1996),** "Fire Safety Engineering Design of Structures, Department of Civil Engineering", Aston University

19. **M.K. Kassir, K.K. Bandyopadhyay and M. Reich (1996**), "Thermal degradation of concrete in the temperature range from ambient to 315°C (600°F)"

20. **Khoury G, Grainger B, Sullivan P (1985),** "Transient thermal strain of concrete: literature review, conditions within specimen and behaviour of individual constituents". Mag Concrete Res 132:131–144

21. **Kirby B.R. and Preston R.R., (1988),** "High Temperature Properties of Hot-Rolled Structural Steel for Use in Fire Engineering Design Studies", Fire Safety Journal, 13, pp. 27-37

22. **Khoury, G.A. (2000)**, "Effect of fire on concrete and concrete Structures", Progress in Structural Engineering and Materials, vol. 2, no. 4, pp. 429-447.

23. **Kodur V., (2014),** "Properties of Concrete at Elevated Temperatures", Department of Civil and Environmental Engineering, Michigan State University, East Lansing (USA)

24. **Kodur, V.K.R., (2003),** "Fire resistance design guidelines for high strength concrete columns", National Research Council, Canada, Internal Report No. 46116, pp. 1-11

25. **Kodur, V.K.R., Cheng, F.P. and Wang, T.C. (2003)**, "Effect of Strength and Fiber Reinforcement on the Fire Resistance of High Strength Concrete Columns," ASCE Journal of Structural Engineering, Vol. 129, No. 2, pp. 253–259

26. **Kowalski R., (2010),** "Mechanical Properties of Concrete Subjected to High Temperature", Architecture Civil Engineering Environment, Silesian University of Technology, pp.61-70

27. **Lie, T.T. and Woolerton, J.L., (1988).** "Fire Resistance of Reinforced Concrete Columns: Test Results, National Research Council of Canada, Institute for Research in Construction, Internal Report No. 569, Ottawa, Ontario"

28. **Lie, T.T. and Irwin, R.J. (1990),** Evaluation of the Fire Resistance of Reinforced Concrete Columns with Rectangular Cross-Section, IRC Internal Report No. 601, Institute for Research in Construction, National Research Council of Canada, Ottawa

29. **N. K. Raut and V. K. R. Kodur, (2011),** "Response of High-Strength Concrete Columns under Design Fire Exposure", Journal of Structural Engineering

30. **Naus D.J., (2005),** The Effect of Elevated Temperature on Concrete Materials and Structures- A Literature Review, NRC Fin No. Y6741, U.S. Nuclear Commission, Oak Ridge, TN, USA

31. **P.K. Mehta and P.J.M. Monteiro, (2006),** "Concrete: Microstructure, Properties, and Materials, McGraw-Hill, New York, NY, USA

32. **Phan, L.T., Nicholas J. Carino, (2000),** "Fire Performance of High Strength Concrete: Research Needs", National Institute of Standards and Technology Internal, Gaithersburg, Maryland, USA,

33. **Sadaoui, A. and A. Khennane, (2009),** "Effect of transient creep on the behaviour of reinforced concrete columns in fire". Engineering Structures, In Press, Corrected Proof.

34. **SAFIR, (2016),** User Manual of Thermal Analysis

35. **SAFIR, (2016),** User Manual of Mechanical Analysis

36. **SAFIR, (2016),** User Manual of Material Properties

37. **Schneider U., (1985),** Properties of Materials at High Temperatures: Concrete, Department of Civil Engineering, University of Kassel, Kassel (Germany)

38. **Schneider U., (1988)**, "Concrete at high temperatures- A general review", Fire Safety Journal, 13 (1), pp. 55-68.

39. **Terro M, (1998),** "Numerical modelling of the behaviour of concrete structures in fire". ACI Struct J 95:183–193

40. **Youssef, M.A & Moftah, M., (2007),** "General stress-strain relationship for concrete at elevated temperatures", Engineering Structures, vol. 29, no. 10, pp. 2618-2634

41. **Zhu, H. L.; Lie, T. T., (1993),** "Fire Resistance Evaluation of Reinforced Concrete Columns", IRC Internal Report No. 639, Institute for Research in Construction, National Research Council of Canada, Ottawa

Appendices

Appendix A

PC1

a) **b)**

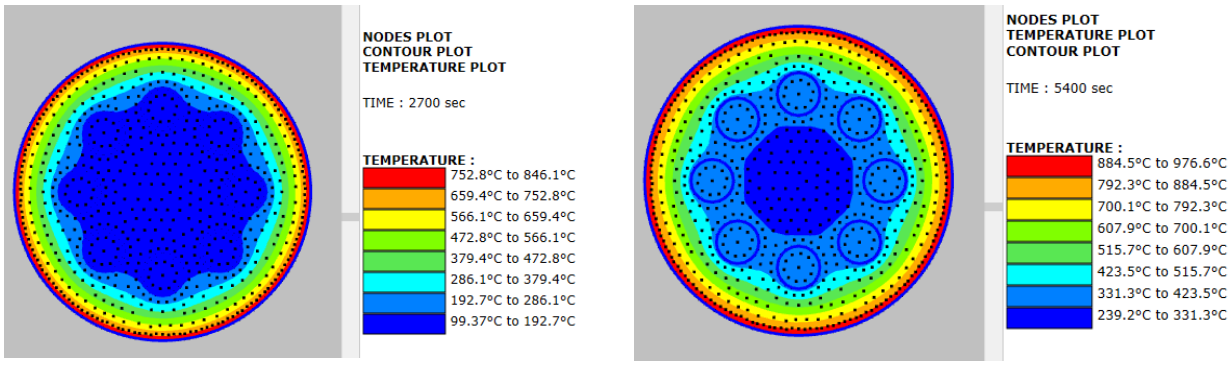

c)

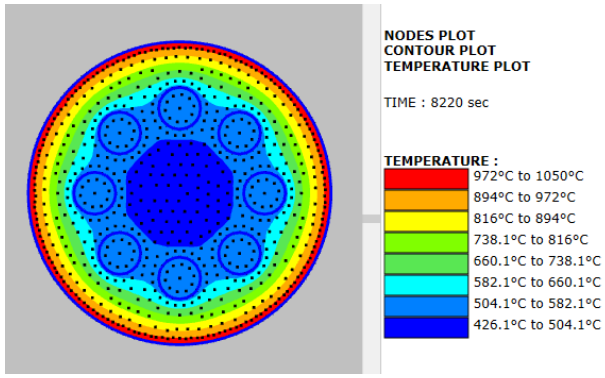

Figure B. 1 Temperature map for PC1 at a) 45 min b) 90 min and c) failure time

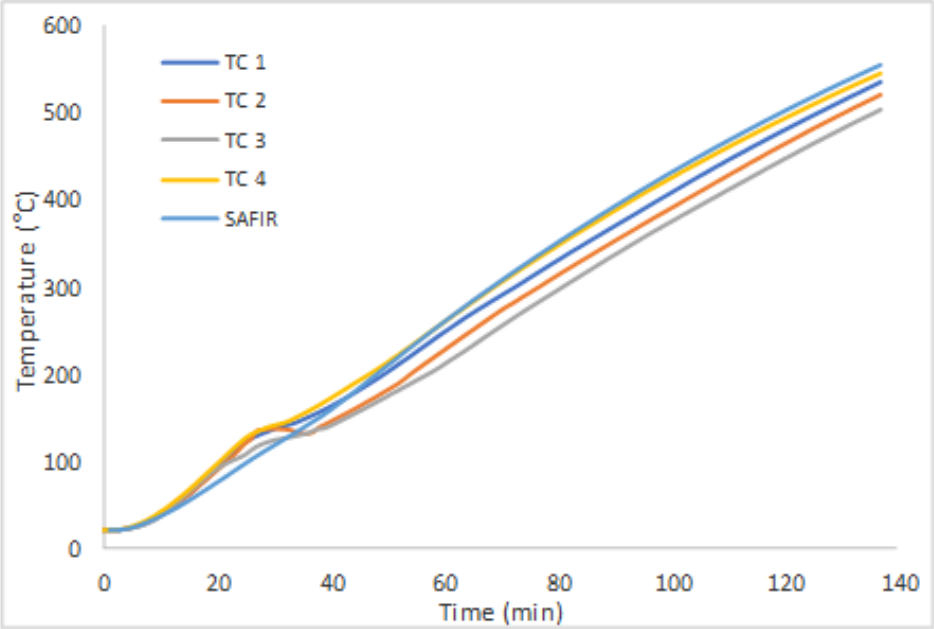

Figure B. 2 The calculated and measured temperature in thermocouples

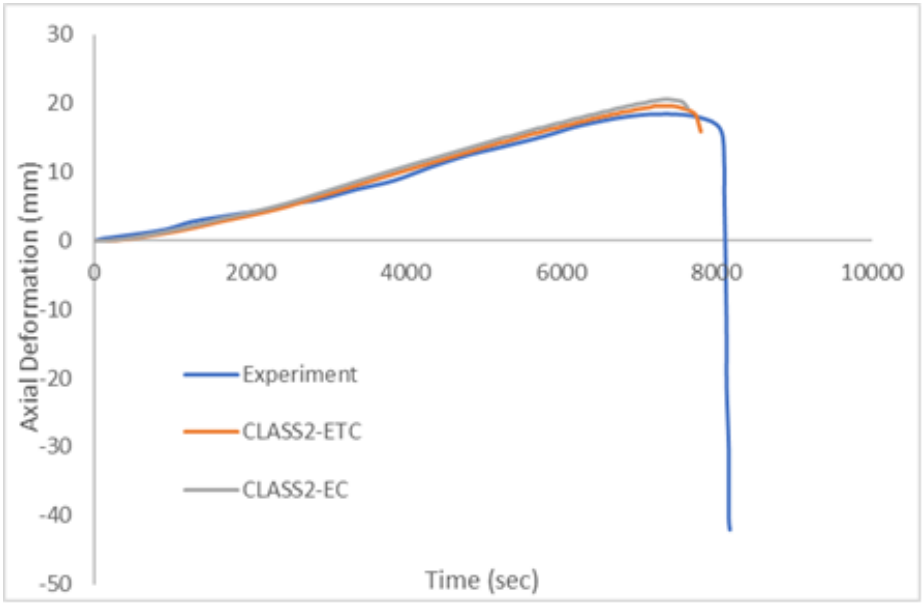

Figure B. 3 Comparison of calculated axial deformations with measured axial deformations for PC1

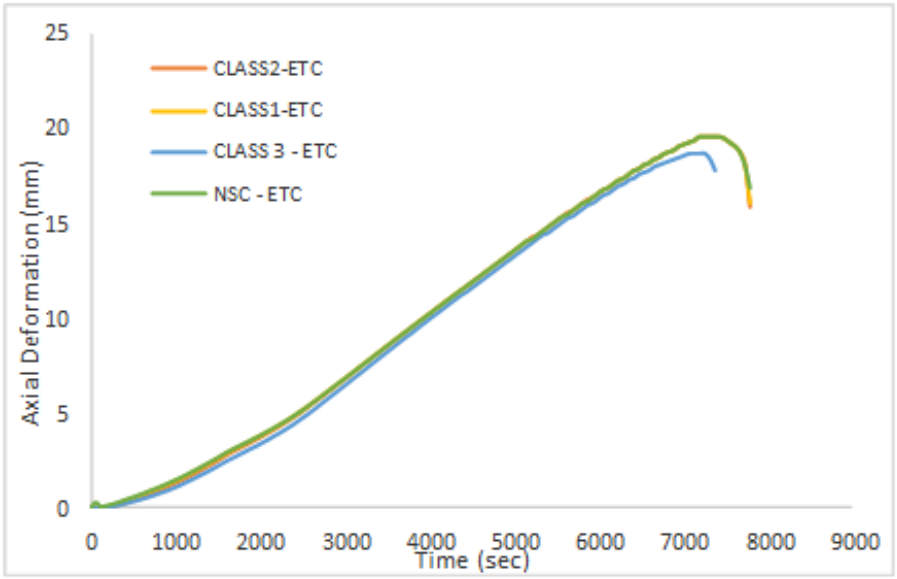

Figure B. 4 Axial deformations for different concrete compressive strengths

PC2

a) **b)**

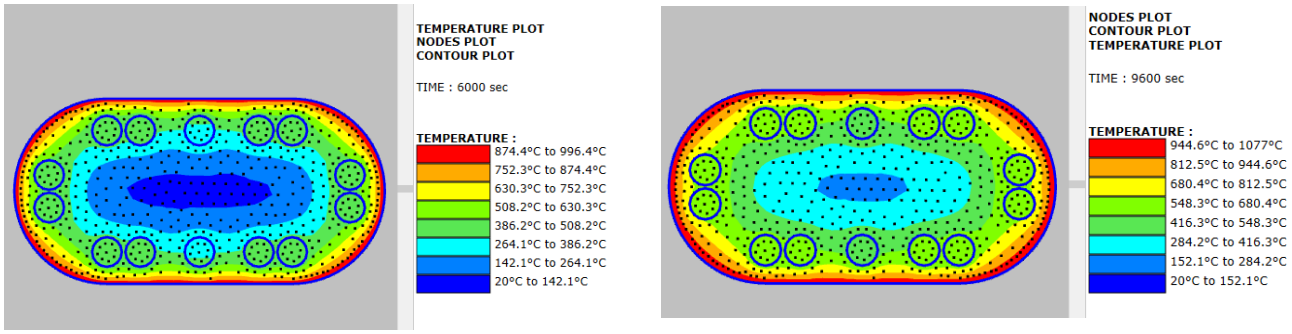

c)

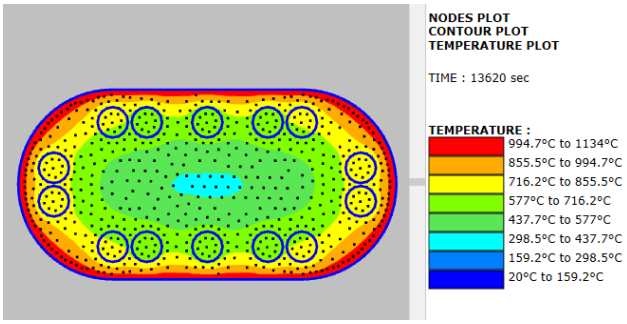

Figure B. 5 Temperature map for PC2 at a) 100 min b) 160 min and c) failure time

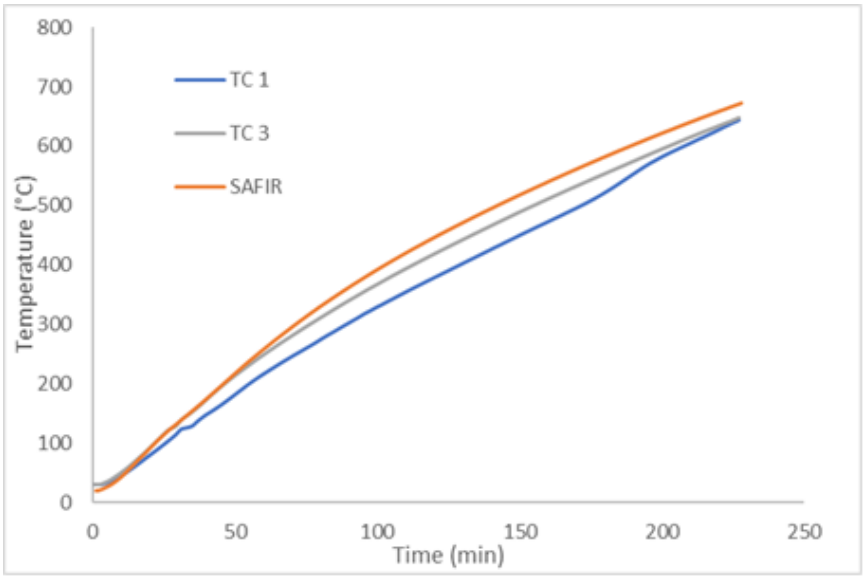

Figure B. 6 The calculated and measured temperature in thermocouples

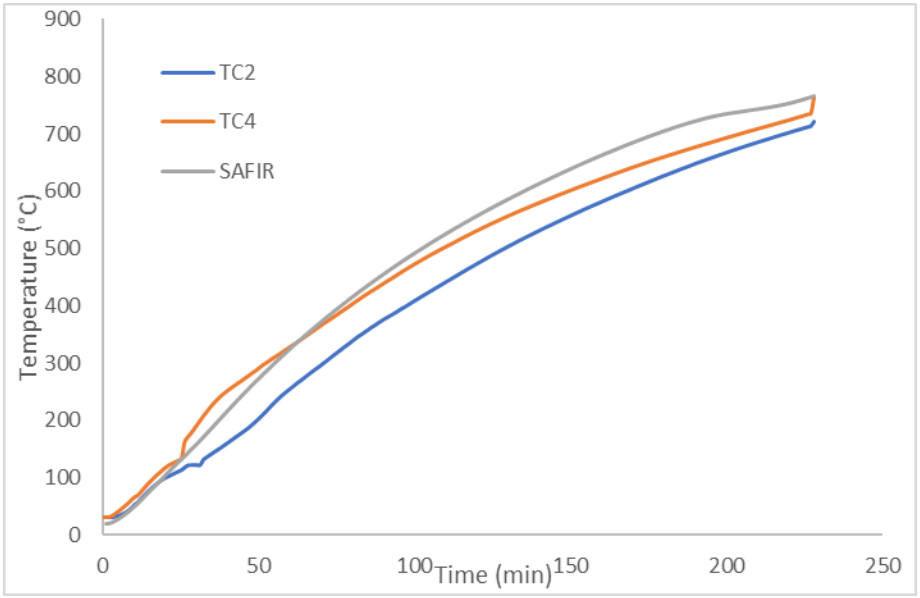

Figure B. 7 The calculated and measured temperature in thermocouples

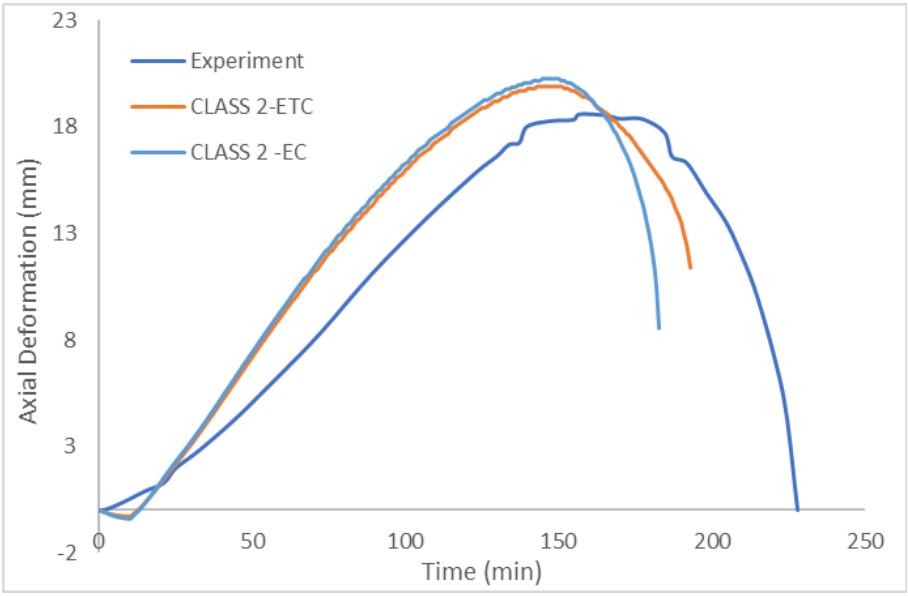

Figure B. 8 Comparison of calculated axial deformations with measured axial deformations for PC2

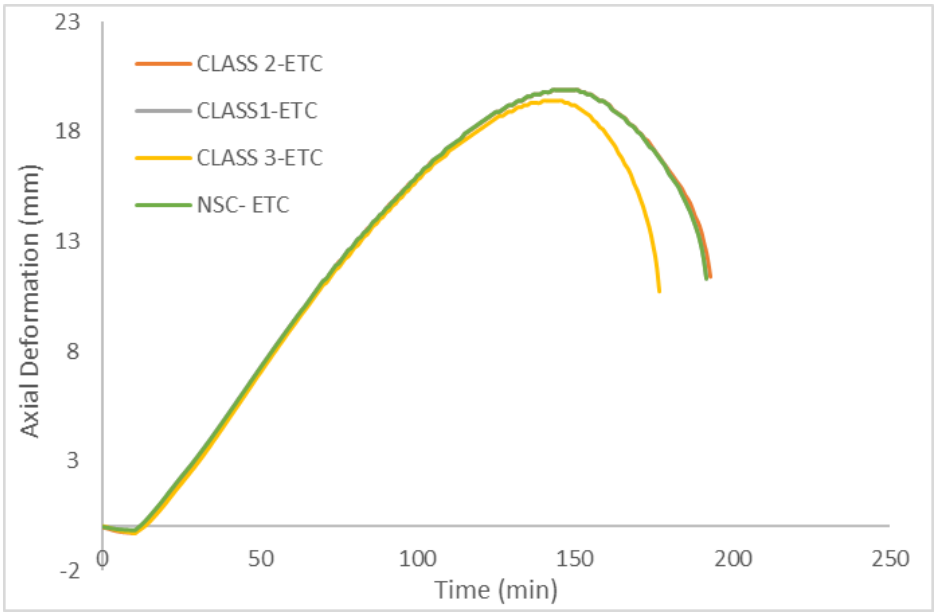

Figure B. 9 Axial deformations for different concrete compressive strengths

PC3

a)

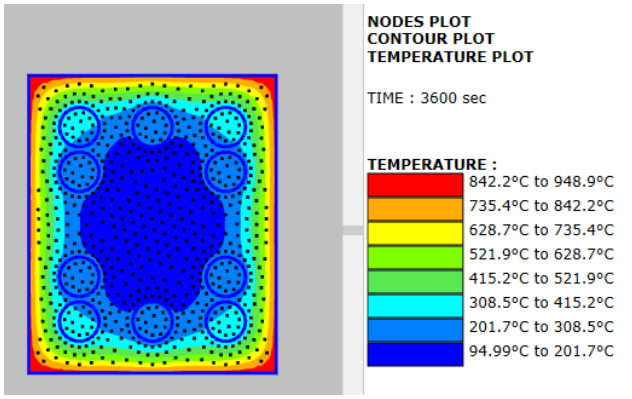

b)

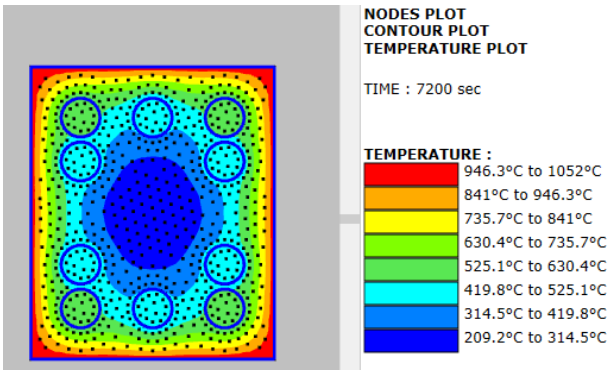

c)

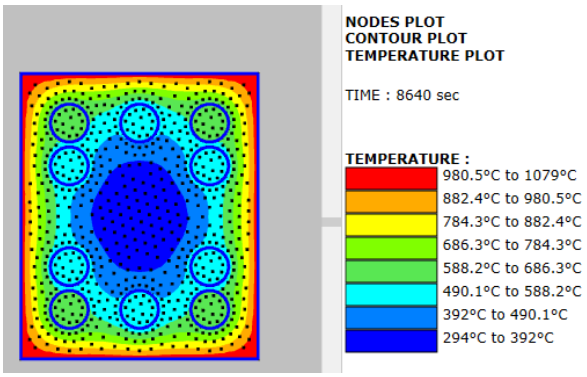

Figure B. 10 Temperature map for PC3 at a) 60 min b) 120 min and c) failure time

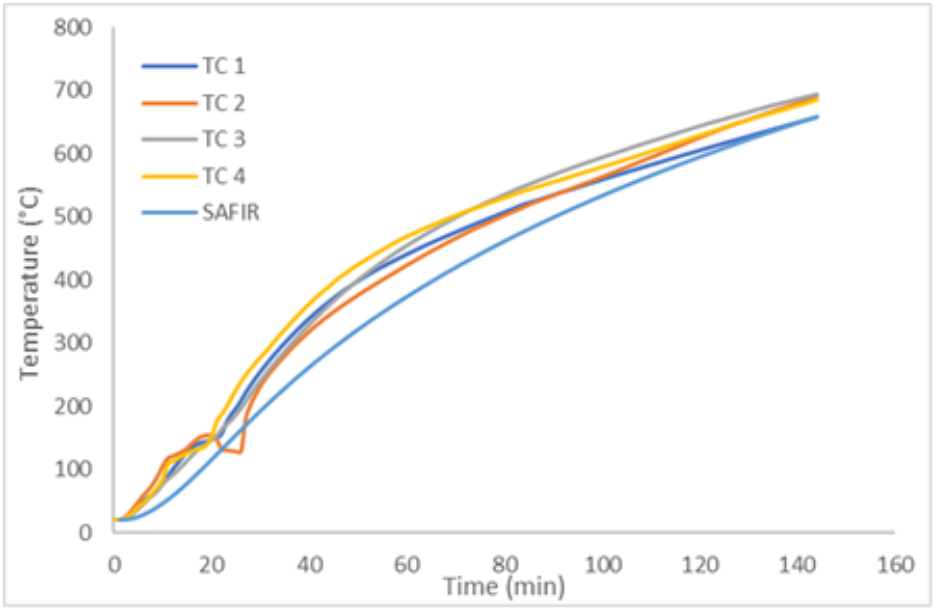

Figure B. 11 The calculated and measured temperature in thermocouples

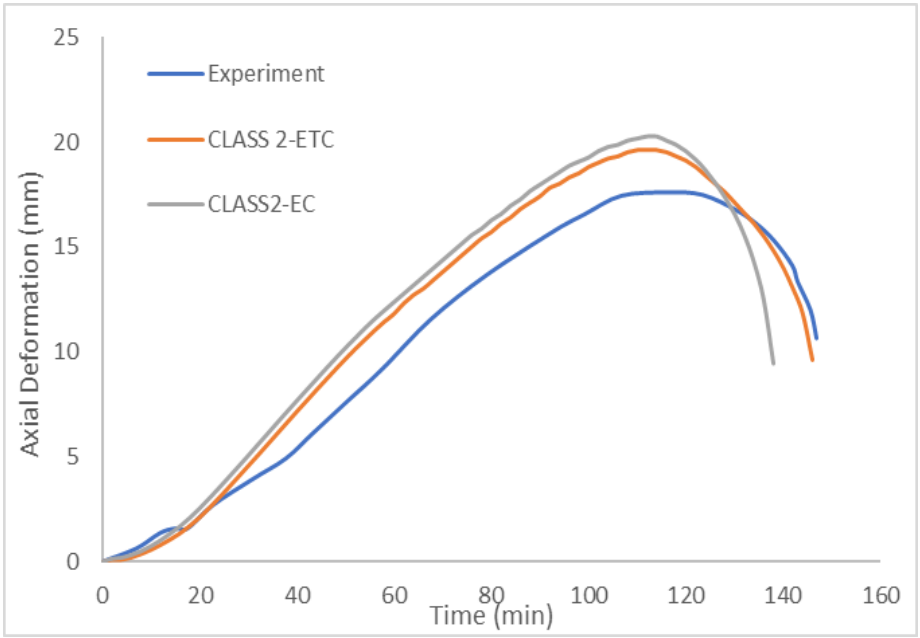

Figure B. 12 Comparison of calculated axial deformations with measured axial deformations for PC3

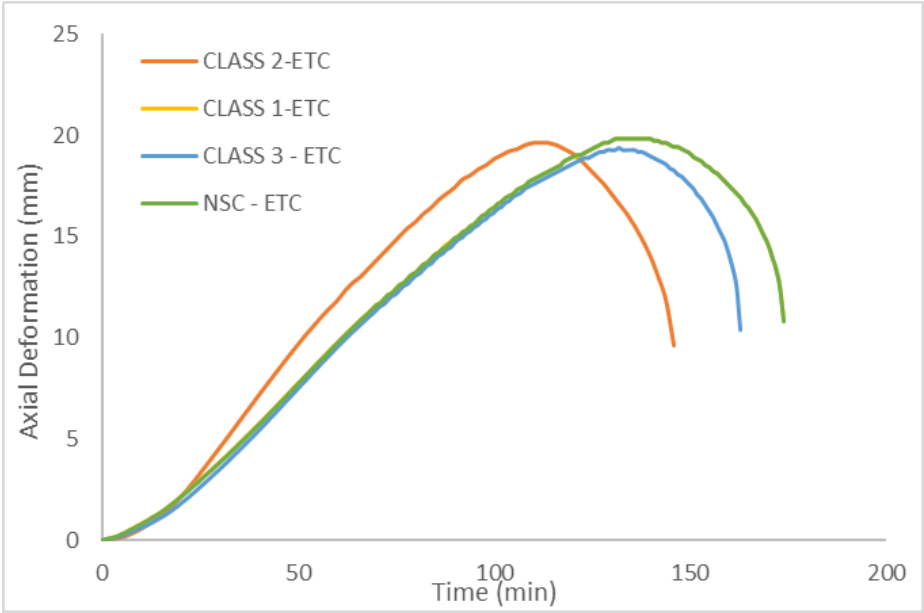

Figure B. 13 Axial deformations for different concrete compressive strengths

PC4

a)

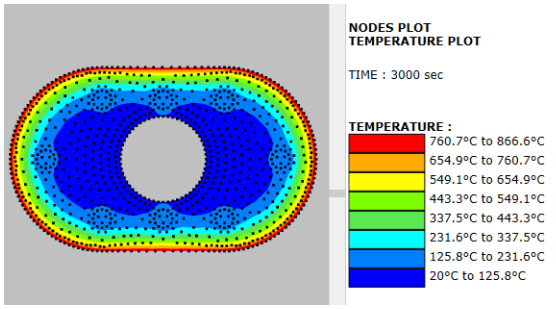

b)

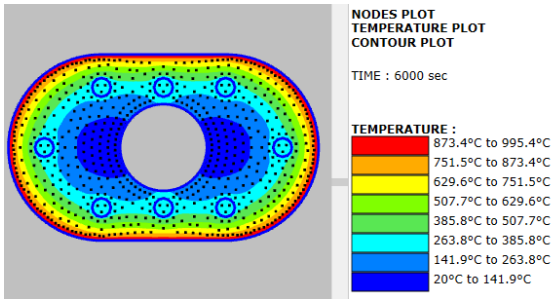

c)

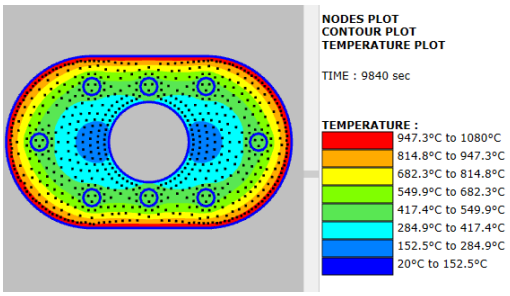

Figure B. 14 Temperature map for PC4 at a) 50 min b) 100 min and c) failure time

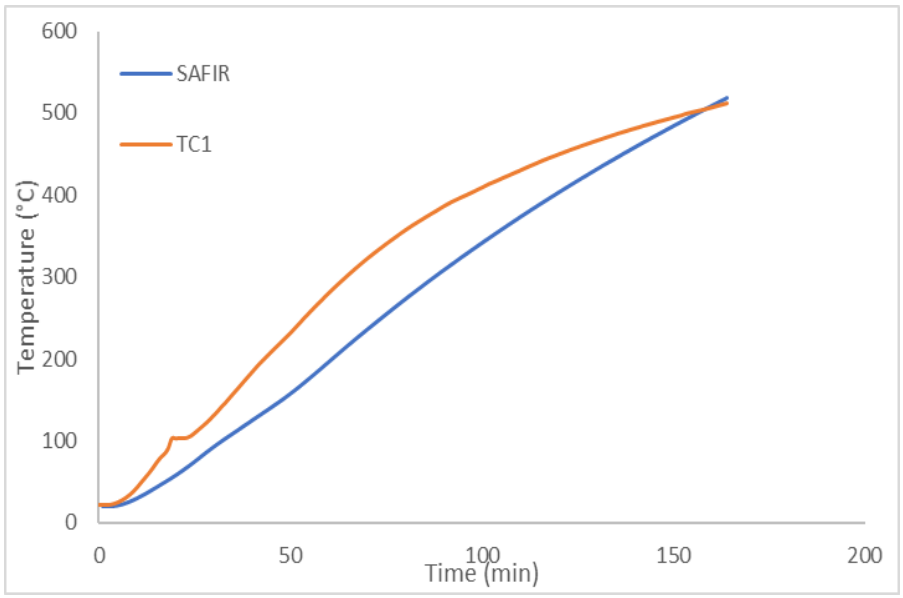

Figure B. 15 The calculated and measured temperature in thermocouple

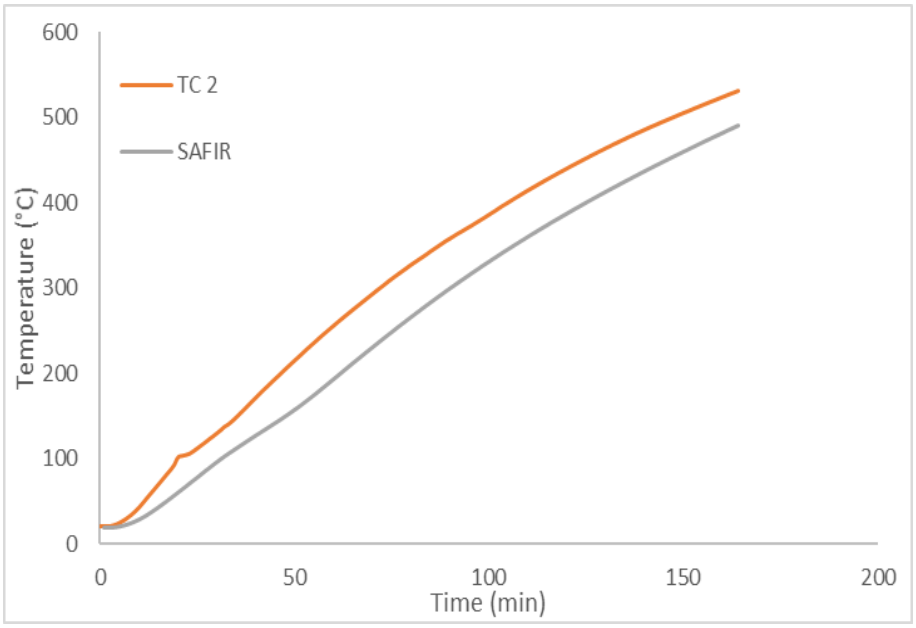

Figure B. 16 The calculated and measured temperature in thermocouples

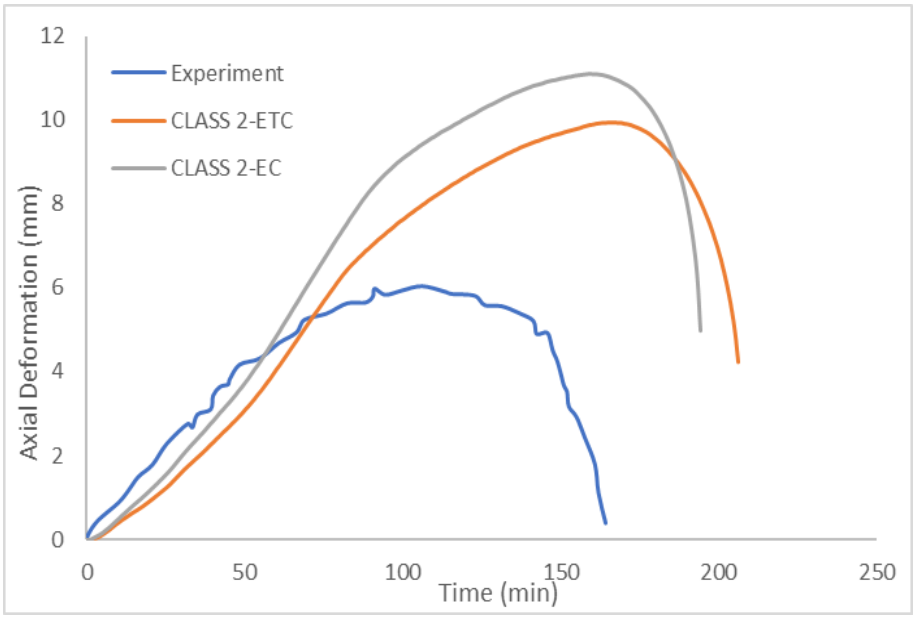

Figure B. 17 Comparison of calculated axial deformations with measured axial deformations for PC4

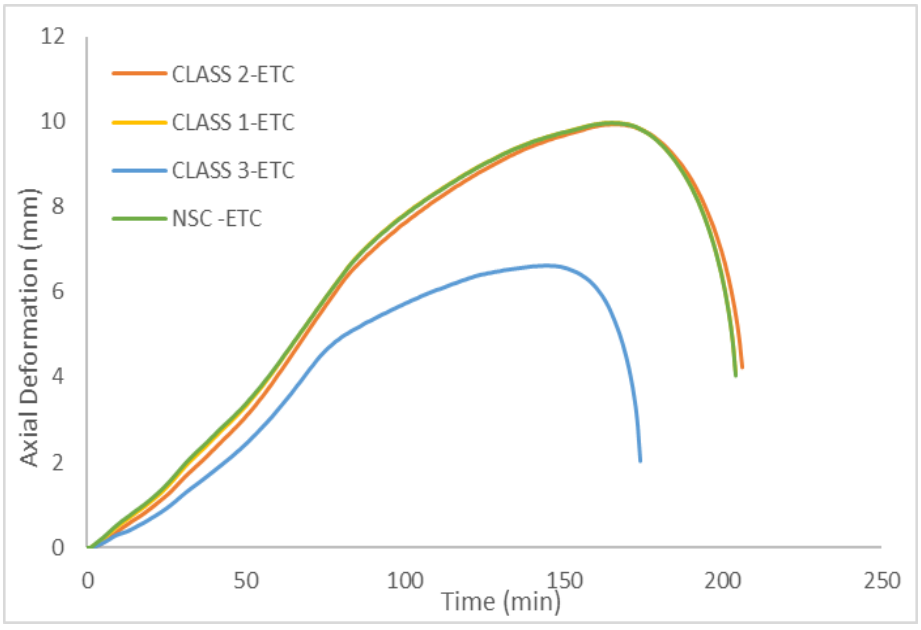

Figure B. 18 Axial deformations for different concrete compressive strengths

PC5

a)

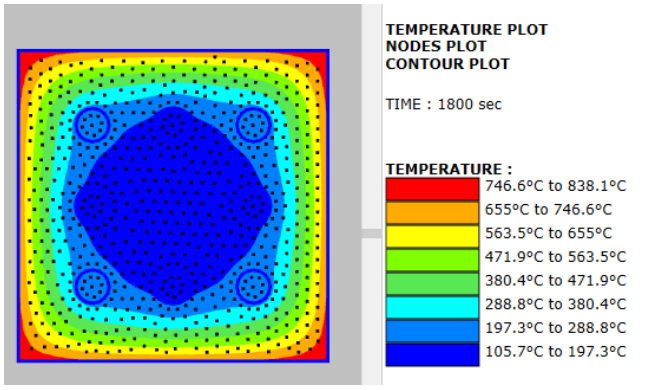

b)

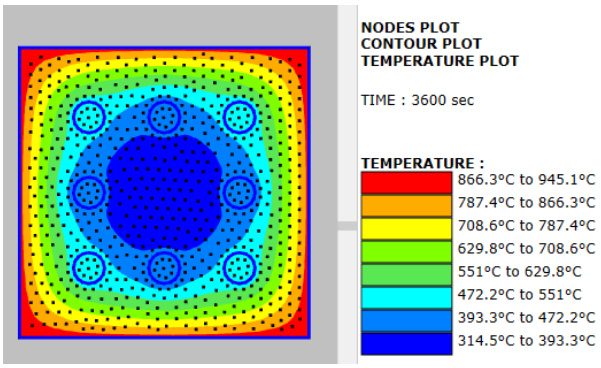

c)

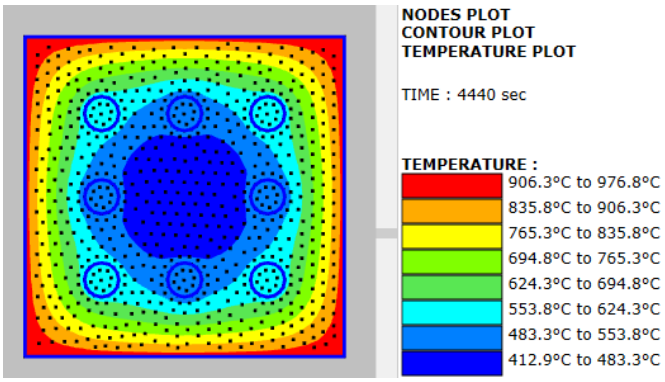

Figure B. 19 Temperature map for PC5 at a) 30 min b) 60 min and c) failure time

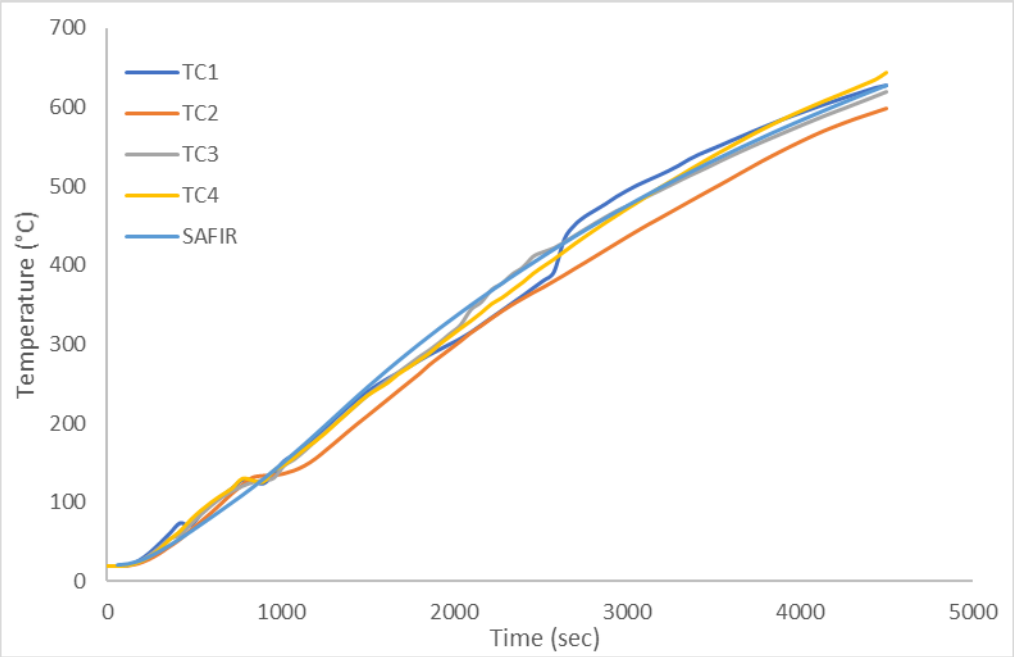

Figure B. 20 The calculated and measured temperature in thermocouples

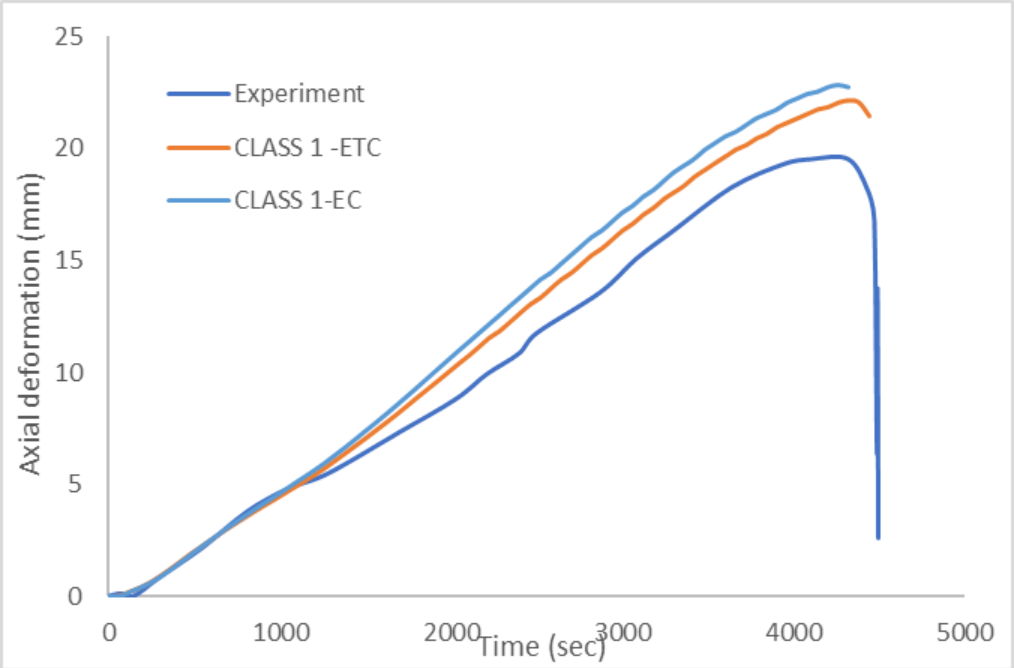

Figure B. 21 Comparison of calculated axial deformations with measured axial deformations for PC5

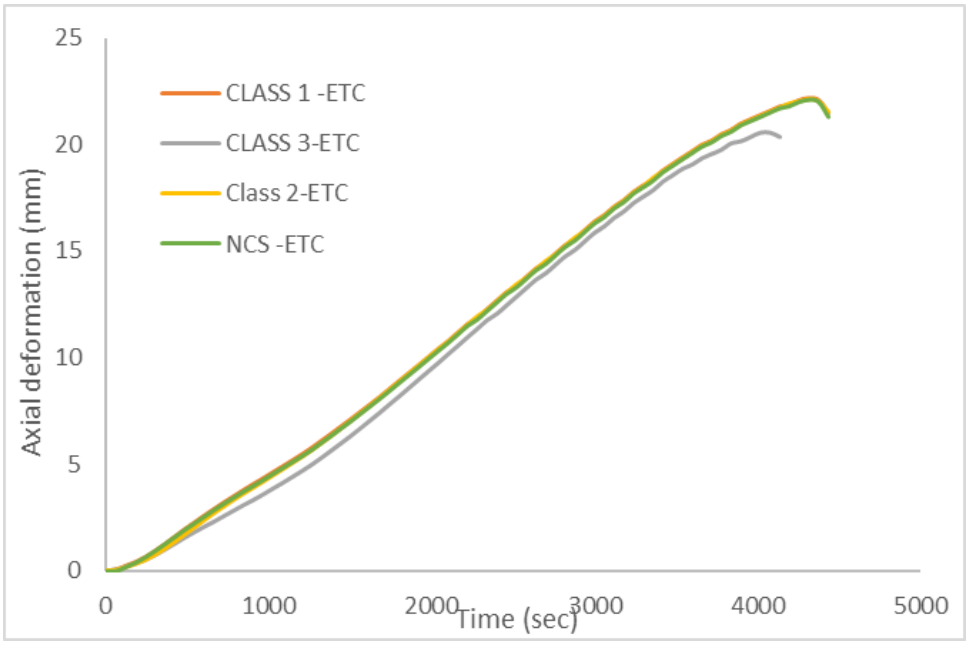

Figure B. 22 Axial deformations for different concrete compressive strengths

PC6

a)

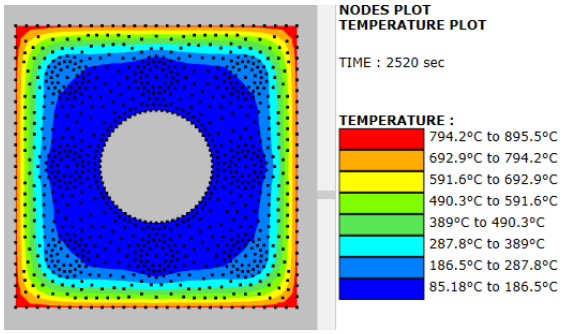

b)

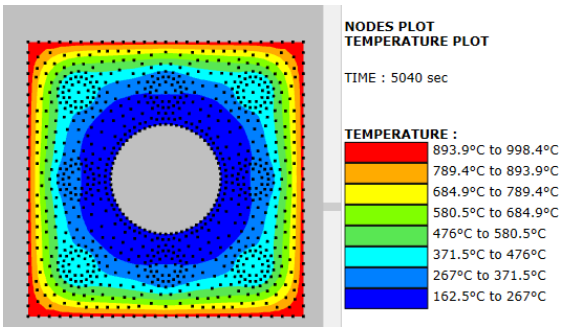

c)

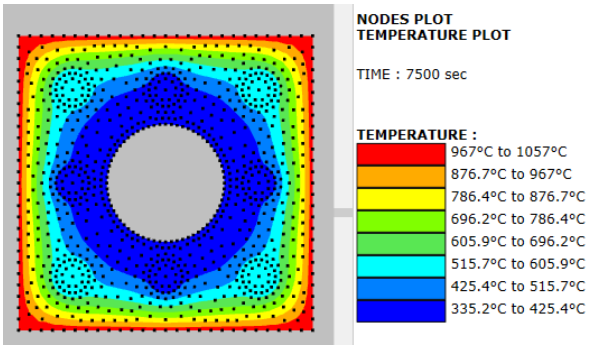

Figure B. 23 Temperature map for PC6 at a) 42 min b) 84 min and c) failure time

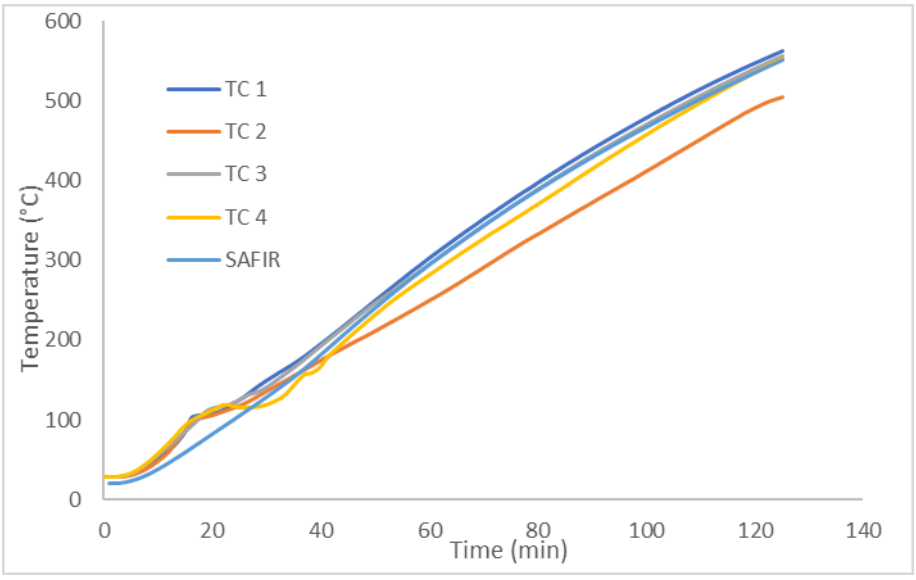

Figure B. 24 The calculated and measured temperature in thermocouples

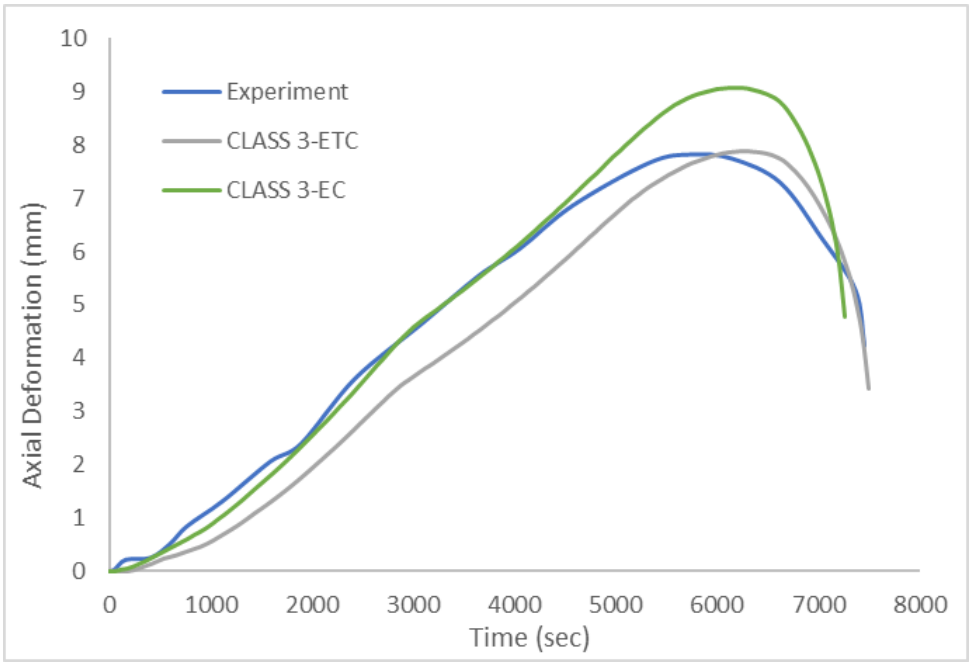

Figure B. 25 Comparison of calculated axial deformations with measured axial deformations for PC6

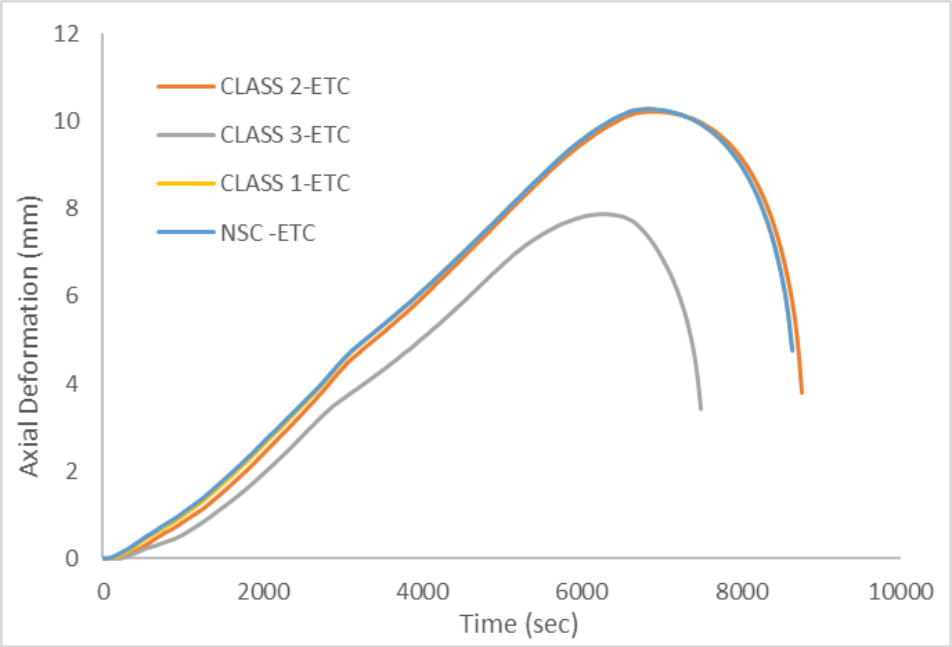

Figure B. 26 Axial deformations for different concrete compressive strengths

PC7

a)

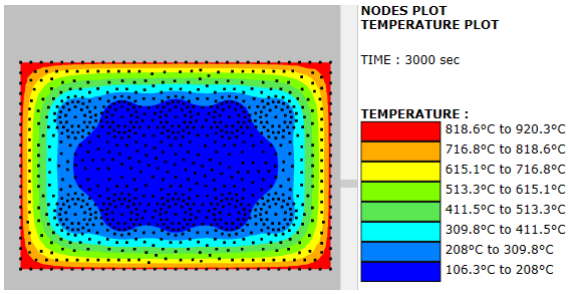

b)

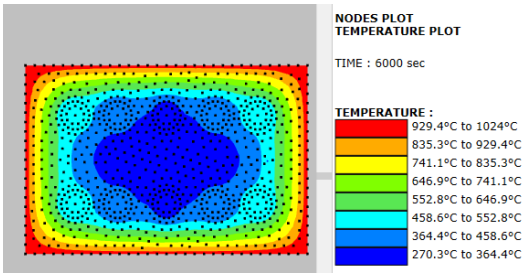

c)

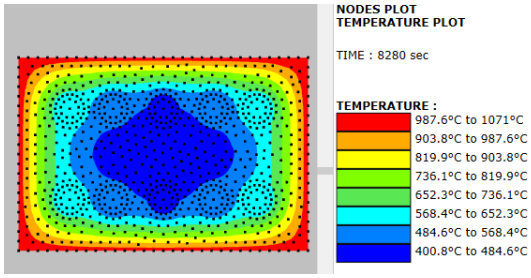

Figure B. 27 Temperature map for PC7 at a) 50 min b) 100 min and c) failure time

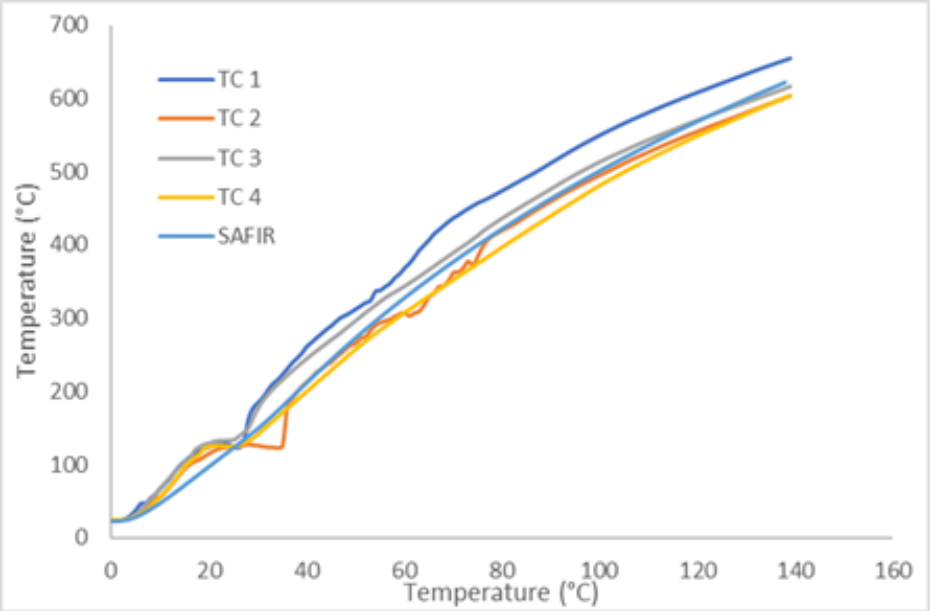

Figure B. 28 The calculated and measured temperature in thermocouples

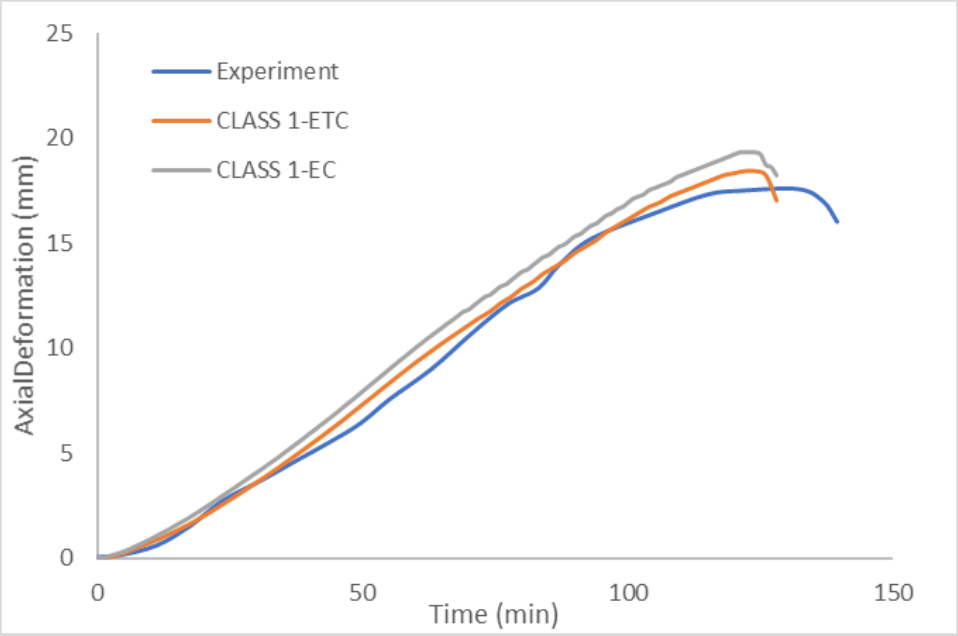

Figure B. 29 Comparison of calculated axial deformations with measured axial deformations for PC7

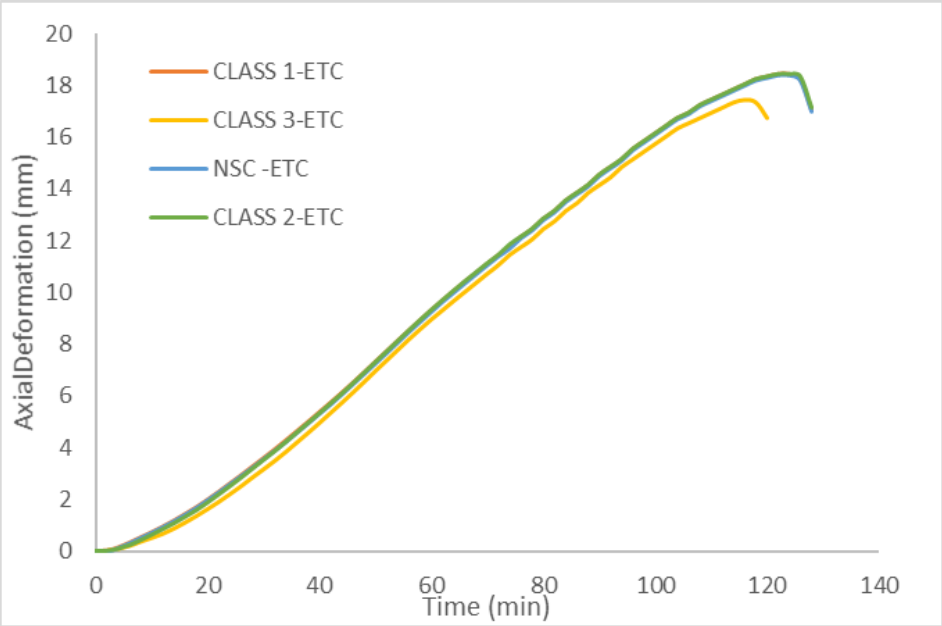

Figure B. 30 Axial deformations for different concrete compressive strengths

PC8

a)

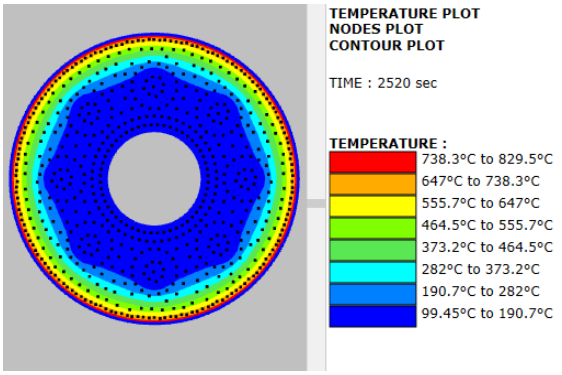

b)

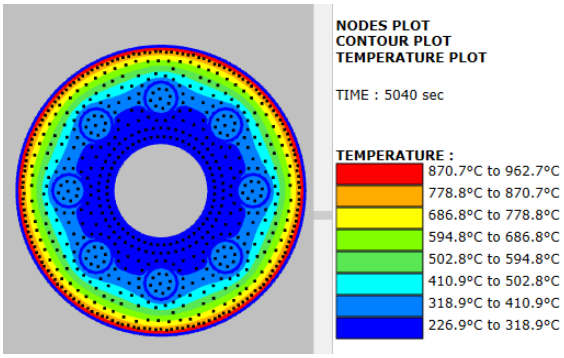

c)

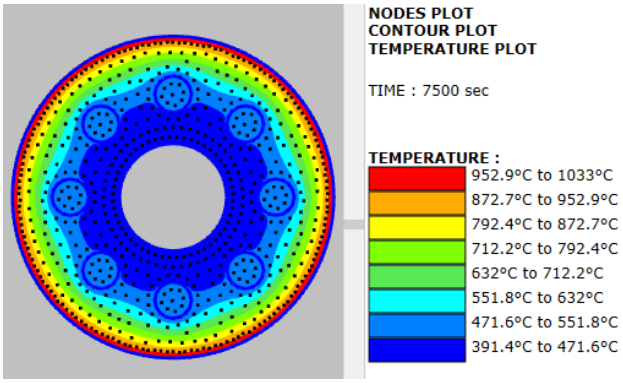

Figure B. 31 Temperature map for PC8 at a) 42 min b) 84 min and c) failure time

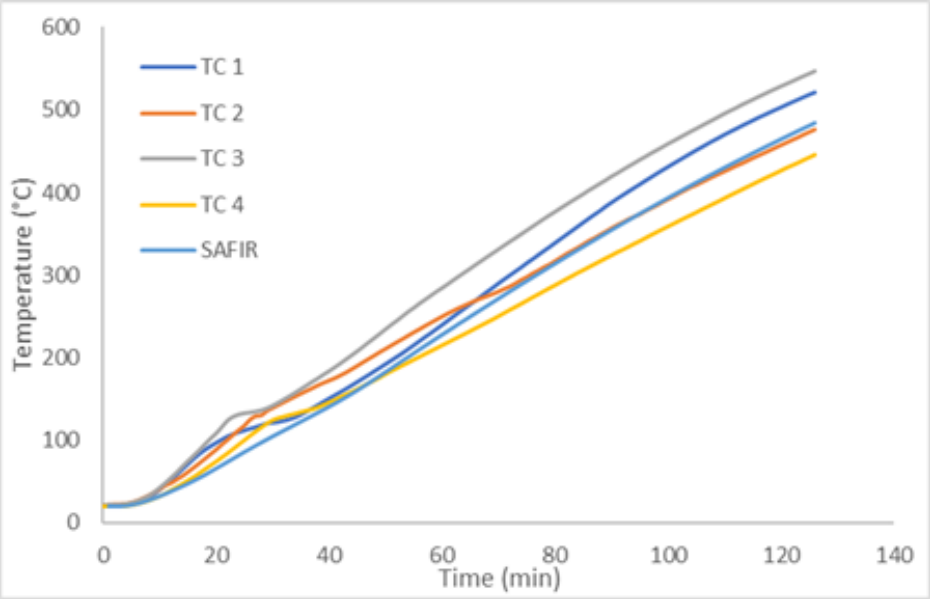

Figure B. 32 The calculated and measured temperature in thermocouples

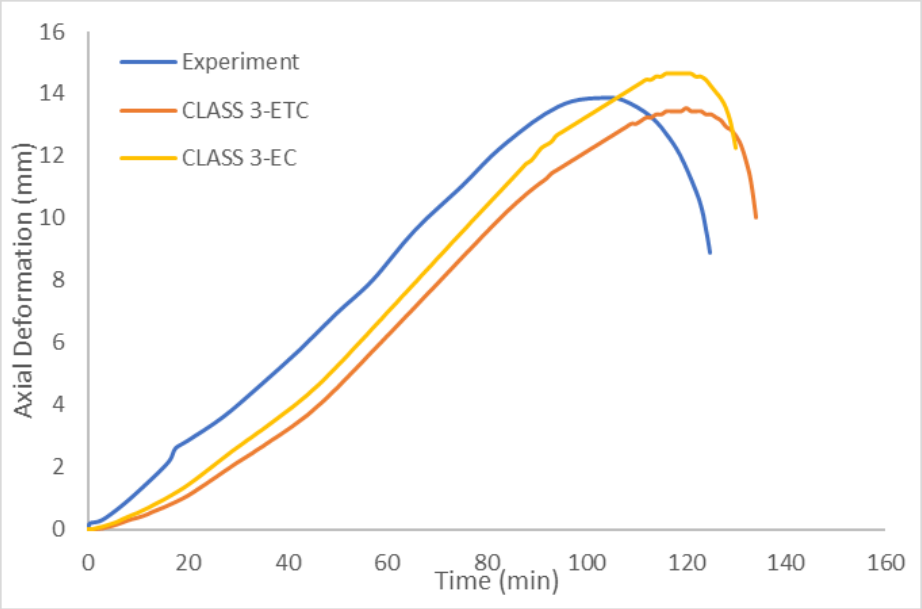

Figure B. 33 Comparison of calculated axial deformations with measured axial deformations for PC8

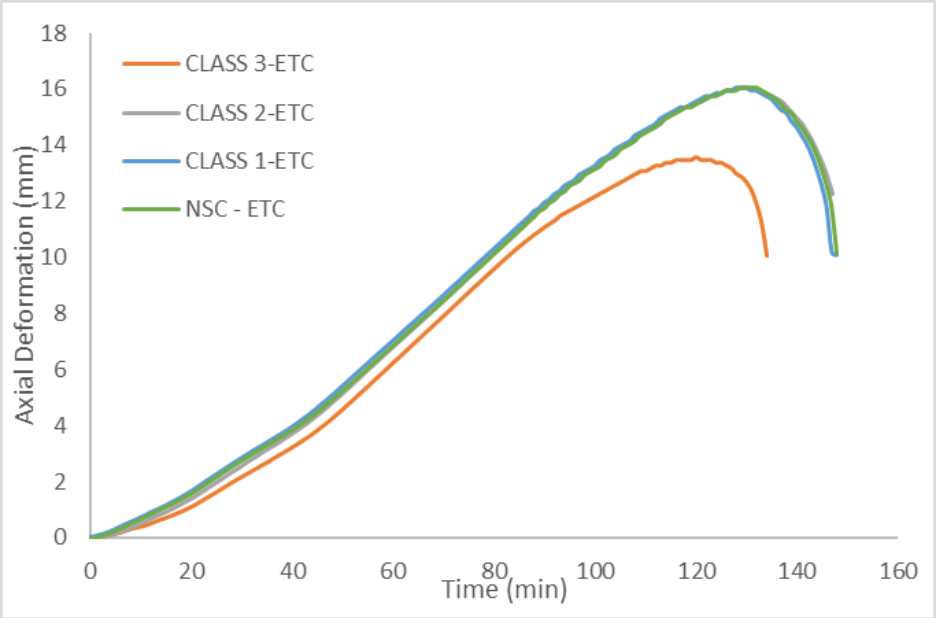

Figure B. 34 Axial deformations for different concrete compressive strengths

PC9

a)

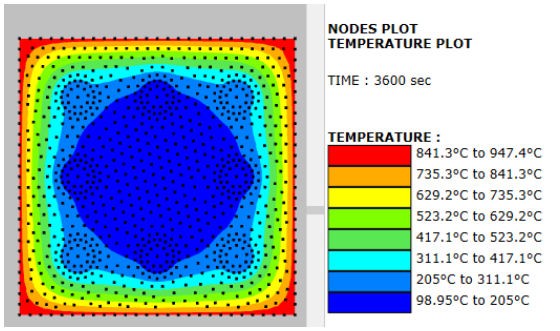

b)

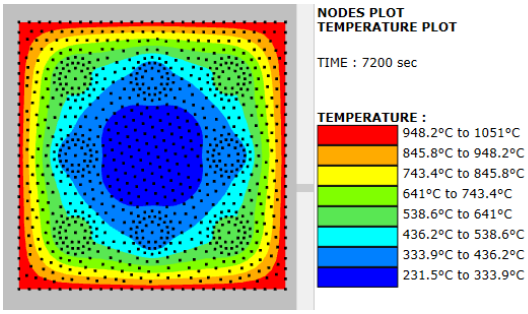

c)

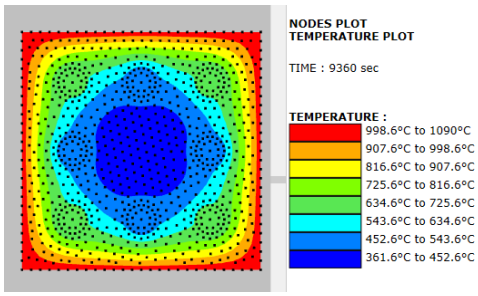

Figure B. 35 Temperature map for PC9 at a) 60 min b) 120 min and c) failure time

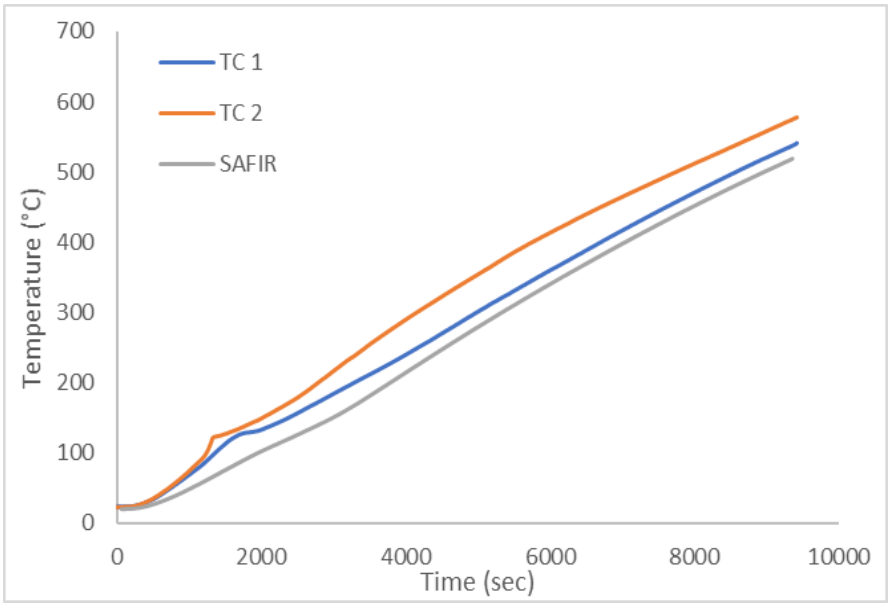

Figure B. 36 The calculated and measured temperature in thermocouples

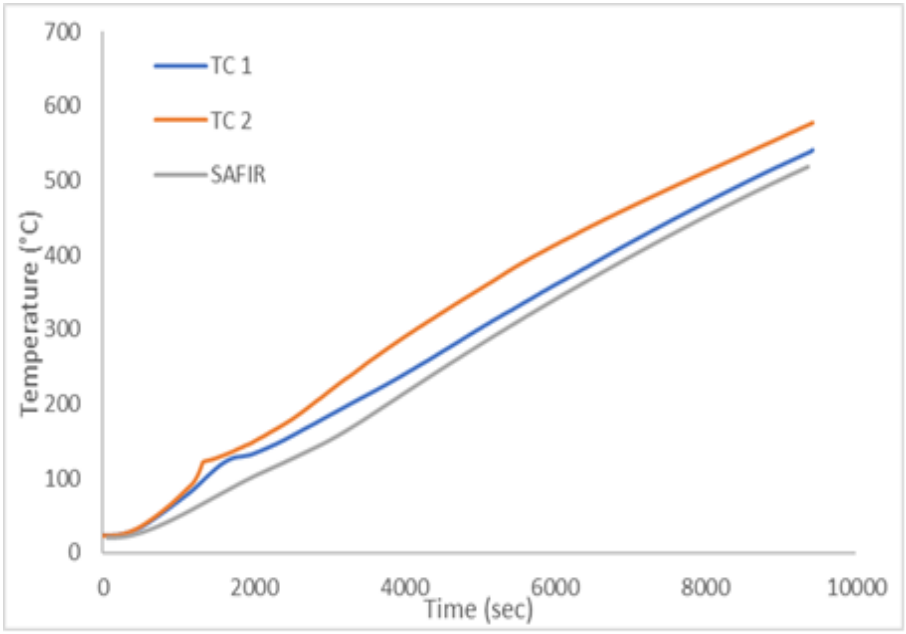

Figure B. 37 The calculated and measured temperature in thermocouples

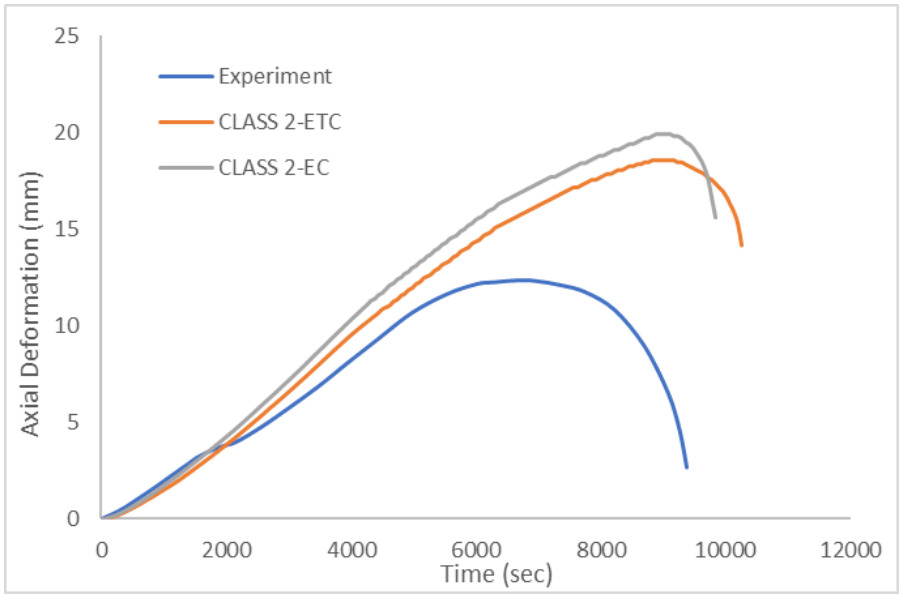

Figure B. 38 Comparison of calculated axial deformations with measured axial deformations for PC9

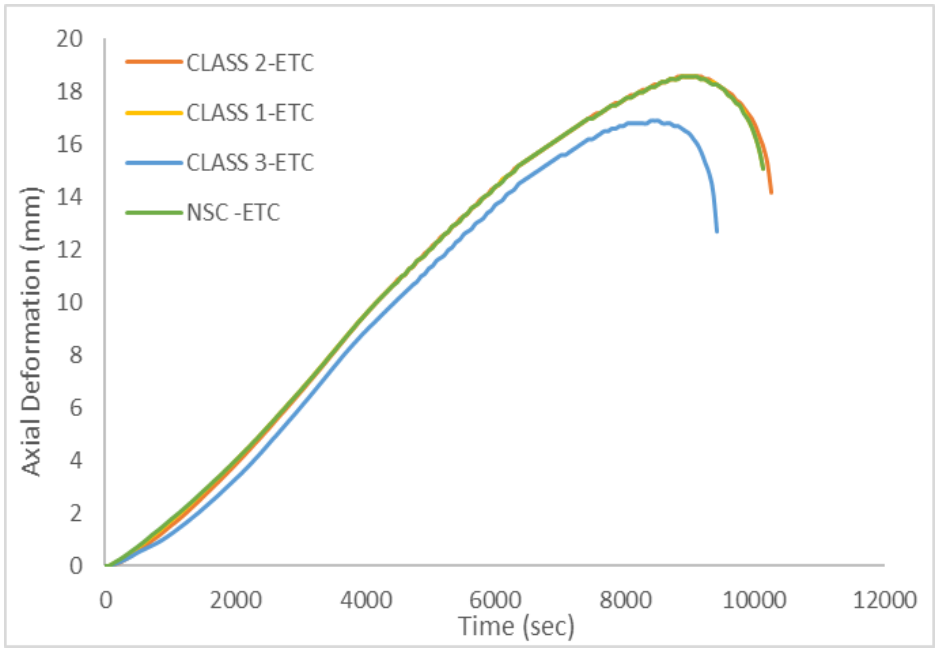

Figure B. 39 Axial deformations for different concrete compressive strengths

PC10

a)

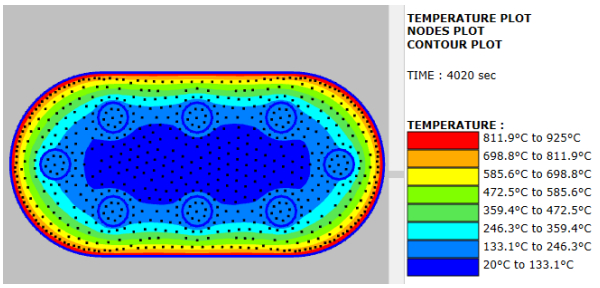

b)

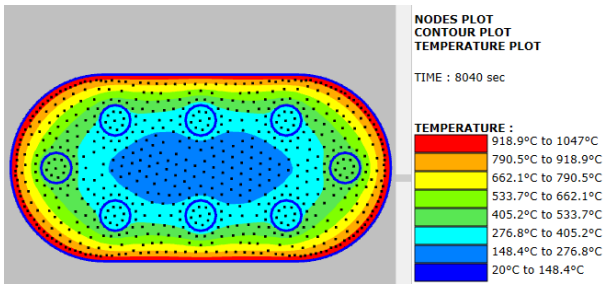

c)

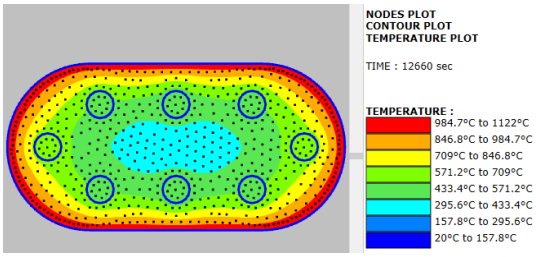

Figure B. 40 Temperature map for PC10 at a) 67 min b) 134 min and c) failure time

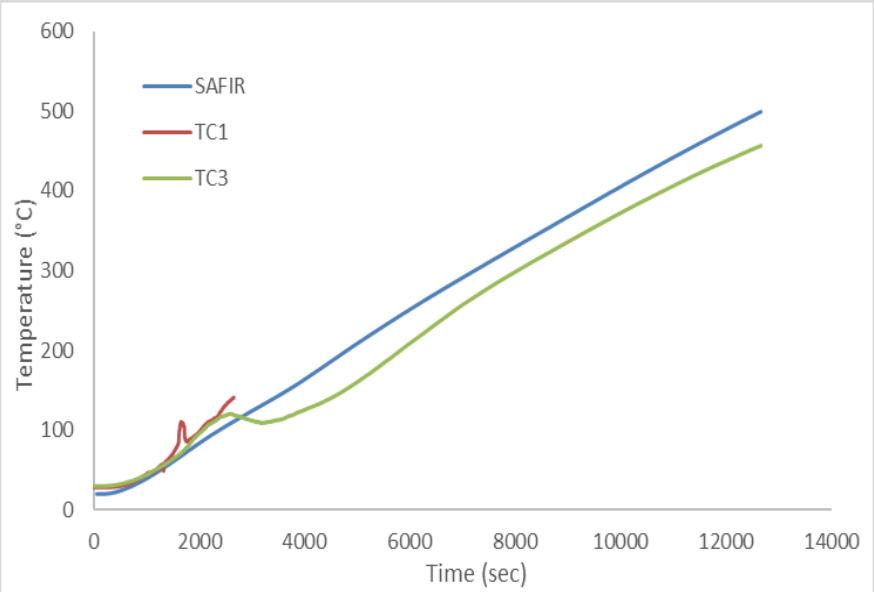

Figure B. 41 The calculated and measured temperature in thermocouples

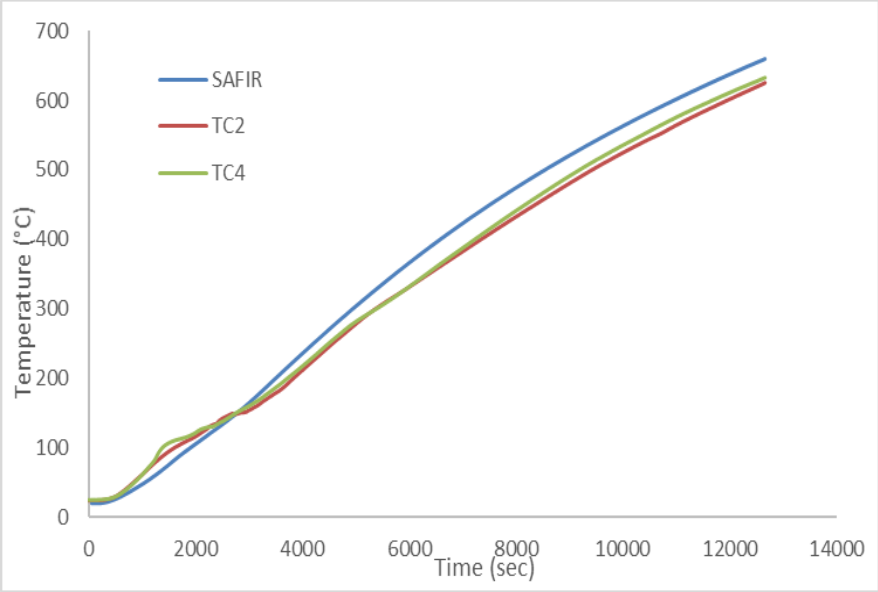

Figure B. 42 The calculated and measured temperature in thermocouples

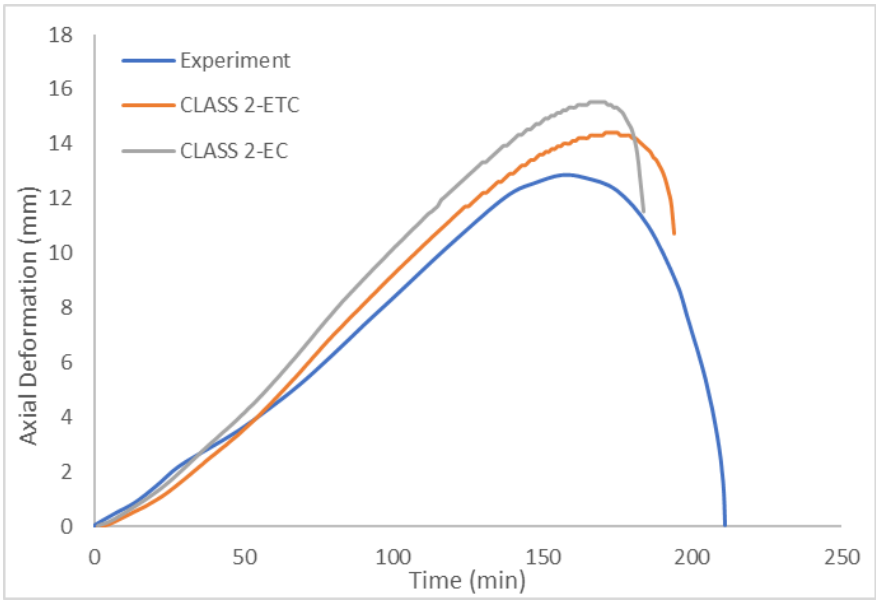

Figure B. 43 Comparison of calculated axial deformations with measured axial deformations for PC10

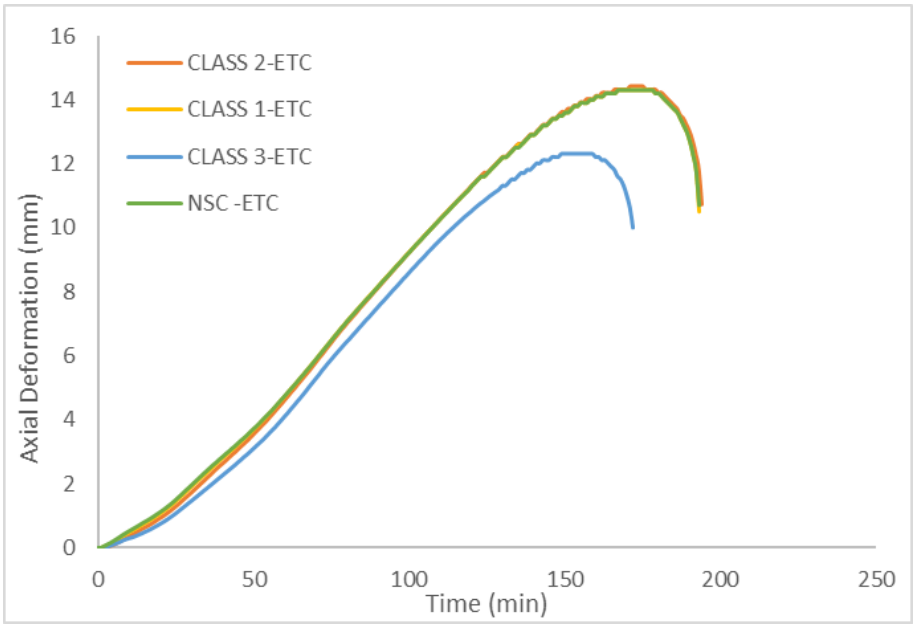

Figure B. 44 Axial deformations for different concrete compressive strengths

PC11

a)

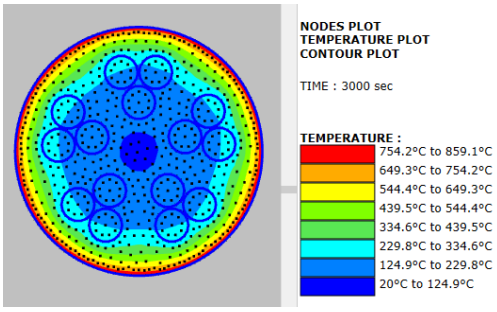

b)

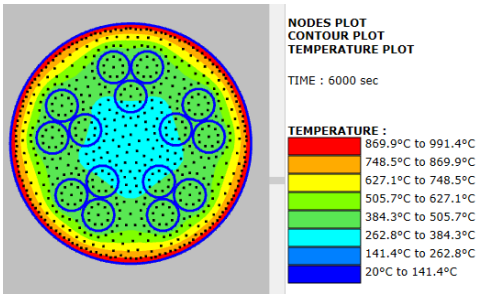

c)

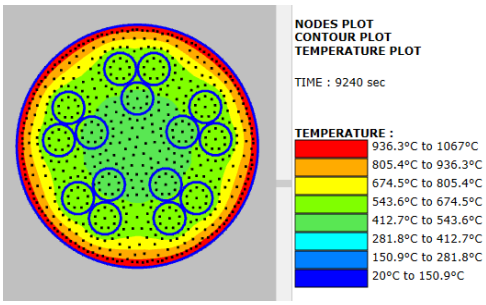

Figure B. 45 Temperature map for PC11 at a) 50 min b) 100 min and c) failure time

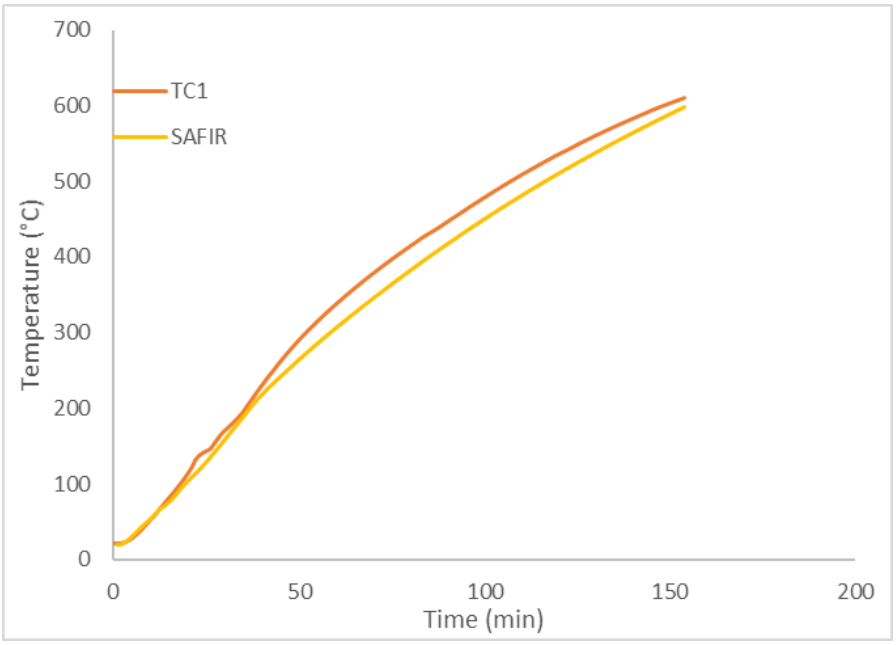

Figure B. 46 The calculated and measured temperature in thermocouple

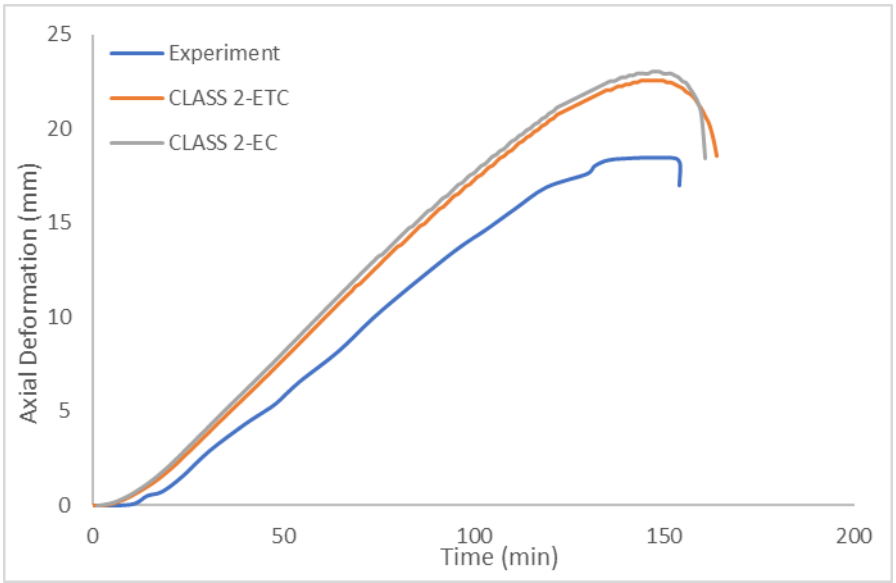

Figure B. 47 Comparison of calculated axial deformations with measured axial deformations for PC11

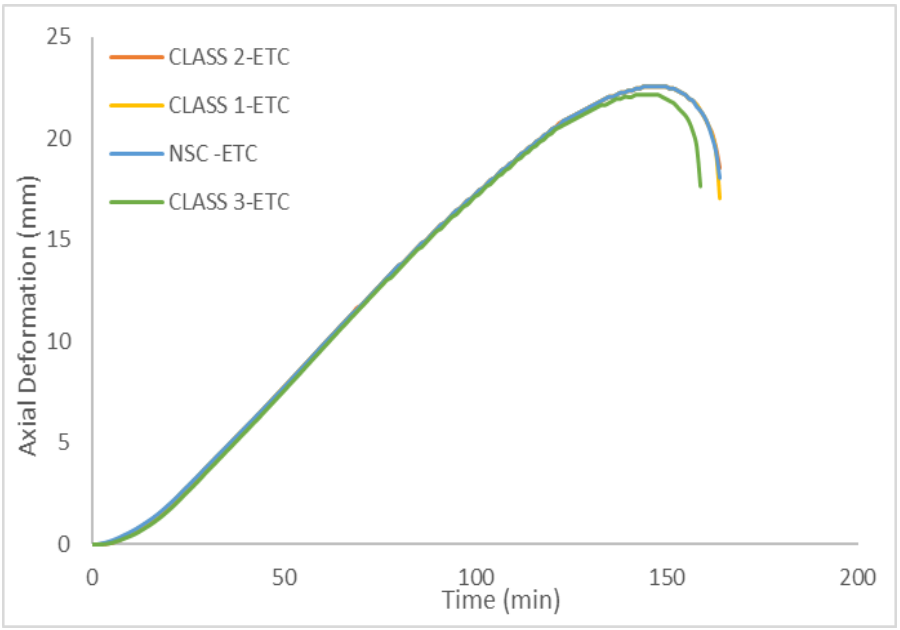

Figure B. 48 Axial deformations for different concrete compressive strengths

PC12

a)

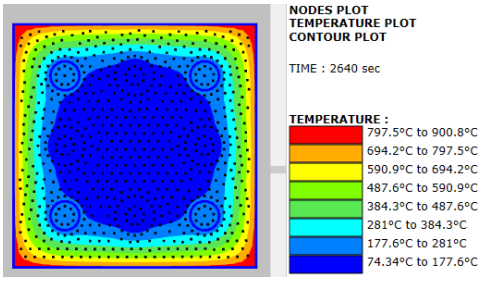

b)

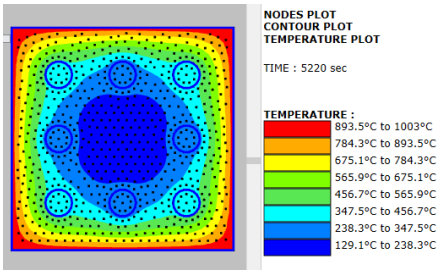

c)

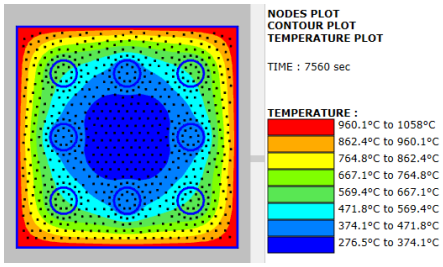

Figure B. 49 Temperature map for PC12 at a) 34 min b) 87 min and c) failure time

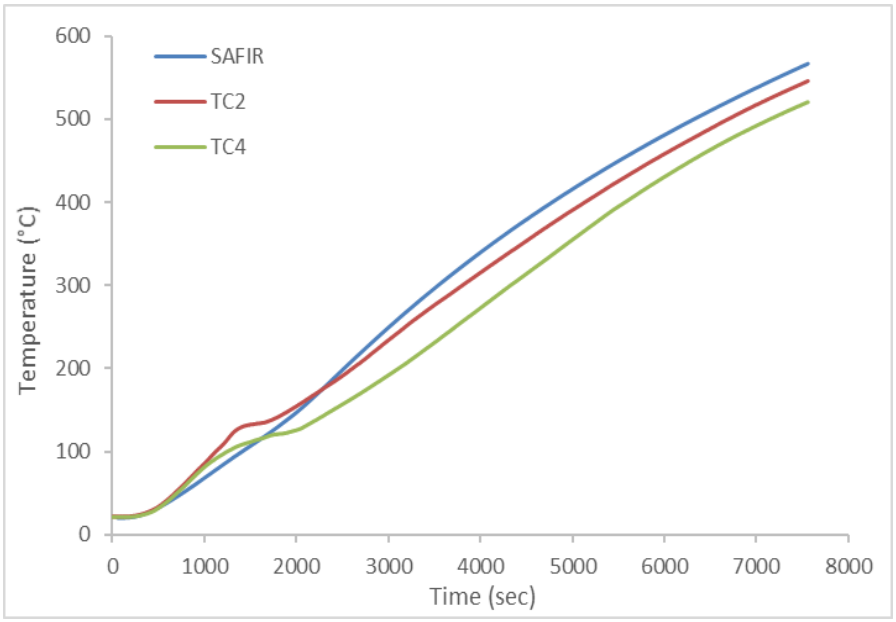

Figure B. 50 The calculated and measured temperature in thermocouples

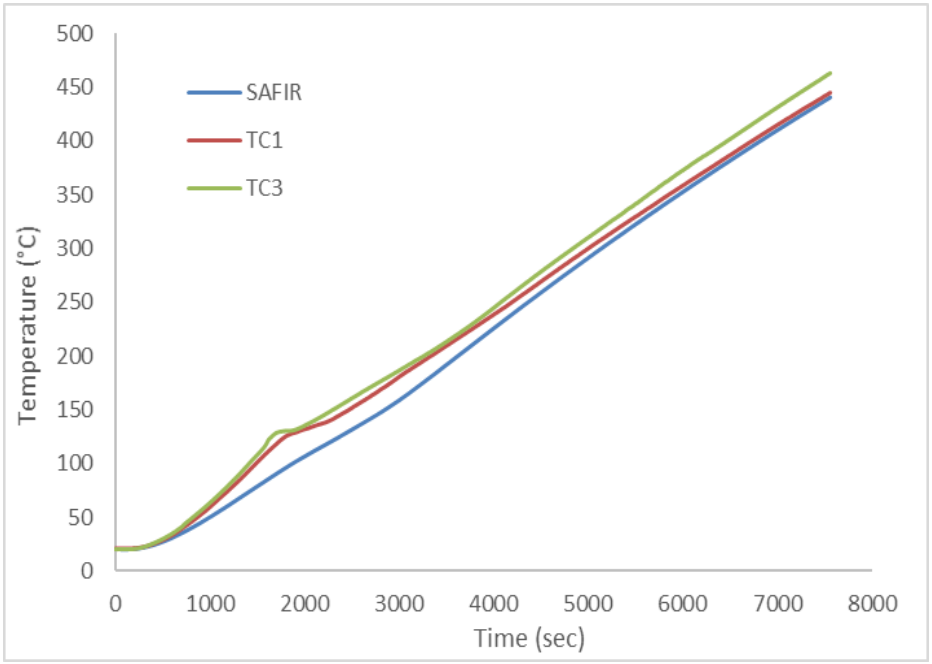

Figure B. 51 The calculated and measured temperature in thermocouples

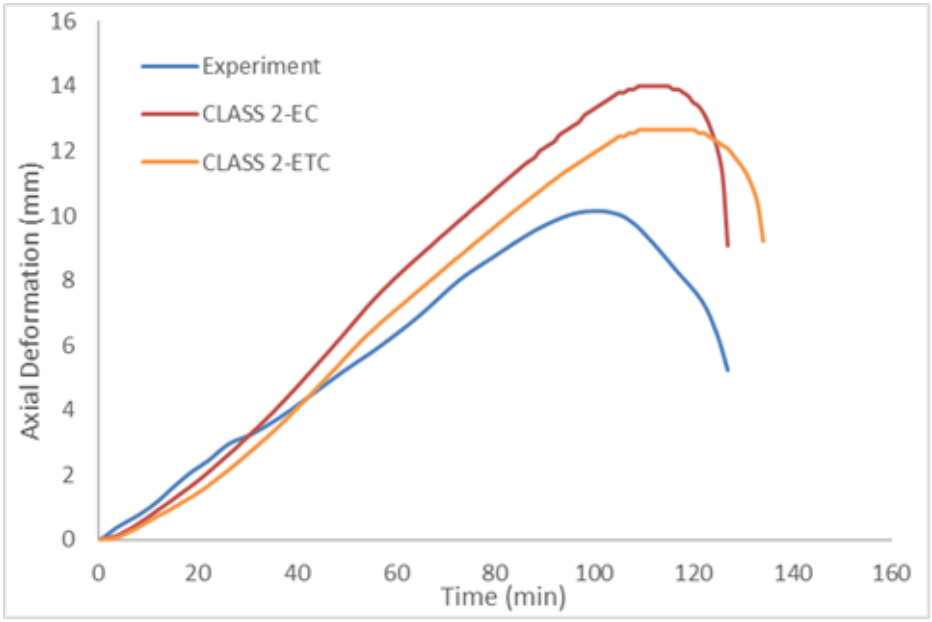

Figure B. 52 Comparison of calculated axial deformations with measured axial deformations for PC12

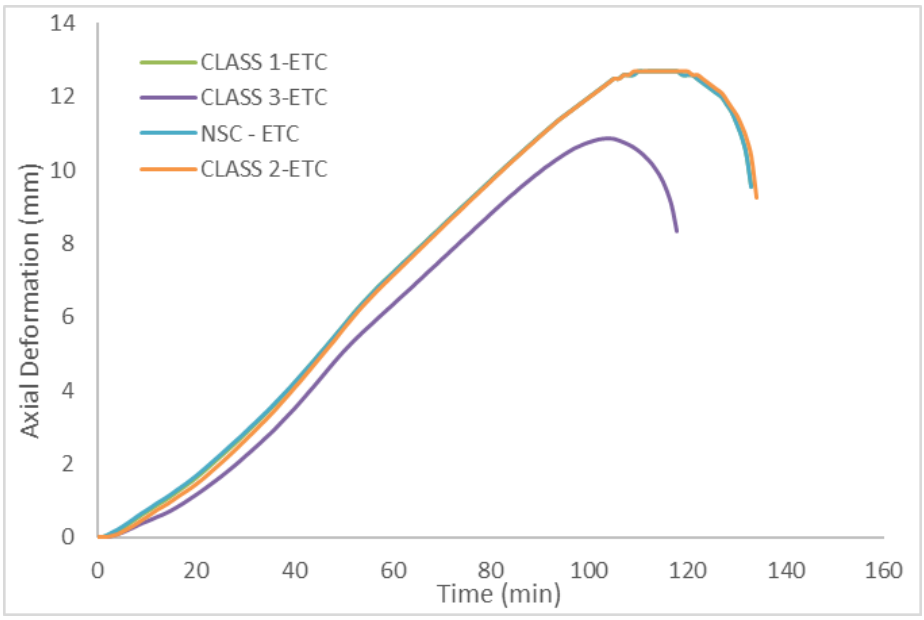

Figure B. 53 Axial deformations for different concrete compressive strengths

PC14

a) **b)**

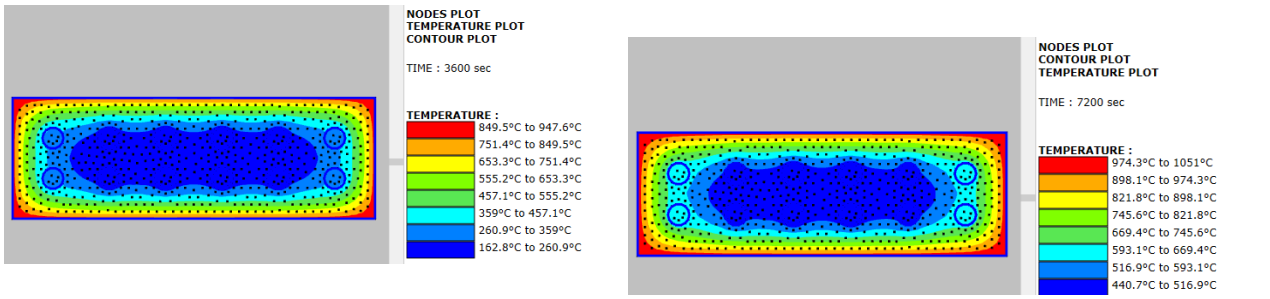

c)

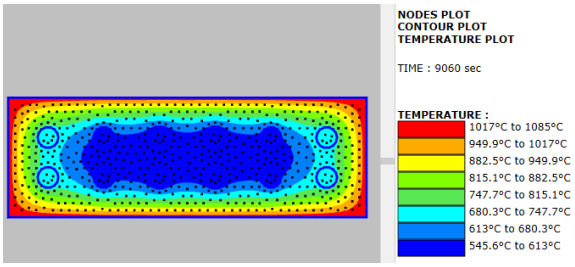

Figure B. 54 Temperature map for PC14 at a) 60 min b) 120 min and c) failure time

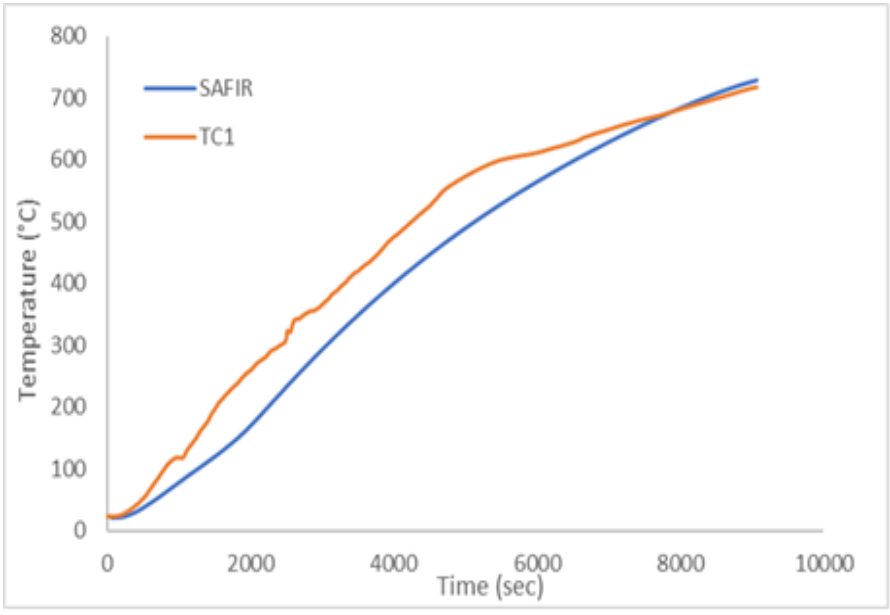

Figure B. 55 The calculated and measured temperature in thermocouple

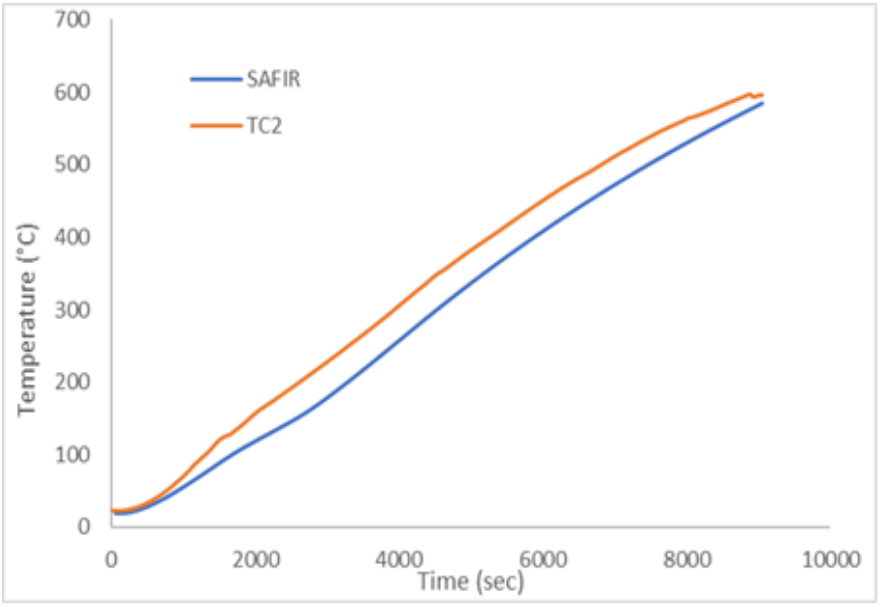

Figure B. 56 The calculated and measured temperature in thermocouples

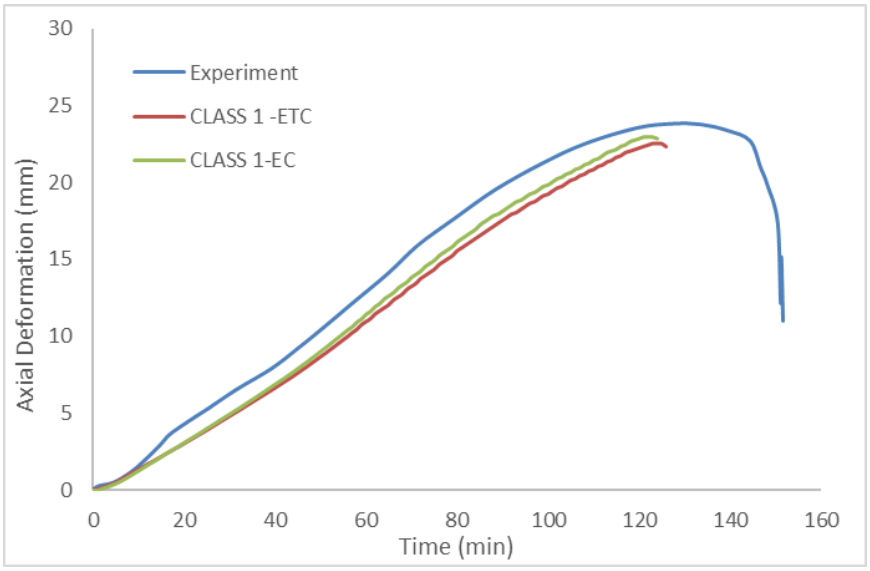

Figure B. 57 Comparison of calculated axial deformations with measured axial deformations for PC14

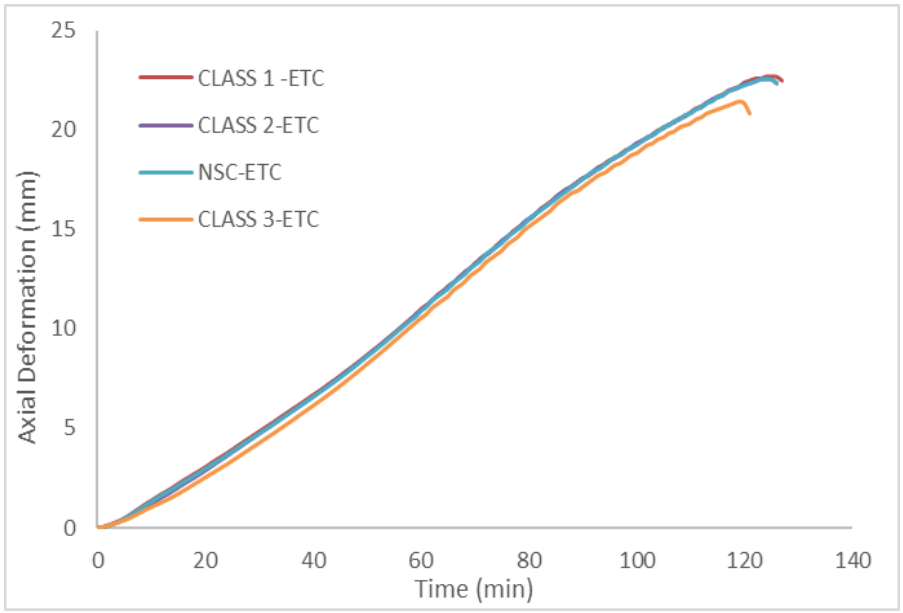

Figure B. 58 Axial deformations for different concrete compressive strengths

PC16

a)

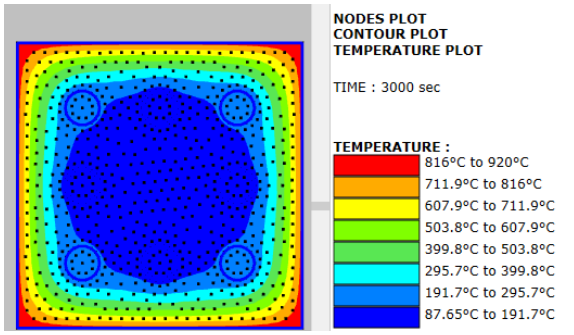

b)

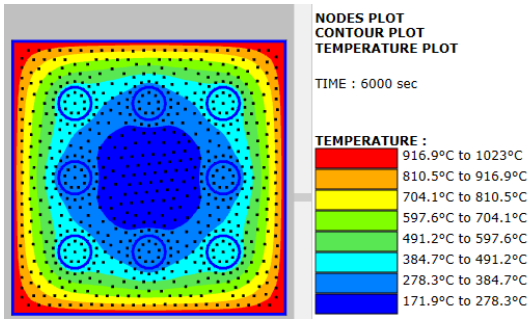

c)

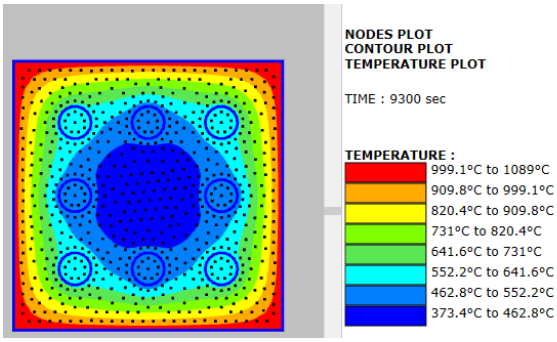

Figure B. 59 Temperature map for PC16 at a) 50 min b) 100 min and c) failure time

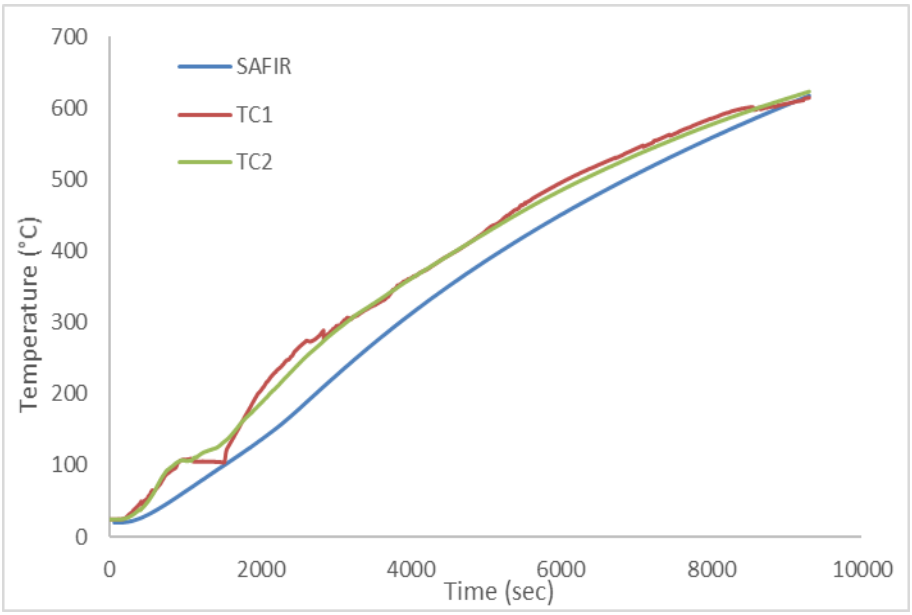

Figure B. 60 The calculated and measured temperature in thermocouples

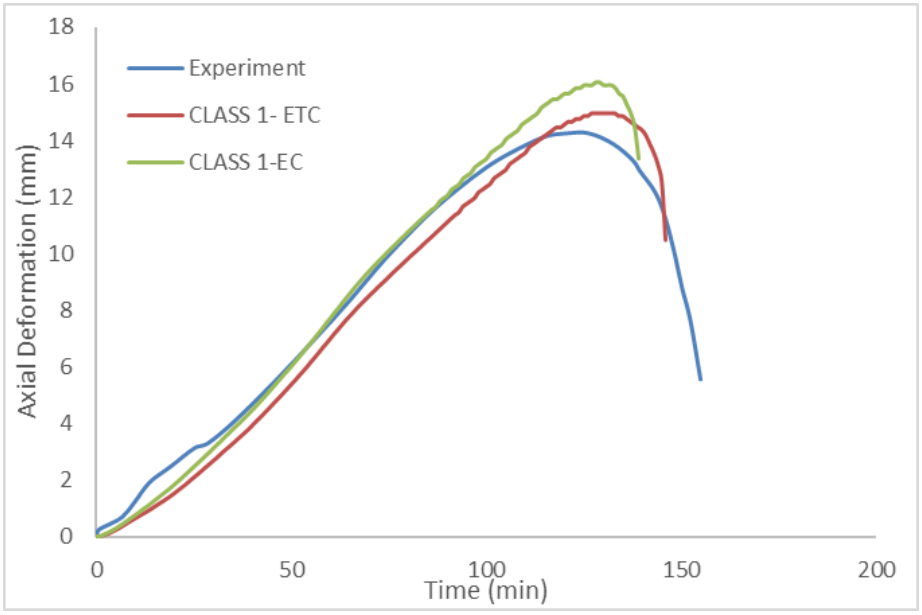

Figure B. 61 Comparison of calculated axial deformations with measured axial deformations for PC16

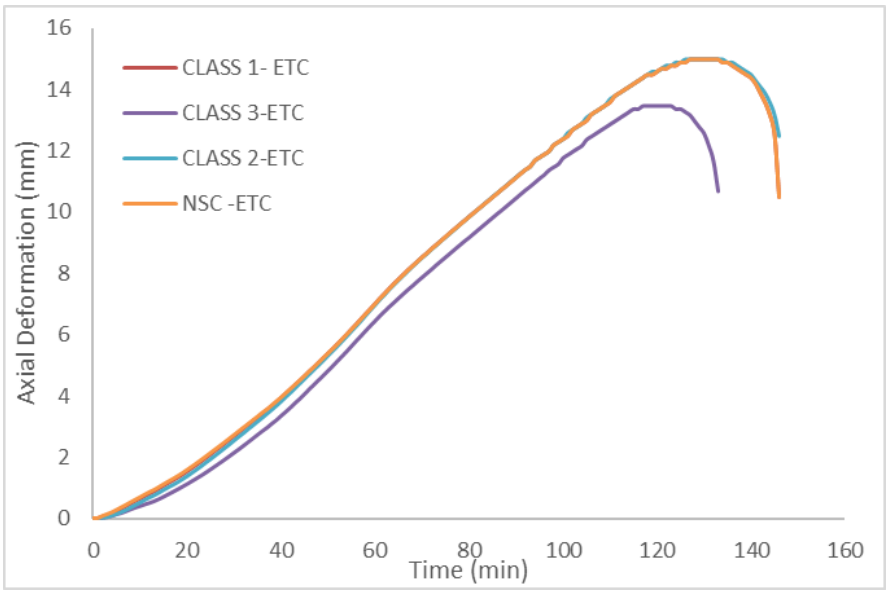

Figure B. 62 Axial deformations for different concrete compressive strengths

PC17

a)

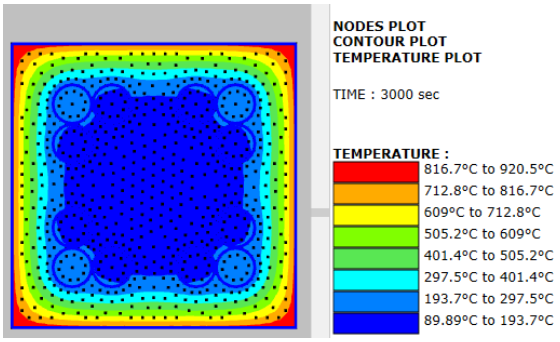

b)

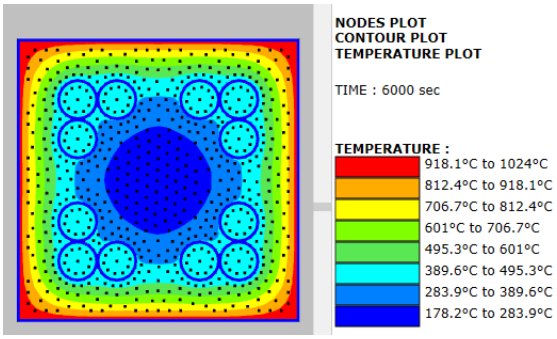

c)

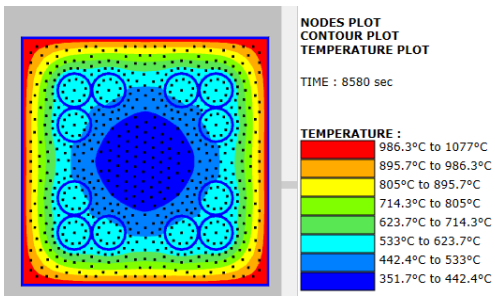

Figure B. 63 Temperature map for PC17 at a) 50 min b) 100 min and c) failure time

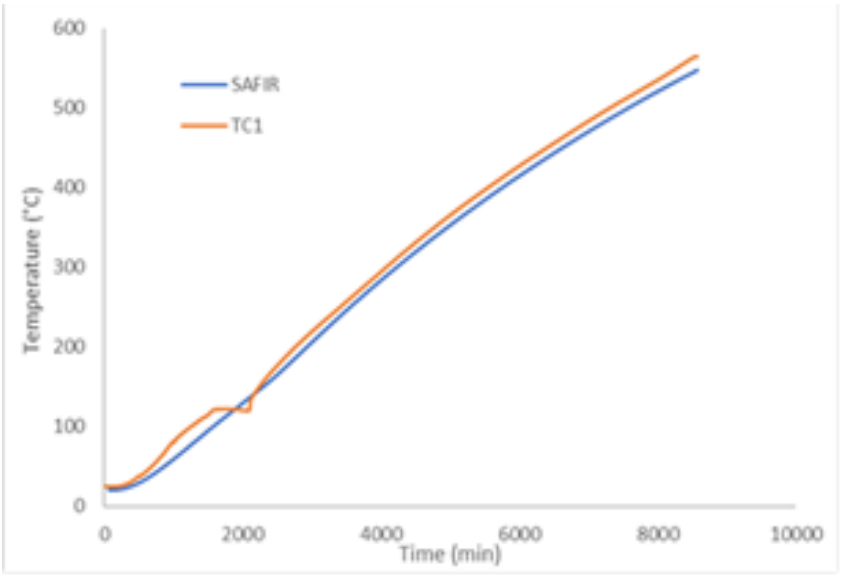

Figure B. 64 The calculated and measured temperature in thermocouple

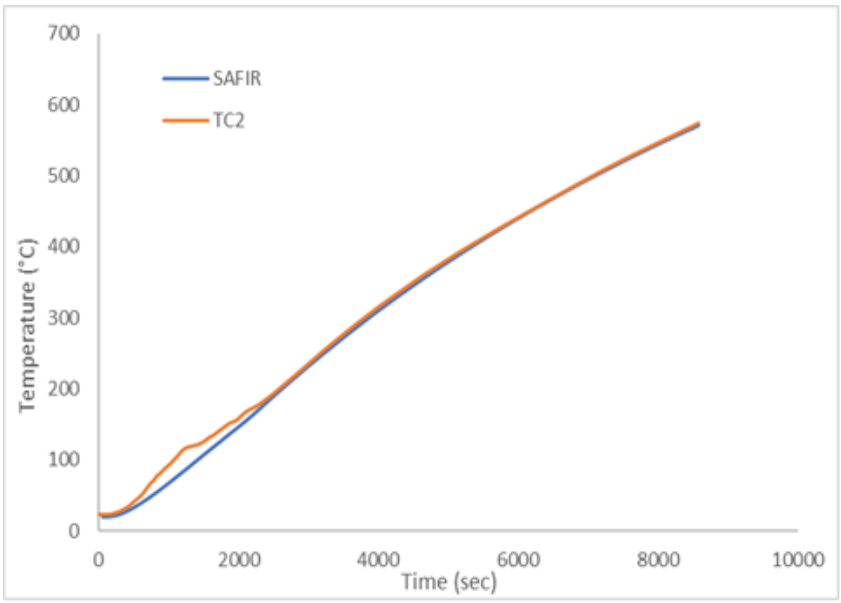

Figure B. 65 The calculated and measured temperature in thermocouple

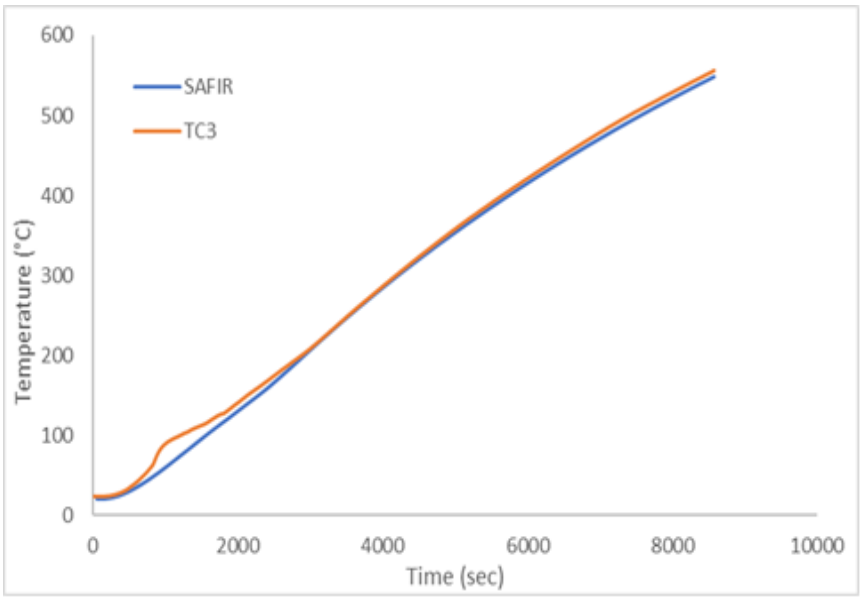

Figure B. 66 The calculated and measured temperature in thermocouple

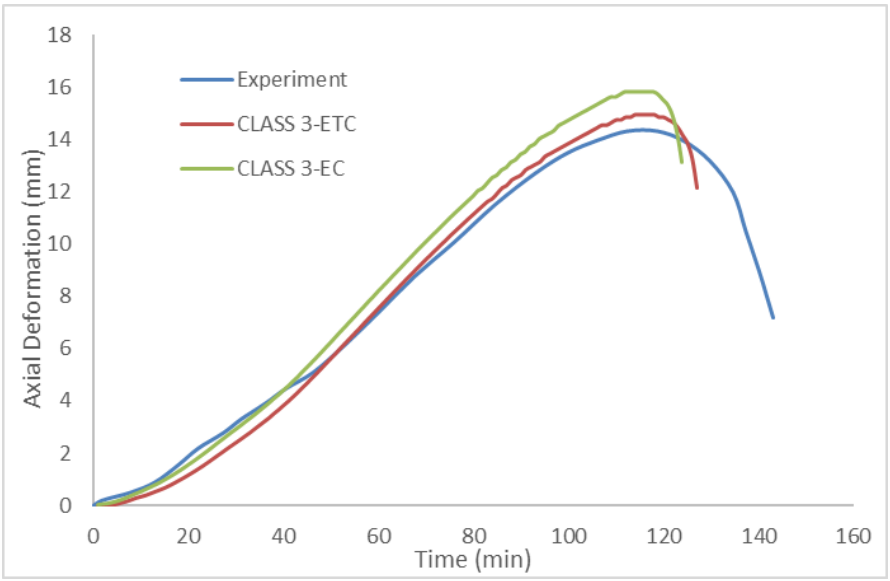

Figure B. 67 Comparison of calculated axial deformations with measured axial deformations for PC17

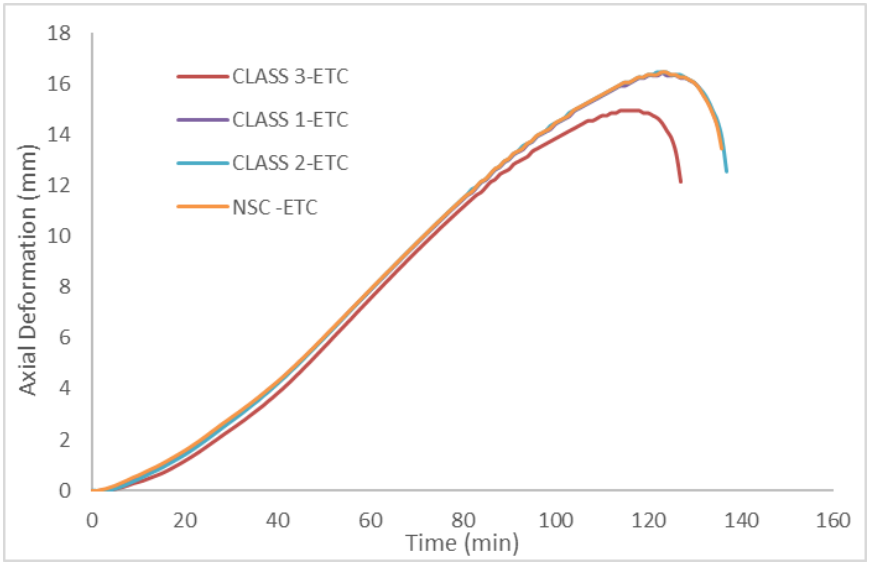

Figure B. 68 Axial deformations for different concrete compressive strengths

PC18

a) **b)**

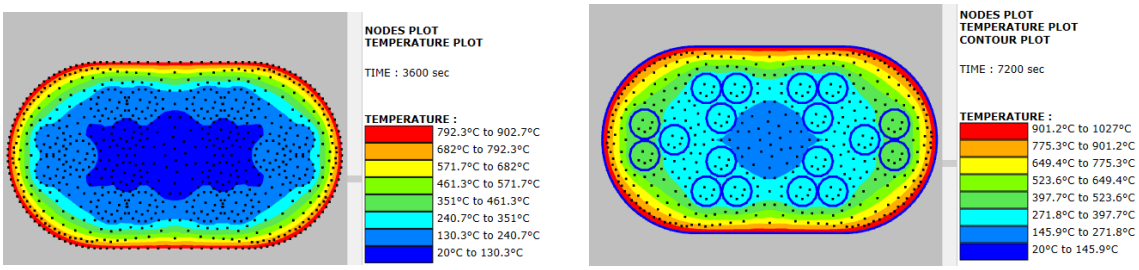

c)

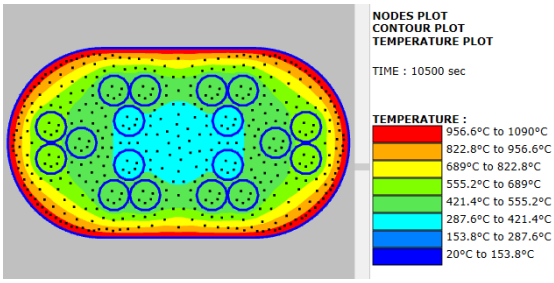

Figure B. 69 Temperature map for PC18 at a) 60 min b) 120 min and c) failure time

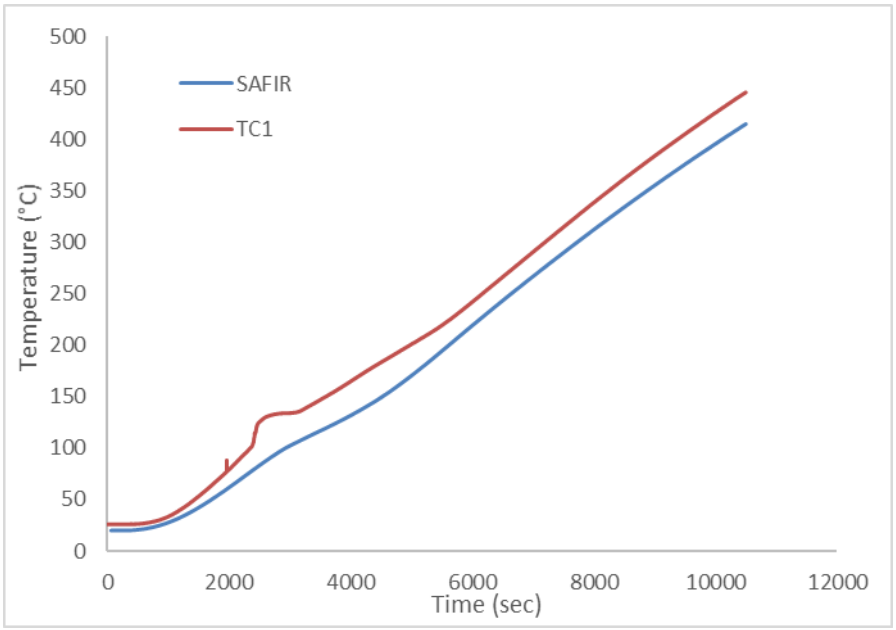

Figure B. 70 The calculated and measured temperature in thermocouple

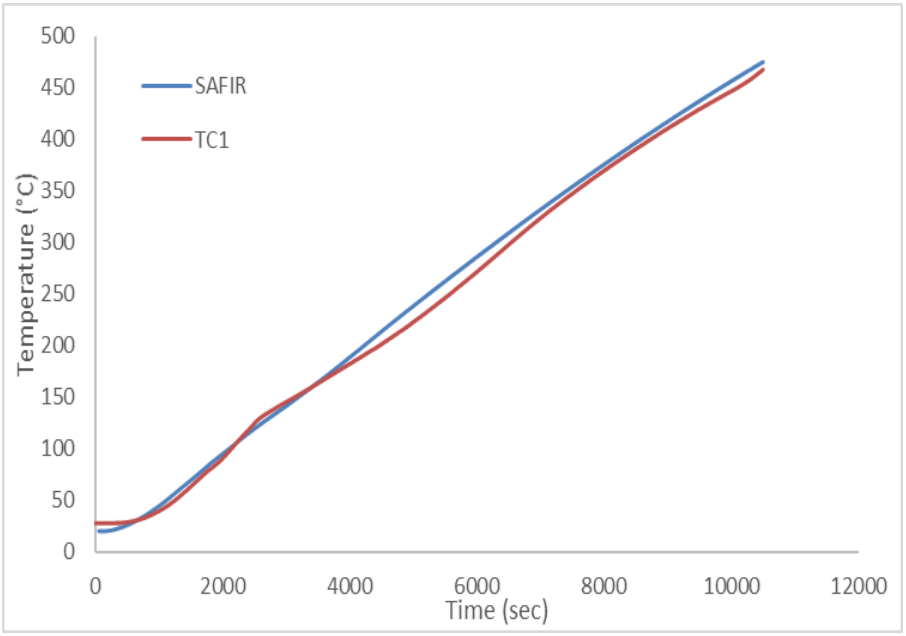

Figure B. 71 The calculated and measured temperature in thermocouple

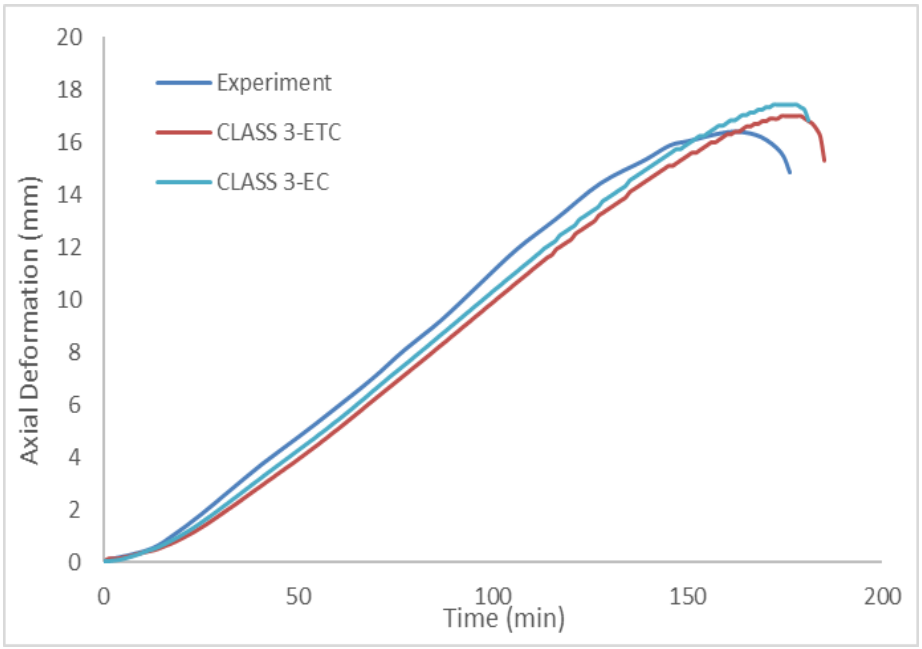

Figure B. 72 Comparison of calculated axial deformations with measured axial deformations for PC18

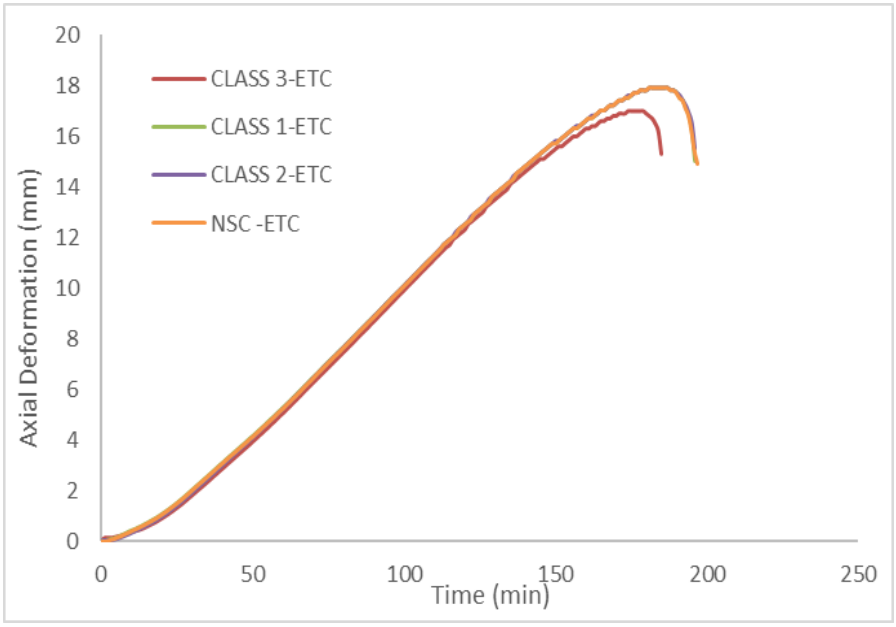

Figure B. 73 Axial deformations for different concrete compressive strengths

PC19

a)

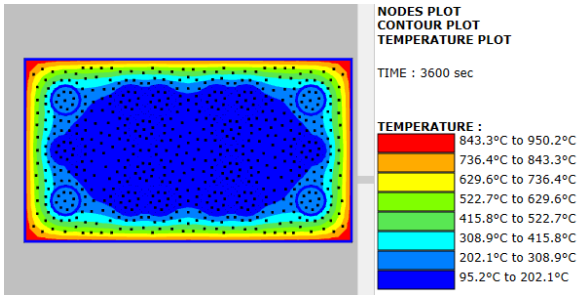

b)

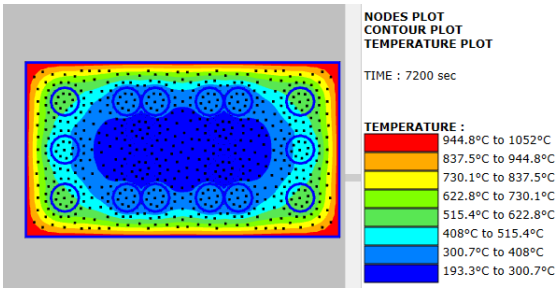

c)

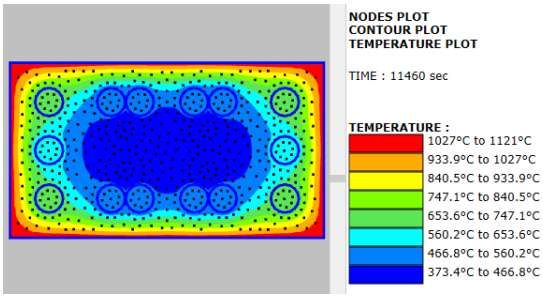

Figure B. 74 Temperature map for PC19 at a) 60 min b) 120 min and c) failure time

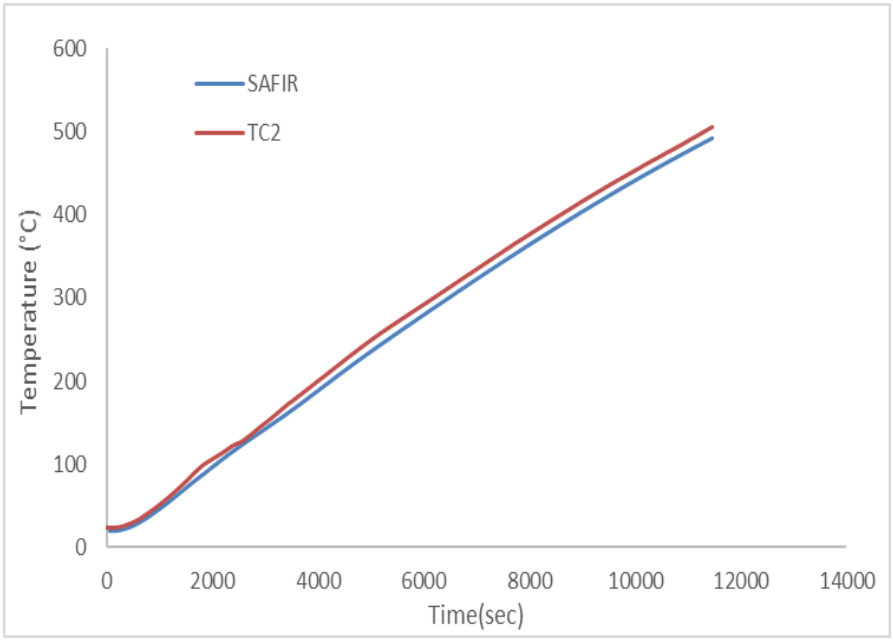

Figure B. 75 The calculated and measured temperature in thermocouple

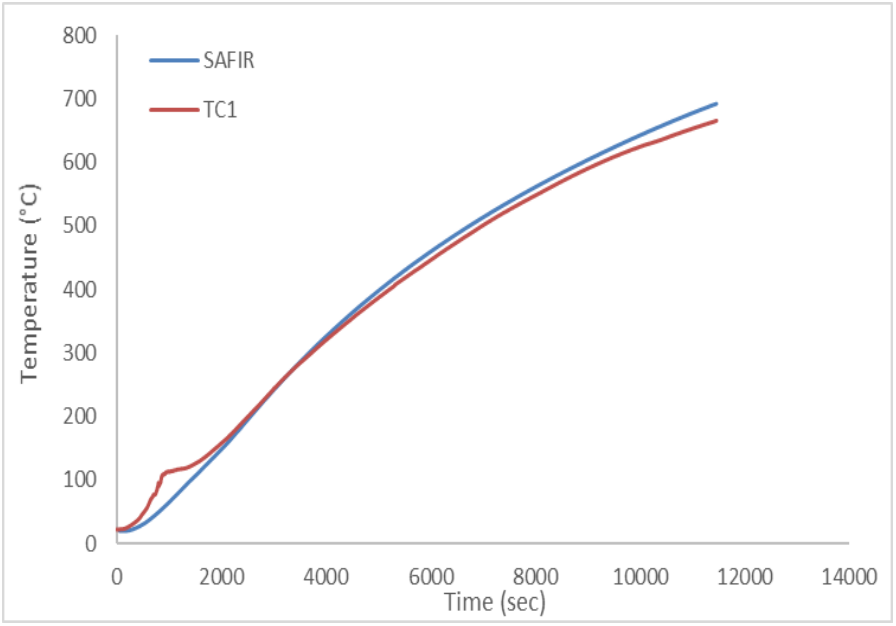

Figure B. 76 The calculated and measured temperature in thermocouple

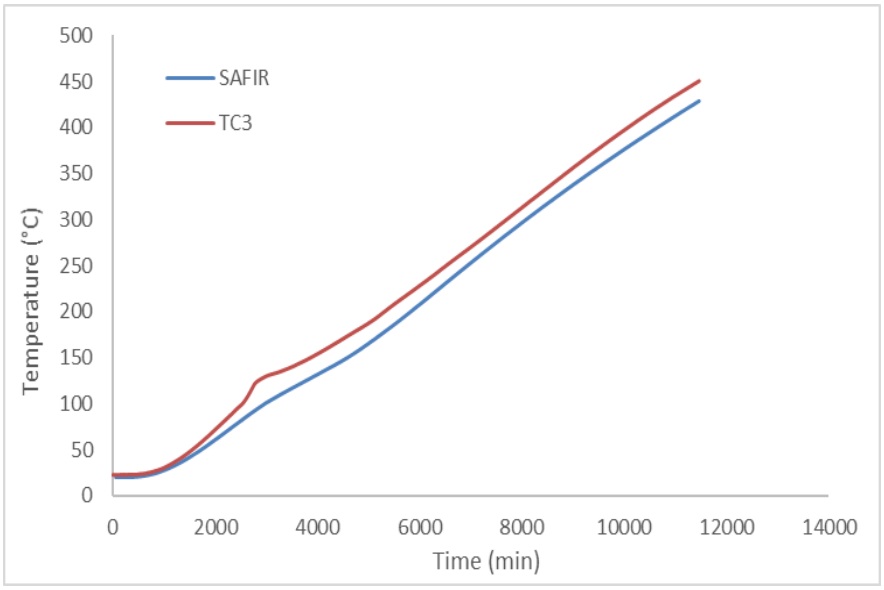

Figure B. 77 The calculated and measured temperature in thermocouple

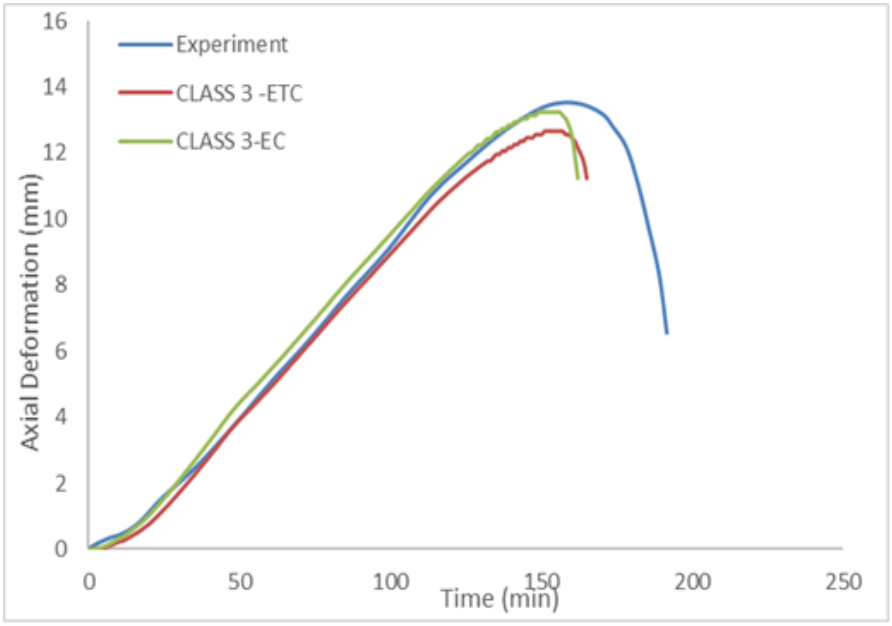

Figure B. 78 Comparison of calculated axial deformations with measured axial deformations for PC19

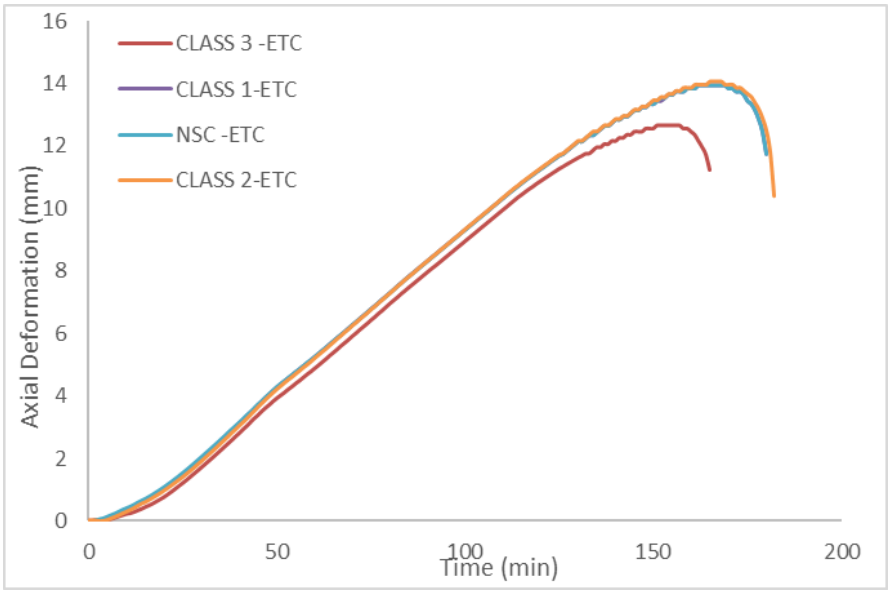

Figure B. 79 Axial deformations for different concrete compressive strengths

PC20

a) **b)**

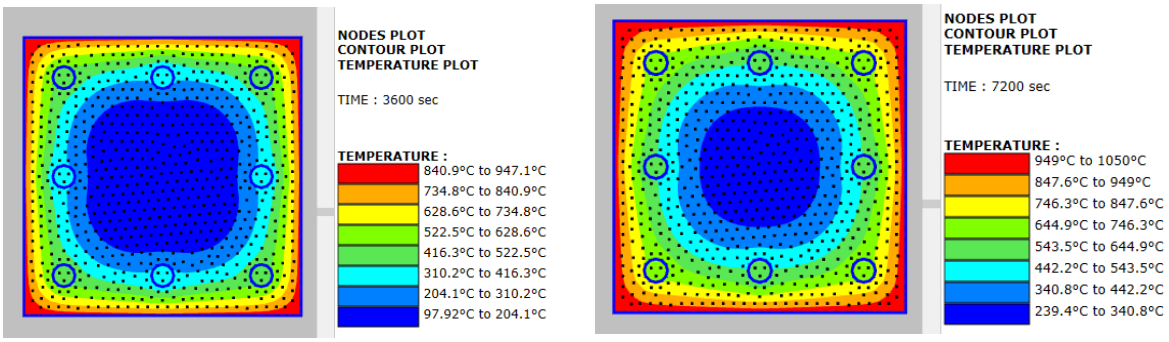

c)

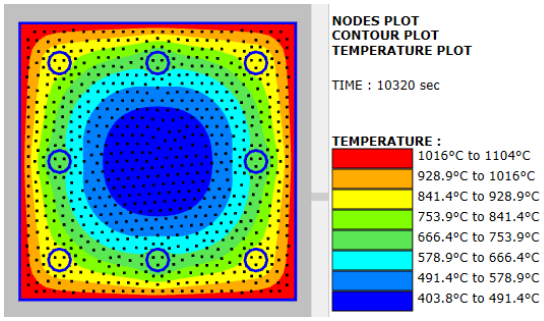

Figure B. 80 Temperature map for PC20 at a) 60 min b) 120 min and c) failure time

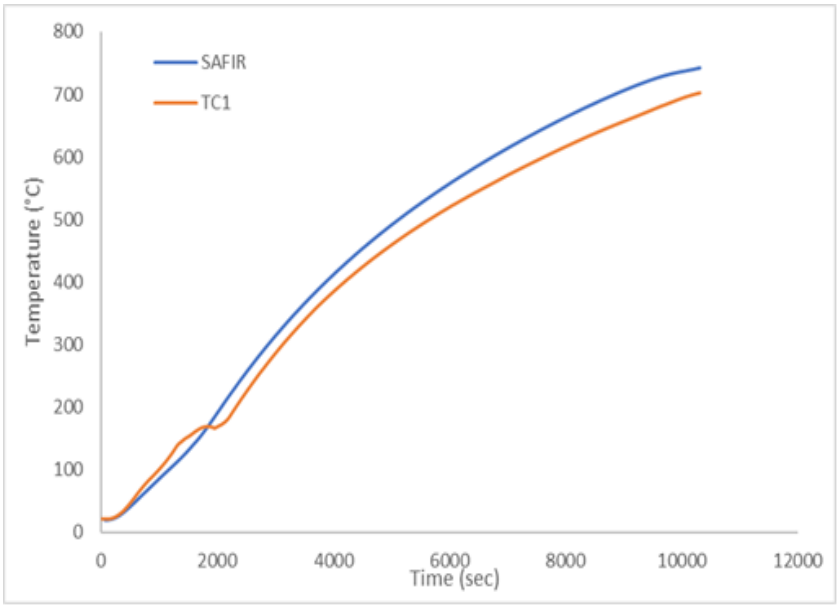

Figure B. 81 The calculated and measured temperature in thermocouple

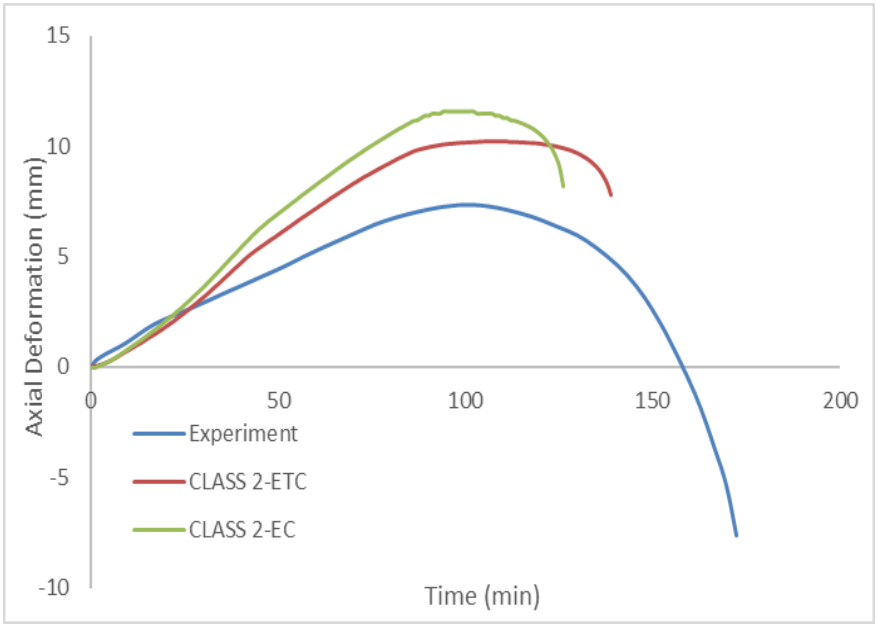

Figure B. 82 Comparison of calculated axial deformations with measured axial deformations for PC20

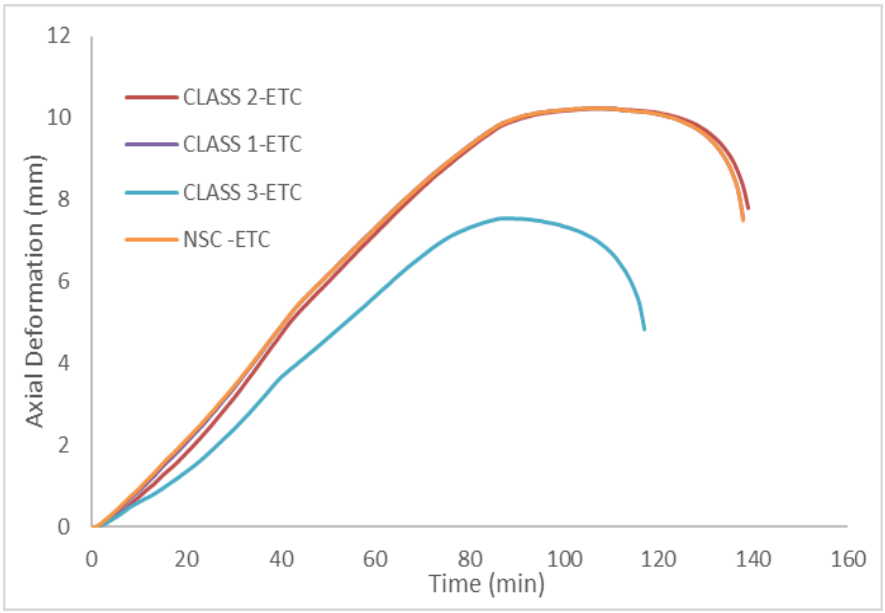

Figure B. 83 Axial deformations for different concrete compressive strengths

PC21

a)

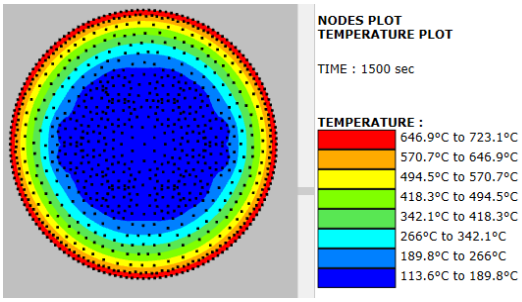

b)

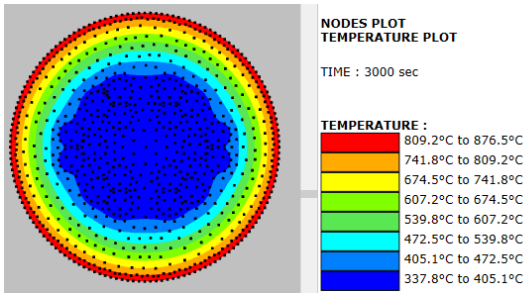

c)

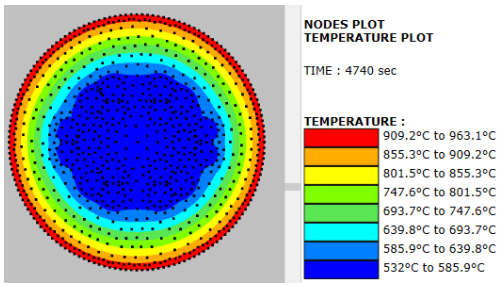

Figure B. 84 Temperature map for PC21 at a) 25 min b) 50 min and c) failure time

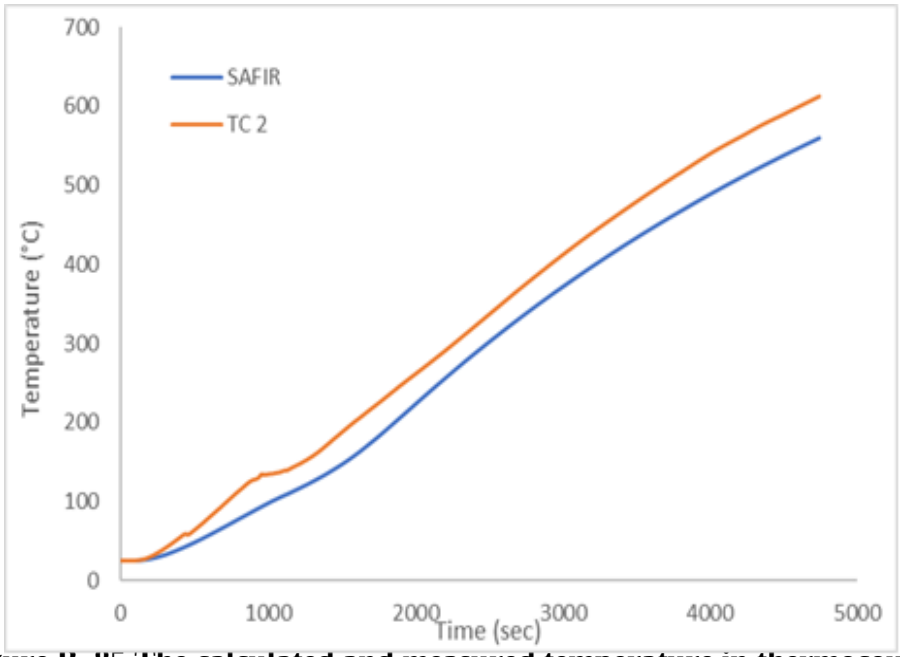

Figure B. 85 The calculated and measured temperature in thermocouple

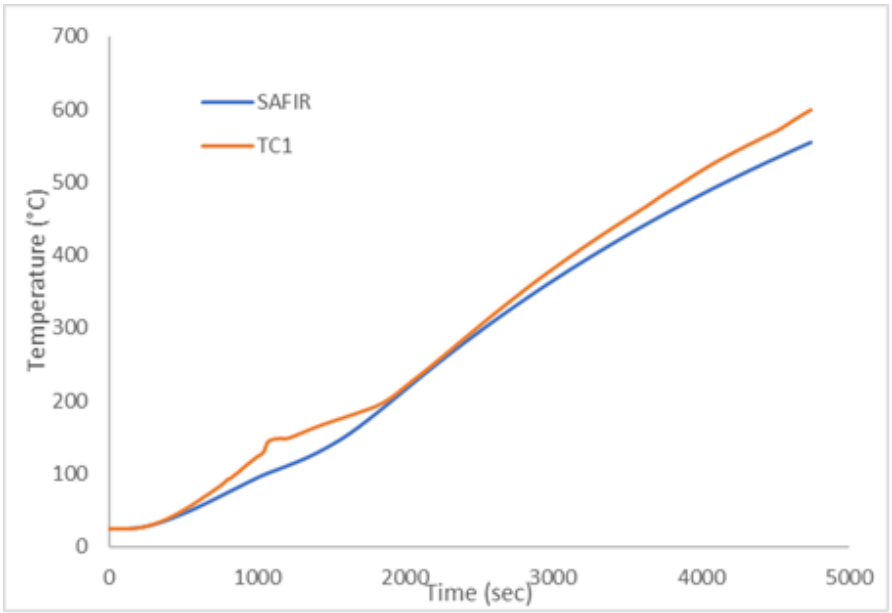

Figure B. 86 The calculated and measured temperature in thermocouple

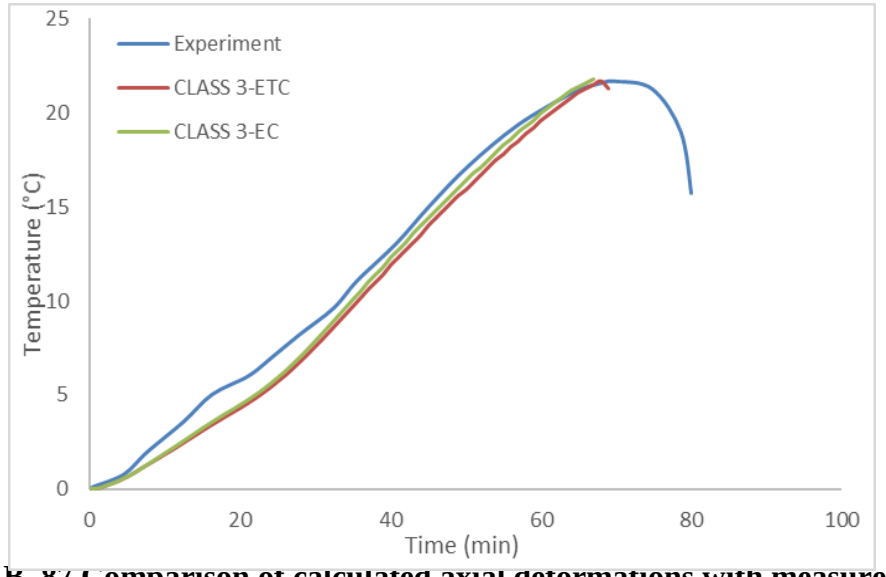

Figure B. 87 Comparison of calculated axial deformations with measured axial deformations for PC21

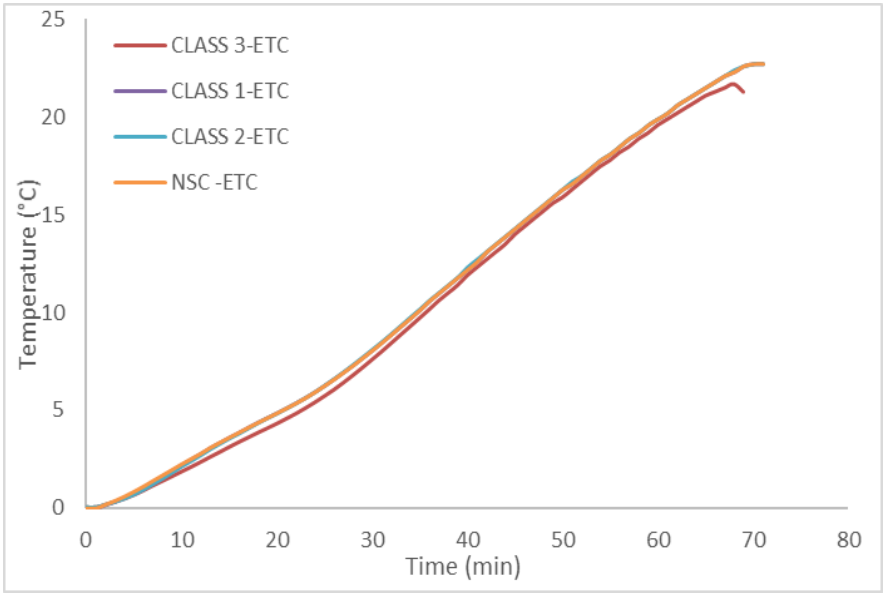

Figure B. 88 Axial deformations for different concrete compressive strengths

PC22

a)

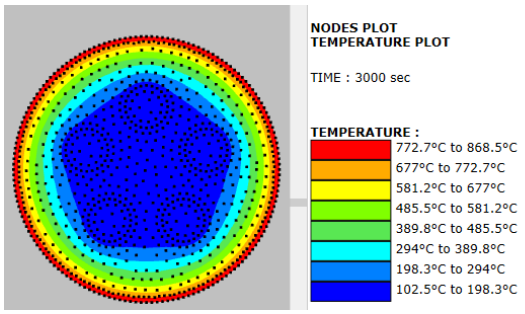

b)

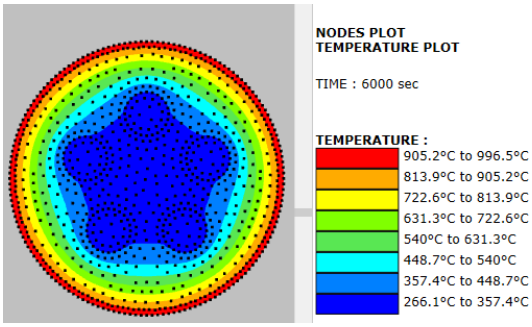

c)

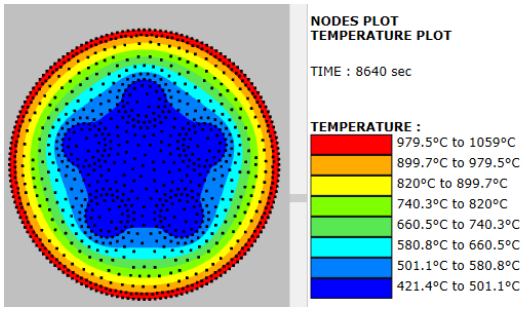

Figure B. 89 Temperature map for PC22 at a) 50 min b) 100 min and c) failure time

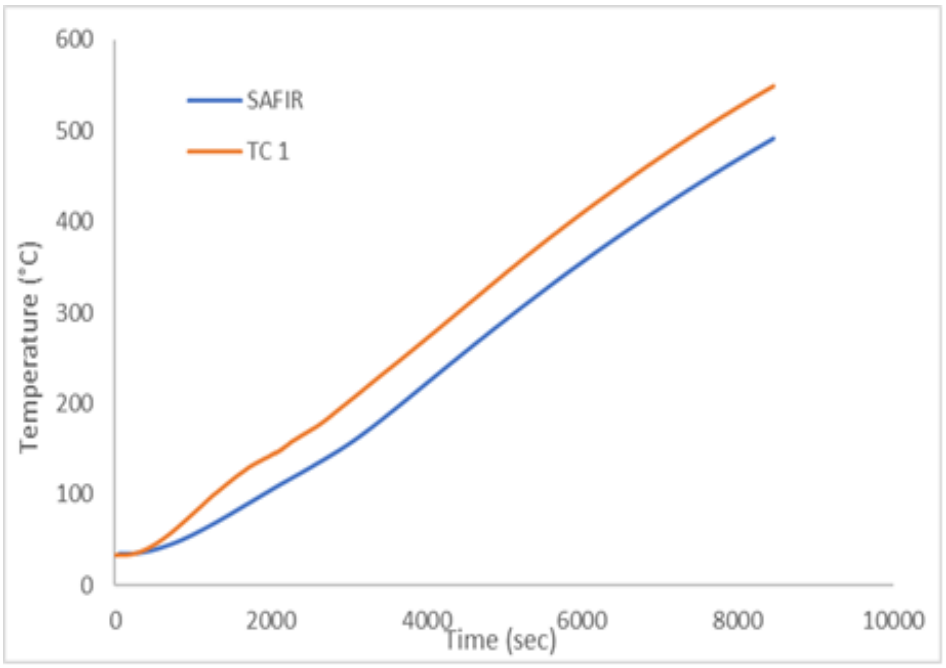

Figure B. 90 The calculated and measured temperature in thermocouple

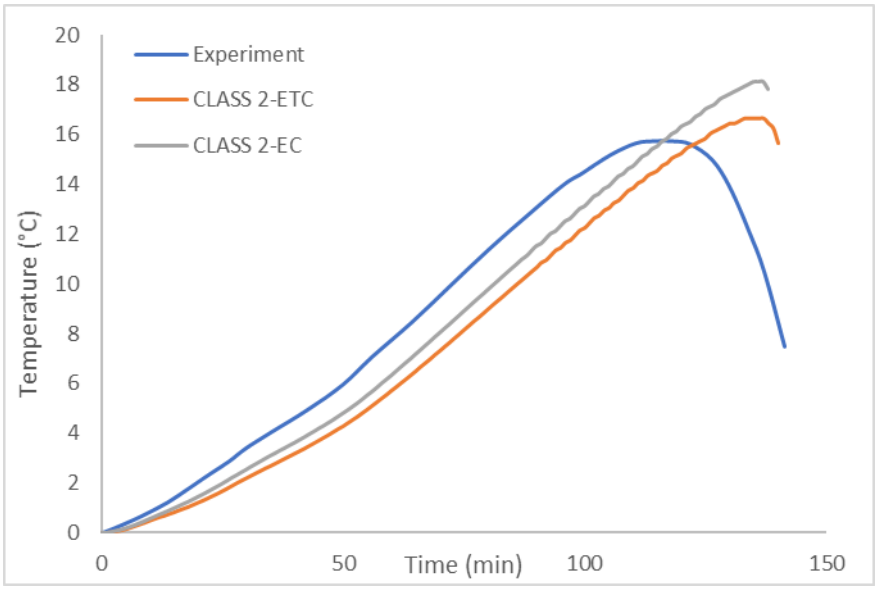

Figure B. 91 Comparison of calculated axial deformations with measured axial deformations for PC22

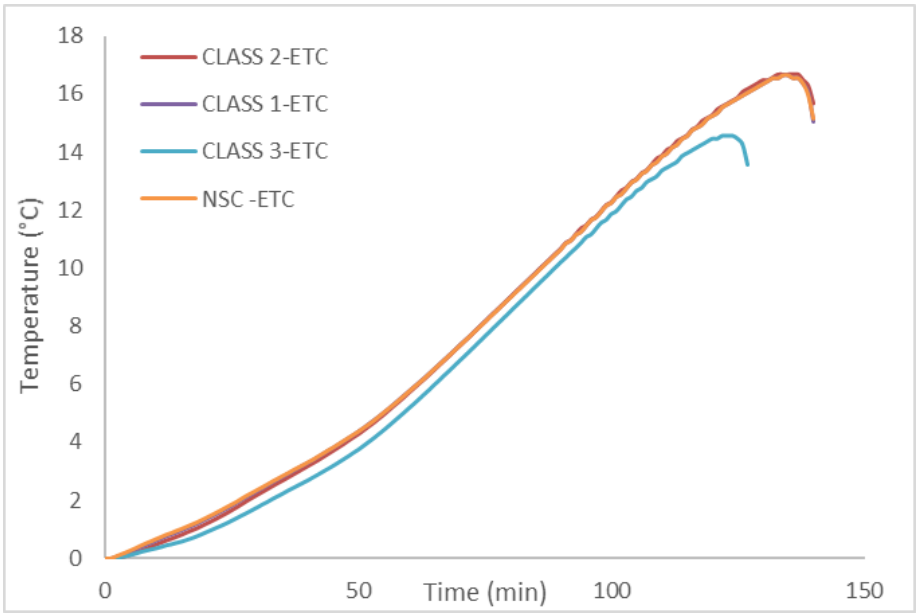

Figure B. 92 Axial deformations for different concrete compressive strengths